Tiedemann, R., Mix, A.C., Richter, C., and Ruddiman, W.F. (Eds.)
Proceedings of the Ocean Drilling Program, Scientific Results Volume 202

4. Astronomically Calibrated Timescales from 6 to 2.5 Ma and Benthic Isotope Stratigraphies, Sites 1236, 1237, 1239, and 1241[1]

Ralf Tiedemann,[2] Arne Sturm,[2] Silke Steph,[2] Steven P. Lund,[3] and Joseph S. Stoner[4]

ABSTRACT

We present benthic isotope stratigraphies for Sites 1236, 1237, 1239, and 1241 that span the late Miocene–Pliocene time interval from 6 to 2.4 Ma. Orbitally tuned timescales were generated for Sites 1237 and 1241 by correlating the high-frequency variations in gamma ray attenuation density, percent sand of the carbonate fraction, and benthic $\delta^{13}C$ to variations in Earth's orbital parameters. The astronomical timescales for Sites 1237 and 1241 are in agreement with the one from Atlantic Site 925/926 (Ocean Drilling Program Leg 154). The comparison of benthic $\delta^{18}O$ and $\delta^{13}C$ records from the east Pacific sites and Atlantic Site 925/926 revealed a surprising clarity of the "41-k.y. signal" in $\delta^{13}C$ records and a remarkably good correlation between their $\delta^{13}C$ records. This suggests that the late Miocene–Pliocene amplitudes of obliquity-related $\delta^{13}C$ cycles reflect a magnitude of global response often larger than that provided by obliquity-related $\delta^{18}O$ cycles. At Site 1237, the orbitally derived ages of Pliocene magnetic reversal boundaries between the base of Réunion and the top of Thvera confirm astronomical datings of the generally accepted ATNTS2004 timescale, except for the top of Kaena and the base of Sidufjall. Our astronomical age for the top of Kaena is about one obliquity cycle older. The base of Sidufjall appears to be about one precession cycle younger. The age models of Sites 1236 and 1239 were established by correlating their benthic $\delta^{18}O$ and $\delta^{13}C$ records directly to the orbitally tuned isotope record of Site 1241.

[1]Tiedemann, R., Sturm, A., Steph, S., Lund, S.P., and Stoner, J.S., 2007. Astronomically calibrated timescales from 6 to 2.5 Ma and benthic isotope stratigraphies, Sites 1236, 1237, 1239, and 1241. *In* Tiedemann, R., Mix, A.C., Richter, C., and Ruddiman, W.F. (Eds.), *Proc. ODP, Sci. Results,* 202: College Station, TX (Ocean Drilling Program), 1–69. doi:10.2973/odp.proc.sr.202.210.2007
[2]IFM-GEOMAR, Wischhofstrasse 1-3, 24148 Kiel, Germany. Present address: Alfred Wegener Institute for Polar and Marine Research (AWI), Am Alten Hafen 26, 27568 Bremerhaven, Germany. Correspondence author: **rtiedemann@awi-bremerhaven.de**
[3]Department of Earth Sciences, University of Southern California, University Park, Los Angeles CA 90089-0740, USA.
[4]College of Oceanic and Atmospheric Sciences, Oregon State University, 104 COAS Administration Building, Corvallis OR 97331-5503, USA.

Initial receipt: 4 February 2005
Acceptance: 4 October 2006
Web publication: 6 March 2007
Ms 202SR-210

INTRODUCTION

Our goal is to establish an astronomical timescale (ATS) from 12 to 2.5 Ma at Sites 1237 and 1241 that integrates the framework of magnetostratigraphy, biostratigraphy, tephrachronology, and oxygen isotope stratigraphy. Here, we present a progress report that documents our results of an orbitally tuned stratigraphy for the early Pliocene time interval from 6 to 2.5 Ma. The tuned ages of magnetic reversals (Site 1237) and oxygen isotope records (Sites 1237 and 1241) are directly compared with other orbitally tuned age models from Ceara Rise (Tiedemann and Franz, 1997), the equatorial east Pacific (Shackleton et al., 1995), and the Mediterranean (Lourens et al., 1996).

The astronomical tuning technique is at present the most accurate dating method for sediment records spanning the time interval of the last 35 m.y. for which astronomers provide a valid and precise orbital solution for variations in Earth's orbital parameters (Laskar, 1999). Changes in the eccentricity of Earth's orbit are marked by main periods of 413 and 100 k.y., and the tilt and precession of Earth's axis are dominated by periods of 41 and 23/19 k.y., respectively. These astronomical records provide the basis to date Neogene sediment records by matching patterns of cyclic variation in climate proxy records with patterns of changes in solar radiation that are controlled by cyclic variations in Earth's orbital parameters. The astronomical tuning method is based on the fact that cyclic changes in climate proxy records respond statistically convincingly to variations in insolation. The application of this tuning procedure made a high-precision time calibration possible because the "astronomical clock" is very accurate and cyclic changes in orbital parameters give very small-scale time markers on geological timescales (Laskar, 1999; Berger and Loutre, 1991). At best, the ATS could provide an age control point every 10,000 or 20,000 years, corresponding to half of a precession or obliquity cycle. The orbital tuning method is far more precise than that achievable by radiometric dating alone (Hilgen et al., 1999). The error of an astronomically tuned timescale is systematic and includes a few thousand years, based on the assumption of a constant (mostly unknown) time lag between a change in orbital insolation and the following climate response. Within this inaccuracy, the tuning approach provides a reliable and absolute timescale for magnetic reversal stratigraphy, biostratigraphy, oxygen isotope stratigraphy, and, of course, records of climate and oceanographic variability that transfer the astronomical record of varying insolation into quasi-cyclic sedimentological variability. The orbitally tuned geological timescale became the standard chronology for the Pleistocene and Pliocene (0–5.3 Ma) when the tuned ages of magnetic reversals were adopted to the geological timescale (Cande and Kent, 1995).

The improvement of the Pleistocene astronomical polarity timescale (APTS) and its expansion into the Miocene has been primarily pushed forward by two scientific criteria, using sedimentary cycle patterns in both, marine successions exposed on land in the Mediterranean (Hilgen and coworkers, Utrecht, Netherlands) and marine records from Ocean Drilling Program (ODP) sites located in the equatorial Pacific and Atlantic (Shackleton and coworkers, Cambridge, UK). Hilgen (1991a, 1991b) developed a Pliocene APTS back to 5.3 Ma by correlating sedimentary cycles from land-based sections to the astronomical record (Berger and Loutre, 1991). Lourens et al. (1996) improved this record by tuning to the astronomical solution of Laskar et al. (1993). The work of Hilgen et

al. (1995), Krijgsman et al. (1999), and Hilgen et al. (2003) expanded the Mediterranean APTS back to 13.6 Ma.

Based on marine records from ODP Leg 138 in the eastern equatorial Pacific, Shackleton et al. (1995) developed an APTS for the past 6 m.y. by matching cyclic variations in gamma ray attenuation (GRA) density records to the orbital insolation record of Berger and Loutre (1991) and advanced the Pliocene oxygen isotope stratigraphy from 2.5 to 6 Ma. At the same time, Tiedemann et al. (1994) developed an astronomically calibrated oxygen isotope timescale for northeast Atlantic Site 659 off the coast of Africa by tuning Pliocene variations in dust flux (2.5–5 Ma) to the astronomical solution of Berger and Loutre (1991). These studies provided a common benthic oxygen isotope stratigraphy and nomenclature for the Pliocene. The work of Shackleton et al. (1995) also provided a preliminary tuning from 6 to 10 Ma by using an astronomically calibrated age of 5.9 Ma for the magnetic reversal C3A.n(t) as a starting point and an age of 9.6 Ma for C5n.1n(t) as a fixed endpoint that, however, was based on radiometric dating. The APTS from Leg 138 suggests that the ages of the late Miocene reversal boundaries are as much as 180 k.y. younger than those derived from the Mediterranean area (Hilgen et al., 1995; Krijgsman et al., 1999). The offset seems to develop in the interval from 5.3 to 6 Ma (Kent, 1999).

More recently, Tiedemann and Franz (1997), Shackleton and Crowhurst (1997), and Shackleton et al. (1999) established an ATS from 2.5 to 34 Ma in sediment records from Leg 154 (Ceara Rise) by tuning sedimentary cycles to the astronomical record of Laskar et al. (1993). The work of Tiedemann and Franz (1997), Billups et al. (1997), and Shackleton and Crowhurst (1997) provided an oxygen isotope stratigraphy for the interval from 2.5 to 7 Ma (Site 925/926). The application of the Laskar solution (instead of Berger and Loutre, 1991) improved the calibration of the early Pliocene isotope stages, especially prior to ~4 Ma. Unfortunately, the sediment records from Leg 154 provided no magnetostratigraphic information, which complicates comparisons with other timescales. The latest APTS that summarizes the ages of magnetic reversals is given by Lourens et al. (2004) and is referred to the ATNTS2004 timescale, whereas the ages of reversal boundaries between 5 and 13 Ma are mainly derived from continental successions.

Rapid progress in advancing the marine APTS to the Neogene/Paleogene boundary is limited by the availability of good reference sections. The sediment record from Site 1237, which was drilled during Leg 202 on Nazca Ridge, meets nearly all aspects of providing such a reference section:

1. It comprises a complete Neogene sequence that was drilled by the advanced piston corer (APC) technique. The composite depth section documents complete recovery for the sequence from 0 to ~31.5 Ma without any detectable stratigraphic breaks as indicated by microfossil and magnetic stratigraphy.
2. Various types of data, indicative of changes in chemical sediment composition and physical properties, document the evident orbital cycles.
3. High carbonate concentrations allow establishment of high-resolution benthic oxygen and carbon isotope records and offer excellent potential for refining the foraminiferal and nannofossil biostratigraphy.
4. The paleomagnetic stratigraphy at Site 1237 is excellent with clear definitions of all chrons and subchrons over the last 5 m.y.

as well as from 7 to 13 Ma. The polarity assignments for the interval from 5 to 7 Ma and for the lowermost part of the sequence between 13 and 31 Ma are still preliminary because the polarity sequence allows several possible interpretations.

At Site 1237 so far, we developed an astronomically tuned age model for the time interval from 2.5 to 6 Ma that includes benthic oxygen isotope stratigraphy from 4 to 6 Ma.

To verify our tuning at Site 1237, we also established an orbitally tuned timescale at Site 1241. Site 1241 yielded a complete and continuous sediment record for the time interval of the last 9 m.y. Here, we measured a benthic isotope record from 2.5 to 5.7 Ma that enables a comparison with that from Site 1237 within the overlapping time interval from 4 to 5.7 Ma.

DATA AND METHODS

For orbital tuning, we considered shipboard core logging data (magnetic susceptibility, bulk density, and color spectra) as well as carbonate percentages, sand fraction percentages of the carbonate fraction, and benthic isotope records. Core logging shipboard data (Mix, Tiedemann, Blum, et al., 2003) were measured at intervals of 2.5 cm (Site 1237) and 5 cm (Site 1241) and provide a temporal resolution of 1000–2500 yr, which corresponds to sedimentation rates ranging from 1 to 3 cm/k.y. at Site 1237 and from 2 to 5 cm/k.y. at Site 1241. Isotope data, carbonate, and sand percentages were measured every 5 cm at Site 1237 and every 10 cm at Site 1241.

Isotope data from Sites 1237 and 1241 were analyzed at the IFM-GEOMAR Institute in Kiel (Germany) using a Finnigan/MAT-252 mass spectrometer equipped with a fully automated Finnigan/Kiel-Carbo-II carbonate preparation device. For each isotope analysis, up to five specimens of the epibenthic foraminifers *Cibicidoides wuellerstorfi* or *Cibicidoides mundulus* were picked from the 250- to 500-µm fraction. The laboratory standard was calibrated to Peedee belemnite through National Bureau of Standards reference material NBS-19. Analytical reproducibility of the laboratory standard typically was about ±0.06‰ for $\delta^{18}O$ and ±0.03‰ for $\delta^{13}C$ (±1σ). Isotope data from Site 1236 were measured at the Leibniz Labor for Radiometric Dating and Isotope Research at Kiel University (Kiel, Germany) using a Finnigan/Delta-Plus-XL mass spectrometer coupled to a Finnigan/Gas-Bench-II. Precision of the local carbonate standard was ±0.07‰ for $\delta^{18}O$ and ±0.05‰ for $\delta^{13}C$ (±1σ) over the period of analyses.

The $CaCO_3$ contents were determined by infrared absorption of total CO_2 (organic and inorganic carbon) released by combustion with a LECO analyzer. Early Pliocene organic carbon contents are lower than 0.4 wt% at Sites 1236, 1237, and 1241 (Mix, Tiedemann, Blum, et al., 2003). Hence, carbonate percentages might be overestimated by as much as 3.3 wt% (equal to an organic carbon content of 0.4 wt%).

The sand fraction represents the wet-sieved residue of the >63-µm fraction, which consists of nearly 100% carbonate. The content of the dry sand fraction is given as weight percent of total $CaCO_3$ to compensate for dilution effects caused by noncarbonate dilutants.

For orbital tuning and spectral analyses, we use the software package AnalySeries 2.0 (Paillard et al., 1996). AnalySeries especially facilitates the transformation of "proxy data vs. depth" records into "proxy data

vs. age" records by graphically adjusting cyclic fluctuations of paleoclimatic proxy records to the astronomical target record. The age of each data point was estimated by linear interpolation between age-depth control points. AnalySeries also provides filters and a set of spectral analysis methods that are partly complementary in terms of robustness vs. resolution. We preferred to use the classical Blackman-Tukey method (Blackman and Tukey, 1958) for spectral analysis in the time and depth domain. The algorithm computes first the autocovariance of the data, applies a window, and finally applies a Fourier transform to compute the spectrum. It is a very robust method, unlikely to present spurious spectral features. The main drawback is its poor resolution in the spectral domain because sharp features can be considerably smoothed. This method allows the user to choose a resolution vs. confidence parameter: the length of the autocovariance series, which is generally set to 60% of the input series. The confidence level associated with the error bar on the spectrum is typically set to 80%. For filtering and spectral analysis in the time domain, we interpolated each record at equidistant intervals, corresponding to the average time resolution of the proxy record. Tukey bandpass filters with a central frequency of 0.045 cycles/k.y. (bandwidth = 0.01) and 0.024 cycles/k.y. (bandwidth = 0.009) were used to extract the precession- and obliquity-related components from the proxy records, respectively.

We used the orbital solution from Laskar et al. (2004) for Pliocene variations in Northern Hemisphere summer insolation (June 21–July 21), obliquity, and precession as a tuning target. Until 1996, orbitally derived age models were based on the astronomical solution of Berger and Loutre (1991). Lourens et al. (1996) demonstrated, however, that unrealistic large time lags will occur between obliquity and the obliquity-related variations in the proxy records if the orbital data from Berger and Loutre (1991) are used as a tuning target. Lourens et al. (1996) pointed out that the geological record can be calibrated most accurately to the summer insolation record calculated from the Laskar et al. (1993) solution $La93_{(1,1)}$ with a dynamically ellipticity of the Earth of 1 and a tidal dissipation term of 1, both close to present-day values. The new solution La2004 for the astronomical computation of the insolation quantities on Earth (Laskar et al., 2004) improved the solution La93 by using a direct integration of the gravitational equations for the orbital motion and by improving the dissipative contributions, in particular in the evolution of the Earth–Moon System. This orbital solution has been used for the latest calibration of the astronomically tuned Neogene timescale (ATNTS2004; Lourens et al., 2004) and is expected to be used for age calibrations of paleoclimatic data over the last 40–50 m.y.

Verification of Depth Scales

A major precondition for tuning marine paleoclimate records to the astronomical record is to ensure the recovery of complete and undisturbed sediment records. This is achieved by drilling multiple offset holes at the same site location to splice across coring gaps and distorted sediment sequences through interhole correlations using closely spaced core logging measurements. This strategy (Ruddiman et al., 1987) became a standard during paleoceanographic ODP legs. At Sites 1236, 1237, 1239, and 1241, the construction of the composite depth was based on core logging magnetic susceptibility and GRA density data. We reinspected the composite depth of Sites 1237 and 1241 by considering in addition the core logging color data, which was not possible

during the cruise because of time constraints. We did not verify the composite depth at Sites 1236 and 1239.

Only at Site 1241, the correlation of overlapping sections from adjacent holes by means of color data suggests a mismatch between Cores 202-1241C-11H and 202-1241A-16H (Fig. F1). The former correlation resulted in a doubling of a 63-cm-long sediment section. Our new splice suggests a switch point at 175.77 meters composite depth (mcd), from Section 202-1241C-11H-7, 20 cm (same as before), to Section 202-1241A-16H-4, 72 cm. This deletes 63 cm from the former composite depth (interval 202-1241A-16H-4, 7–72 cm; corresponding to an interval of 65 cm on the meters below seafloor scale). The revision leads to a small reduction of the composite depth scale, as 63 cm is subtracted from the mcd below Section 202-1241A-16H-4, 72 cm.

F1. Revision of former mcd splice, Site 1241, p. 22.

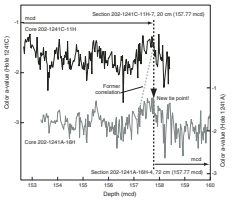

Tuning Procedure

At best, the tuning medium should be marked by cyclic, high-amplitude fluctuations and a high signal-to-noise ratio. From our experience, however, we know that a single climate proxy record often includes an interval of low signal-to-noise ratios, where a clear interpretation of the geological record with regard to its orbitally induced variability is difficult to derive. Therefore, we used a multiproxy approach for orbital tuning to overcome such problems. Discrete ash layers (Mix, Tiedemann, Blum, et al., 2003) were removed from the data sets to avoid misinterpretations of the climate signal and distortions of sedimentation rates. The sediment record from Site 1237 was especially affected by the frequent deposition of ash layers. Fourteen ash layers were identified in the time interval from 2.4 to 6 Ma by the Leg 202 shipboard party, some of them ranging in thickness from 15 to 36 cm. Inspection of the sand fraction record indicated that the range with significant amounts of ash often spanned a larger interval than simply suggested by a discrete ash layer. Although we deleted discrete ash layers from the composite depth, the "normal pelagic sedimentation rate" is overestimated by the amount of dispersed ash in such intervals.

The first step toward astronomical calibration was to identify dominant cycles of selected proxy records in the depth domain by means of spectral analyses on succeeding 10-m-long intervals. This approach helped to trace long-term changes in sedimentation rates (e.g., an increase in sedimentation rate would move dominant precession- or obliquity-related frequencies [cycles/m] to lower frequencies). The spectral comparison between different proxy records also clearly identifies precession- and obliquity-related cycles and indicates which of the proxy records are best suited for tuning to the precession and/or obliquity.

In a second step, we extracted the precession- and obliquity-related components from the proxy records by bandpass filtering each of the succeeding 10-m-long sections. We then used the merged filter outputs for a first tuning. We started with tuning to obliquity for two reasons. First, most proxy records revealed a stronger response to obliquity than to precession. More than one proxy for tuning to obliquity improved the continuous and reliable detection of the 41-k.y. cycle from 2.5 to 6 Ma. Second, the effect of obliquity on insolation is symmetric across hemispheres. That is, cold summers occur in both hemispheres at the same time (in phase). This increases the likelihood that proxy records indicative of global climate change respond to obliquity forcing with possibly different but relatively constant phase lags. Pliocene variations in benthic $\delta^{18}O$ and $\delta^{13}C$ are dominated by 41-k.y. cycles and are

thought to respond with relatively constant phase lags to obliquity forcing. Fluctuations in benthic $\delta^{18}O$ records are linked to high-latitude processes because they are sensitive to variations in global ice volume and to changes in deepwater temperature/salinity. Provided that the effect of obliquity on insolation is symmetric across hemispheres, the mid-Pliocene shift from unipolar to bipolar glaciations or changes in the location of predominant deepwater formation (Southern Ocean vs. North Atlantic) should not have significantly affected the phase of the obliquity-related benthic $\delta^{18}O$ variations (Clemens, 1999). The work of Imbrie and Imbrie (1980) and Imbrie et al. (1984) suggested a lag between obliquity and obliquity-controlled variations in ice volume of 8 k.y. for the Pleistocene time interval. Their model also implied that the time lag strongly depends on the size of the ice sheet, whereas a smaller ice sheet would result in a smaller phase lag. For the relatively warm Pliocene interval prior to Northern Hemisphere glaciation, the true phase lag may have been close to 6 k.y., as suggested by Chen et al. (1995). The disadvantage of solely using Pliocene benthic $\delta^{18}O$ records for orbital tuning is their low signal-to-noise ratio because the small variability in global ice volume prior to Northern Hemisphere glaciation (>3 Ma) distinctly decreased the $\delta^{18}O$ amplitudes. In some intervals of the early Pliocene, the signal-to-noise ratio is so low that it is difficult to decide whether 41-k.y. cycles are registered or not (Tiedemann et al., 1994; Shackleton et al., 1995). In this context, the benthic $\delta^{13}C$ records are an alternative for tuning to obliquity. Obliquity-related fluctuations in benthic $\delta^{13}C$ are thought to be largely controlled by global variations in marine productivity and the mass of organic matter stored in forests, soils, and shallow marine sediments (Shackleton, 1977), presumably related to glacial–interglacial climate change. Although the globally correlative nature of the Pliocene benthic $\delta^{13}C$ signal has never been examined in detail, several studies indicated that Pliocene benthic $\delta^{13}C$ maxima lag $\delta^{18}O$ minima in the eastern Pacific with a relatively constant phase of ~2 k.y. at the obliquity band (Mix et al., 1995; Shackleton et al., 1995). Considering a phase difference of 6 k.y. between Pliocene variations in orbital obliquity and benthic $\delta^{18}O$, $\delta^{13}C$ maxima may have lagged obliquity maxima by ~8 k.y. For an unambiguous tracing of 41-k.y. cycles, we also considered other proxy records like GRA density, magnetic susceptibility, and color reflectance data. After determining their phase relationships with respect to $\delta^{18}O$ minima (warm stages), we established a preliminary age model that is based on tuning their 41-k.y. components to orbital obliquity. At this stage, the tuning provided constant phase relationships between the proxy records and orbital obliquity but did not include the possible phase lags for $\delta^{18}O$ and $\delta^{13}C$, as mentioned above. Instead of that, we continued with tuning to precession; matching the obliquity-related filter output of a proxy record to orbital obliquity is not as easy as tuning to precession because the amplitudinal variability in orbital obliquity is low and thus provides no eye-catching control points for a correct match.

The advantage of tuning to orbital precession is that the amplitudinal power of orbital precession is well structured by eccentricity-induced packets of 100- or 400-k.y. intervals. These packets are often easily recognized in proxy records that are dominated by precessional variance (e.g., Tiedemann et al., 1994; Tiedemann and Franz, 1997). Therefore, we also used such packets for aligning climate variables with strong precessional responses. GRA density data from Site 1237 and the sand fraction record from Site 1241 reveal significant response to or-

bital precession forcing. Their precession-related filter outputs provided a powerful independent check on the correlation initially defined by tuning to obliquity. Nevertheless, we are aware of the fact that the amplitudinal variability of precession-related cycles could also be influenced by changes in sedimentation rates or internal processes of the climate system. Low sedimentation rates decrease the time resolution and the signal-to-noise ratio and thus may distort the original, amplitudinal climate response to orbital forcing. Internal processes of the climate system couple specific variables or mutually interact among them. These interactions may either amplify anomalies of one of the interacting elements or damp them. Thus, we only set precession-based age control points, where the alignment with the orbital record is corroborated by both the precession component and the obliquity component of proxy records. A point of discussion is that we have no model linking the precessional response of the proxy records to orbital forcing. Precession insolation forcing is hemispherically asymmetric with Northern Hemisphere summers being 180° (11.5 k.y.) out of phase with Southern Hemisphere summers and we did not examine whether Northern or Southern Hemisphere insolation exerted a stronger control on the precessional signal of the proxy records. We simply assumed that the observed correlation between benthic $\delta^{18}O$ warm stages and obliquity-related maxima or minima in proxy records is similar for precessional minima. For instance, if obliquity-related maxima in GRA density correlate with $\delta^{18}O$ warm stages (maxima in orbital obliquity), we also assumed that precession-related maxima in GRA density correspond to precession-controlled maxima in insolation. We used the summer insolation at 65°N as a target record and assumed an in-phase relationship between insolation and the proxy record. However, we did not tune to precession if the adjustment would lead to unrealistic large time lags between obliquity and glacial-bound variations in proxy records indicative of global climate change.

Development of an Orbitally Derived Age Model for Site 1237

Sedimentation rates are relatively low (<3 cm/k.y.) at Site 1237. For this reason, we first demonstrate that the quality of the logging data from Site 1237 is still appropriate for orbital tuning (Fig. F2). The depth interval from 60 to 80 mcd is especially suited for a test because it has a well-constrained paleomagnetic age model that provides a first approximation of changes in sedimentation rates. Sedimentation rates range from 1.6 to 2 cm/k.y. between the base of Mammoth Chron and the base of Cochiti Chron. Within this interval, cyclic fluctuations of the GRA bulk density and magnetic susceptibility records are characterized by two major clusters of cycles, from 37 to 49 cm and from 77 to 114 cm (Fig. F2). These two clusters clearly identify the response to precession (19- and 23-k.y. cycles) and obliquity (41-k.y. cycle), whereas the range of the clusters is defined by the variability of sedimentation rates.

Spectral analyses in the depth domain suggested that the records of benthic $\delta^{13}C$, magnetic susceptibility, and GRA density are best suited for orbital tuning. The $\delta^{13}C$ and magnetic susceptibility records revealed significant variability at the obliquity frequency band. The GRA density record provided in addition significant variability at precession-related frequencies (Fig. F2). Before tuning, we examined their relationships to obliquity-dominated changes in global climate as indicated by compar-

F2. Cyclic variation in GRA density and magnetic susceptibility, Site 1237, p. 23.

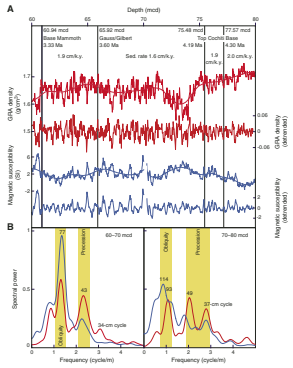

isons with the benthic $\delta^{18}O$ record. The GRA densities vary according to the nature of the sedimentary matrix, which is dominated by carbonate and smaller amounts of siliciclastics and biogenic opal. Maxima in GRA density reflect maxima in carbonate percentages. Obliquity-related maxima in GRA densities are associated with $\delta^{18}O$ warm stages and $\delta^{13}C$ maxima. The magnetic susceptibility record is negatively correlated to the carbonate record and represents the degree of magnetized sediment and, hence, approximates the ratio of siliciclastic vs. biogenic material. Maxima in magnetic susceptibility reflect relatively higher amounts of siliciclastics during $\delta^{18}O$ cold stages. The siliciclastic fraction is mainly derived from eolian deposition, as Site 1237 underlies the modern path of dust that originates in the Atacama Desert of Chile (Mix, Tiedemann, Blum, et al., 2003). Accordingly, we correlated obliquity-related minima in magnetic susceptibility, maxima in GRA density, and maxima in benthic $\delta^{13}C$ with maxima in orbital obliquity (warm stages). We involve the benthic $\delta^{18}O$ record into this process in those intervals where obliquity-related cycles were clearly registered. We started our tuning from the Gauss/Matuyama boundary (47.9 ± 0.1 mcd), which has a well-constrained astronomical age of 2.59 ± 0.01 Ma (Shackleton et al., 1995; Lourens et al., 1996). Other magnetic reversal boundaries were not considered during the tuning process. An initial age model for the interval from 2.1 to 6 Ma was derived by tuning the 41-k.y. component of the magnetic susceptibility record to orbital obliquity. The tuning was then verified via comparisons with the obliquity-related GRA density filter output. In a final approach, we matched the precessional component of the GRA record to the insolation record (Fig. **F3**) and reduced the number of tie points to an amount sufficient to keep the GRA density record approximately in phase with obliquity and precession (Table **T1**).

After tuning, we extracted the precession- and obliquity-related components from the proxy records by using Tukey bandpass filters. The filtered components are compared with the respective orbital time series in Figures **F3** and **F4.** The 21-k.y. component of the GRA density record reveals a remarkably good resemblance with orbital precession in the intervals from 2.2 to 4.7 Ma and from 5.6 to 6.0 Ma, in particular with respect to the eccentricity modulation as reflected in the amplitude variations. In addition, a very consistent relation is found between the 41-k.y. components in our proxy records (GRA density and benthic $\delta^{13}C$ and $\delta^{18}O$) and astronomical obliquity. The age model from 4.7 to 5.6 Ma is mainly based on correlating the 41-k.y. signal of the isotope records to obliquity (Fig. **F4**) because the GRA density record provided a weak variability at the obliquity band, especially between 4.9 and 5.5 Ma, and no clear similarity in amplitude fluctuations between orbital precession and the 21-k.y. GRA component.

In addition, a convincing age model should not produce physically unreasonable changes in sedimentation rates, especially in pelagic regions. The sedimentation rates at pelagic Site 1237 were found to vary from 1.1 to 2.8 cm/k.y., which seems reasonable. This range provides no evidence for distortions caused by the age model (Fig. **F3**) and is close to the values obtained from initial bio- and magnetostratigraphy.

To further examine our timescale, we used cross-spectral analyses to determine the time lags and coherencies of the proxy records with respect to the orbital time series. Coherency between the geological data and the orbital target in the precession band is one of the fundamental methods by which a timescale may be evaluated (Shackleton et al.,

F3. Match between 65°N and GRA density, Site 1237, p. 24.

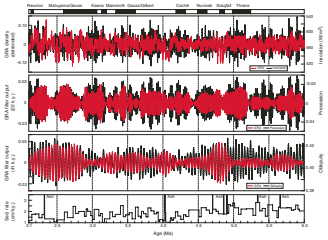

T1. Age model for Site 1237, p. 34.

F4. Benthic $\delta^{13}C$ and $\delta^{18}O$ records, Site 1237, p. 25.

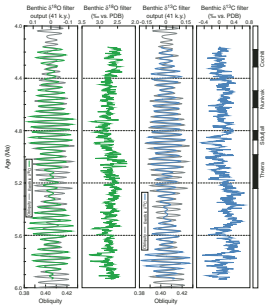

1995). Separating the time interval from 2 to 6 Ma into four succeeding intervals, cross-spectral comparison indicated that Northern Hemisphere summer insolation and GRA density were in phase (as requested by our tuning) and displayed high coherencies at the precession (mainly >0.95) and obliquity (0.91–0.97) frequency bands (Table T2; Fig. F5). The benthic $\delta^{13}C$ record provided coherencies of 0.97 and 0.89 for the time intervals from 4.2 to 5 Ma and from 5 to 5.9 Ma, respectively. Brüggemann (1992) showed that high coherencies are very unlikely to appear by tuning a randomly fluctuating time series to the astronomical record. Thus, the very high coherencies at Site 1237 would not be obtained without a close coupling between changes in insolation and southeast Pacific paleoceanography. Cross-spectral analyses also indicated fairly constant phase relationships between variations in orbital obliquity and benthic isotopes. For consistency of phase calculations, the $\delta^{18}O$ record was multiplied by –1, so that larger values indicate interglacial conditions along with maxima in Northern Hemisphere summer insolation. Variations in benthic $\delta^{13}C$ lag obliquity forcing by ~5 k.y. and obliquity-related variations in $-\delta^{18}O$ by ~2 k.y. Accordingly, the benthic $-\delta^{18}O$ signal, indicative of changes in ice volume, would lag obliquity forcing by ~3 k.y. As a consequence, the tuned ages at Site 1237 might be a few thousand years too old rather than too young, if the true phase lag was close to 6 k.y., as suggested by Chen et al. (1995).

T2. Cross-spectral coherencies and phase relationships, p. 35.

F5. Cross-spectral analyses between 65°N and the GRA density record, Site 1237, p. 26.

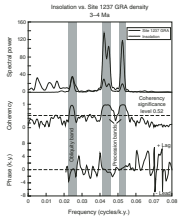

Development of an Orbitally Derived Age Model for Site 1241

The proxy records from Site 1241 contain significant distribution of variance at obliquity-related wavelengths of 100–200 cm. Accordingly, sedimentations rates vary from 2.5 to 5 cm/k.y. and are higher than those at Site 1237. The primary signals that we used for tuning were benthic $\delta^{13}C$ and sand percentages of the carbonate fraction. Both records are highly coherent with $\delta^{18}O$ at the obliquity frequency band. Maxima in $\delta^{13}C$ and sand percentages are associated with $\delta^{18}O$ warm stages. The sand fraction record is additionally marked by strong concentration of variance at precessional frequency bands. Carbonates and GRA density values show distinctly weaker correlations to $\delta^{18}O$, although obliquity-related minima in GRA density and carbonate percentages are mainly associated with $\delta^{18}O$ warm stages. This correlation is opposite to that found at Site 1237. These data were only considered for identifying obliquity- or precession-related cycles in intervals where the variance or the response to orbital forcing was less pronounced in the $\delta^{13}C$ and sand fraction records.

Before using the sand fraction data for tuning, we examined the type of paleoceanographic information provided by this record. Variations in the sand percentages of the carbonate fraction are often used as a proxy to reconstruct either changes in carbonate dissolution or differences in carbonate accumulation between foraminifers and calcareous nannoplankton. The sand fraction consists of nearly 100% of foraminiferal shells at Site 1241. For such environments, it has been shown that the sand content of deep-sea carbonates decreases as dissolution progresses (e.g., Bickert et al., 1997). Foraminiferal shells are weakened by dissolution and tend to break down in small fragments. As a result, material moves from the coarse fraction into finer fractions. At the shallow water depth of Site 1241 (2027 m), carbonate dissolution is ex-

pected to have been low. Therefore, it is not surprising that the Pliocene variability in sand fraction percentages does not correspond to the general pattern of Pacific carbonate dissolution. Over the past 4.5 m.y., carbonate dissolution in the equatorial Pacific was enhanced during interglacials (Farrell and Prell, 1991). Thus, Pliocene changes in carbonate dissolution mainly operated on 41-k.y. cycles. These relationships rather exclude changes in carbonate dissolution as a primary mechanism because high sand percentages at Site 1241 are associated with interglacials and reveal in addition strong precession-related variability. As carbonate dissolution seems to be of secondary importance, changes in the ratio between nannofossil placoliths and foraminiferal shells are regarded as the primary mechanism that could change the relative portion of the coarse fraction (Bickert and Wefer, 1996). Hence, the sand fraction record is indicative of changes in carbonate productivity.

We used the oxygen isotope Stages 96, 98, and 100 as a starting point for calibrating the timescale at Site 1241. These stages were easily recognized in the benthic oxygen isotope record (Fig. F6). Their age assignments to the orbital record are well constrained (e.g., Tiedemann and Franz, 1997) and identified the three corresponding obliquity cycles. We then tuned the 41-k.y. component of the benthic $\delta^{13}C$ record to orbital obliquity assuming no phase difference. This resulted in a preliminary timescale for the interval from 2.4 to 5.7 Ma. In a next step, we compared the sand fraction record with the Northern Hemisphere summer insolation record and tuned the precession-related maxima of the sand record to insolation maxima (Fig. F6). The new age model changed the phase relationship between the $\delta^{13}C$ record and orbital obliquity with $\delta^{13}C$ lagging obliquity insolation forcing relatively constant by ~5 k.y. and lagging $\delta^{18}O$ by ~3 k.y. during the interval from 2.5 to 5.5 Ma (Table T2). Mix et al. (1995) found a similar phase relationship for the Pliocene between benthic $\delta^{13}C$ and $\delta^{18}O$ at tropical east Pacific Site 849 (2 k.y.). Results from cross-spectral analyses from Site 1241 imply that the benthic $\delta^{18}O$ signal, indicative of changes in ice volume, lagged obliquity forcing by ~2 k.y. For comparison, the tuning at Site 1237 yielded a similar phase lag of ~3 k.y. The tuned ages at Site 1241 might be a few thousand years too old rather than too young if a larger phase lag close to 6 k.y. is assumed (Chen et al., 1995). The age-depth control points for Site 1241 are given in Table T3.

To evaluate our tuned age model and the match between the proxy records and the orbital record, we applied the same methods used for Site 1237. Tuning to precession resulted in a concentration of variance over all the main orbital frequencies. For statistical evaluation of the tuned timescale, we applied cross-spectral analyses to estimate the coherencies between the proxy records and the orbital target for the time intervals from 2.5 to 3.5 Ma, 3.5 to 4.5 Ma, and 4.5 to 5.5 Ma (Fig. F7). At the obliquity band, coherency estimates for the sand fraction and benthic $\delta^{13}C$ and $\delta^{18}O$ records are >0.94. At the precession bands, the sand fraction record provided coherency estimates of >0.9. Table T2 summarizes the coherencies and phase estimates of the different proxies for Site 1241. The high coherencies also indicate that the physical linkage between changes in solar insolation and paleoceanography was strong through the entire interval from 2.5 to 5.5 Ma. Sedimentation rates were estimated and vary between 2 and 5 cm/k.y. Higher sedimentation rates mark the older part of the record. This is reasonable because the depositional environment in the equatorial east Pacific was characterized by a late Miocene to early Pliocene biogenic bloom, enhancing

F6. Summary of Site 1241 records, p. 27.

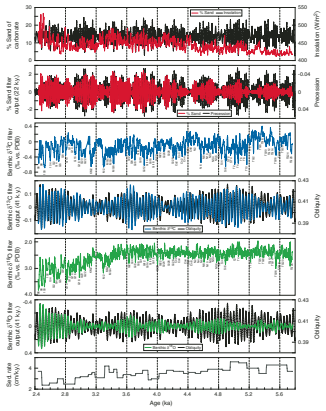

T3. Age model for Site 1241, p. 36.

F7. Cross-spectral analyses between 65°N and the percent sand record, Site 1241, p. 28.

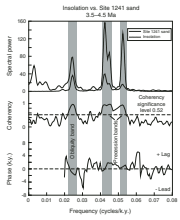

the sediment flux to the seafloor. Finally, we applied bandpass filtering to extract the orbital frequency components from the sand fraction, $\delta^{13}C$, and $\delta^{18}O$ time series and compared them with orbital precession and obliquity. We found a remarkable similarity between the amplitude variation in orbital precession and the precessional components in the sand fraction record (Fig. F6). This implies that we correctly mapped the climate signal onto the orbital record. A mismatch of precession-related cycles (e.g., making one precession cycle too old or too young) would be recognized by an out-of-phase relationship with orbital obliquity. The filtered 41-k.y. components in the sand fraction, $\delta^{13}C$, and $\delta^{18}O$ records show a very consistent relationship with orbital obliquity, with different but relatively constant phase offsets (Table T2). The mismatch between orbital obliquity and the 41-k.y. component of the sand fraction at ~2.9 Ma is caused by relatively high amounts of ash, although we deleted the corresponding interval of the ash layer (77.08–77.10 mcd) (Mix, Tiedemann, Blum, et al., 2003) before tuning. Inspection of the sand fraction, however, revealed relatively high amounts of ash over an interval of ~1.5 m (76.27–77.77 mcd) that clearly distorted the primary signal of the sand fraction record.

COMPARISON OF ASTRONOMICALLY TUNED AGE MODELS

To further examine the quality of the astronomically calibrated timescales from Sites 1237 and 1241, we plotted the benthic $\delta^{18}O$ and $\delta^{13}C$ records from both sites vs. age (Fig. F8). This allows us to compare their age models for the time interval from 4.2 to 5.7 Ma. The oxygen isotope records from the two sites are well correlated and are almost in phase at the precession- and obliquity-related frequency bands (Table T2). Several eye-catching structures and prominent isotope stages are easily recognized and have almost identical ages (within a range of ±2 k.y.). Accordingly, we numbered the unambiguously correlated isotope stages in Figure F8 following the numbering scheme developed by Shackleton et al. (1995). In several intervals, however, patches are seen where the signal-to-noise ratio in the $\delta^{18}O$ records is so low that isotope stages bear no clear resemblance. The comparison of the carbon isotope records further strengthens the stratigraphic correlation between the two sites, as the $\delta^{13}C$ records are exceptionally well correlated, which is also indicated by cross-spectral analyses. Both $\delta^{13}C$ records are highly coherent with each other at the orbital periods of 41 and 23 k.y (Table T2). We used the excellent correlation to complete the numbering of isotope stages for the interval from 5.7 to 4.2 Ma (Fig. F8). In summary, the correlation of isotope stratigraphies between Sites 1237 and 1241 demonstrated that their astronomically calibrated age models are identical within an error range of a few thousand years.

The comparison of the benthic $\delta^{18}O$ and $\delta^{13}C$ records from Pacific Site 1241 and Atlantic Site 925/926 provides another excellent opportunity to test our age model for the late Miocene to Pliocene interval from 5.7 to 2.5 Ma (Fig. F9). The timescale at Atlantic Site 925/926 (Ceara Rise) (Tiedemann and Franz, 1997; Shackleton and Crowhurst, 1997) was developed by tuning precession-related variations in magnetic susceptibility to the same target record used for calibrating Sites 1241 and 1237. The benthic isotope records were established by Tiedemann and Franz (1997), Billups et al., (1997), and Shackleton and Hall (1997). For

F8. Comparison of benthic $\delta^{18}O$ and $\delta^{13}C$ records, Sites 1237 and 1241, p. 29.

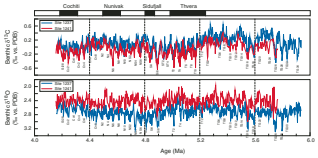

F9. Comparison of benthic $\delta^{18}O$ and $\delta^{13}C$ records, Sites 1241 and 925/926, p. 30.

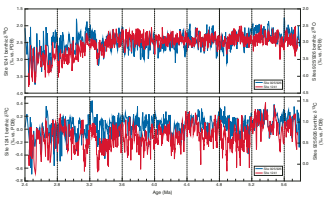

the time interval from 4 to 2.5 Ma, cross-spectral comparison between the $\delta^{18}O$ records from Sites 1241 and 925/926 indicates that the spectral distribution of variance is very similar and coherent for 41-k.y. cycles (Fig. F10). The dominant obliquity-related variations are highly coherent and in phase (Table T2). In the time interval from 5.7 to 4 Ma, the distribution of spectral variance for 41-k.y. cycles is less similar, but variations in $\delta^{18}O$ are highly coherent at the obliquity band. The visual comparison of the oxygen isotope records indicates a remarkably good correlation for the time intervals from 3.75 to 2.5 Ma and 5.1 to 4.5 Ma (Fig. F9), reflecting the global nature of the $\delta^{18}O$ ice volume signal and relatively uniform changes in deepwater temperatures and/or salinity at the two sites. The correlation is less pronounced in the intervals from 5.7 to 5.1 Ma and from 4.5 to 3.75 Ma because the $\delta^{18}O$ amplitude fluctuations are more different between both sites. These differences cannot be ascribed to differences in the time resolution, as the sampling resolution and the sedimentation rates are similar at both sites. Thus, we attribute these deviations to larger local differences in deepwater temperature/salinity fluctuations. The regional overprint of the global $\delta^{18}O$ signal is expected to have been larger at Site 925/926 than at Site 1241, at least for the interval from 4.5 to 3.75 Ma. This has been suggested by the isotope study of Billups et al. (1997). The bathymetric comparison of Pliocene benthic $\delta^{18}O$ records from Ceara Rise indicated anomalous high $\delta^{18}O$ values at Site 925 between 4.2 and 3.7 Ma, which were interpreted to represent a stronger flux of relatively warmer and more saline North Atlantic Deep Water (NADW) at 3000 m water depth. This is consistent with other studies that attribute early Pliocene warmth and enhanced NADW production to an increased northward heat and salt transport, which probably resulted from a critical threshold in the closure history of the Central American Isthmus (Haug and Tiedemann, 1998; Haug et al., 2001).

The benthic $\delta^{13}C$ records from Sites 925/926 and 1241 are exceptionally well correlated between 5.7 and 2.5 Ma (Fig. F9) and surprisingly good in those intervals, where the correlation of the $\delta^{18}O$ signal is relatively weak (5.7–5.1 and 4.5–3.75 Ma). Cross-spectral analyses between the $\delta^{13}C$ records indicate that the spectral distribution of variance is very similar and coherent for 41-k.y. cycles, especially in the older time interval from 5.7 to 4 Ma (Fig. F10; Table T2). The remarkable similarity between the Pacific and Atlantic $\delta^{13}C$ deepwater signal (Fig. F9) with strongest concentration of variance at the 41-k.y. cycle indicates a strong response to global variations in the carbon reservoirs and associated isotope fractionations. The amplitudes and the clarity of the 41-k.y. cycles are more strongly developed in the $\delta^{13}C$ than in the $\delta^{18}O$ records, especially in the late Miocene and early Pliocene intervals. This demonstrates that the benthic $\delta^{13}C$ records are not only a powerful medium for orbital tuning, but also a valuable tool for chronostratigraphic correlations that could assist the late Miocene and early Pliocene benthic oxygen isotope stratigraphy, as the $\delta^{13}C$ signal lags relatively constantly behind $\delta^{18}O$ at the 41-k.y. period (2–3 k.y.). This opportunity may primarily become important when extending the isotope stratigraphy further back in time, particularly for those intervals where the $\delta^{13}C$ response to cyclic changes in global climate is more clearly developed than in the oxygen isotope signal. The comparison between the isotope records from Sites 1241 and 925/926 also suggests that their orbitally tuned age models are almost identical within an error range of a few thousand years.

F10. Cross-spectral analyses, Sites 1241 and 925/926, p. 31.

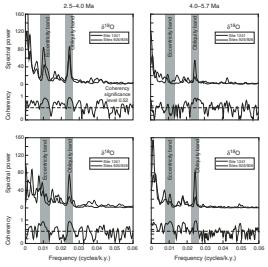

During the review process of our publication, Lisiecki and Raymo (2005) presented an orbitally tuned 5.3-m.y. stack (the "LR04" stack) of globally distributed benthic $\delta^{18}O$ records. Our oxygen isotope nomenclature as well as the timing of oxygen isotope stages is consistent with that presented in Lisiecki and Raymo (2005), except for the interval prior to 4.8 Ma. The comparison between the LR04 $\delta^{18}O$ stack and the $\delta^{18}O$ records from Sites 1237 and 1241 is shown and discussed in **Tiedemann and Mix** (this volume).

Finally, the excellent paleomagnetic stratigraphy at Site 1237 with clear definitions of all Pliocene chrons allows an independent comparison of our age model to the actual ATNTS2004 polarity timescale that has been compiled by Lourens et al. (2004). Our age assignments for the Pliocene magnetic reversal boundaries agree within their error ranges (depth range of magnetic reversals) with the ATNTS2004, except for the top of Kaena and the base of Sidufjall (Table **T4**).

T4. Ages of the magnetic reversals between 2.1 and 6 Ma, p. 37.

Our astronomical age for the top of Kaena is ~30 k.y. older. Apart from the general discrepancy in absolute age control, our age model suggests that Kaena Chron spans a time interval of 54 ± 12 k.y. As this interval is 103 ± 23 cm long, the appropriate sedimentation rate is 1.9 cm/k.y. (Fig. **F3**). Considering the depth range for the top and base of Kaena, the interval of the reversal would be ~30 k.y. shorter than suggested by the ATNTS2004 timescale (Table **T4**). Expanding the interval by ~30 k.y. would significantly drop the sedimentation rate and means that we misinterpreted one or two obliquity cycles as precession cycles. This is not very likely for the following reasons. First, the magnetic reversals of Kaena as well as the top of Mammoth are determined at the same core and the mcd in this interval is not affected by a switch point between holes. Therefore, we can exclude that we missed a sediment section over this interval. Second, the next older magnetic reversals, the base of Kaena and the top of Mammoth, are only ~1 m and ~2 m downcore and their assigned ages agree well with those from the ATNTS2004 (Table **T4**). Our age model suggests a sedimentation rate of ~1.4 cm/k.y. for the interval between the top of Mammoth and the base of Kaena, which is similar to that found for Kaena Chron. Third, spectral variation in both GRA density and color reflectance reveals a dominant precession-related 44-cm cycle for the interval from 54 to 59 mcd (2.92–3.23 Ma). In addition, the spectral variance of the color reflectance is also marked by a pronounced eccentricity-related 222-cm cycle. One may argue that this cycle is statistically not convincing, as it occurs only twice in this short interval. On the other hand, its appearance between 2.92 and 3.23 Ma is not very surprising because the precession-related amplitudes of the color reflectance record may just reflect the strong eccentricity modulation of the astronomical precession record within this interval (Fig. **F3**).

Our astronomical age for the base of Sidufjall is about one precession cycle younger than that provided by the ATNTS2004 timescale (Table **T4**). Our age for the top of Sidufjall, however, is in good agreement with that from the ATNTS2004 timescale. Accordingly, our tuning suggests a time span of ~75 k.y. for Sidufjall Chron instead of 97 k.y. as suggested by the ATNTS2004 timescale. Although the top and base of Sidufjall were determined at sediment intervals that belong to the composite depth, they were determined in different holes: in Hole 1237C and 1237D, respectively (Mix, Tiedemann, Blum, et al., 2003). Therefore, we verified the tie point between the two holes at 89.11 mcd. This tie point occurs within the interval that defines the depth range for the base of Sidufjall (88.77–89.27 mcd) (Table **T4**), whereas the lower limit of the

base of Sidufjall occurs within the composite section. The correlation of GRA density records between Holes 1237C and 1237D reveals a small mismatch for the original tie point in the range of 7–10 cm. Since this small inaccuracy does not add an extra cycle, it does not influence our age assignments. Consequently, the assigned age of 4.888 Ma for the lower limit of the base of Sidufjall at 89.27 mcd will remain unaffected (the depth of the upper limit has been corrected for the small offset) (Table T4). We consider both the age range for the base of Sidufjall and the tuning around Sidufjall Chron as reliable.

The most conspicuous feature within Sidufjall Chron is the occurrence of pronounced obliquity-related GRA density fluctuations and relatively low precession-related variability (Fig. F3). The filtered 22-k.y. component of the GRA density record unfortunately overestimates the amplitudes within this interval, as indicated by visual inspection of the GRA density record. The relatively large amplitudes of the filtered 22-k.y. component most likely resulted from interferences with strong obliquity-related amplitudes. The observed strong response to obliquity is also expected from orbital forcing as amplitude variations in orbital obliquity are strong and those in orbital precession are very small during Sidufjall Chron. Accordingly, the tuning was relatively straightforward in this interval.

The stratigraphic comparison of benthic $\delta^{18}O$ and $\delta^{13}C$ records from Site 1237 and 1241 corroborates our age assignments along Sidufjall Chron (Fig. F8). The isotope records consistently provide a clear 41-k.y. signal over this interval as well as a good match between sites as documented by the simultaneous occurrence of conspicuous isotope stages Si4 and Si6. Any tuning attempt to stretch Sidufjall Chron at Site 1237 by one precession cycle either distorted the sedimentation rates within this interval or led to an out of phase relationship with orbital obliquity.

Apart from the age discrepancies associated with the top of Kaena and base of Sidufjall, our orbitally derived ages for the other geomagnetic reversal boundaries at Site 1237 are in good agreement with those from the ATNTS2004 timescale and suggest that our age model is very similar to that of Lourens et al. (2004) given the error involved in reversal identification and orbital tuning. This result demonstrates the potential for developing an APTS at Site 1237, probably for the entire Neogene.

Stratigraphic Adjustment of Sites 1236 and 1239

The records from Sites 1236 and 1239 are not directly tuned to variations in Earth's orbital parameters. At Site 1236, the main drawback is its poor time resolution. Sedimentation rates vary from 0.5 to 1 cm/k.y. and thus are not suited for orbital tuning. Although Site 1239 has high sedimentation rates of up to 10 cm/k.y., it still lacks a composite depth for the Miocene–Pliocene interval, a major precondition for orbital tuning. However, the opportunity for reconstructing such a composite section is excellent. High-resolution core logging data from two holes as well as high-resolution borehole logging data cover the Miocene–Pliocene interval. Density and natural gamma ray intensity records from borehole and core logging data exhibit strong correlation of meter-scale variability and allow the construction of an equivalent logging depth (eld) scale for the extended core barrel–cored intervals (Mix, Tiedemann, Blum et al., 2003). Such an eld-based composite depth is under construction. The advantage of this depth scale is that it corrects for stretching and squeezing of cored sediment sections. Furthermore, it

provides the best estimate of in situ depth and is ideal for estimating mass accumulation rates.

Instead of orbital tuning, we established an initial age model based on magnetostratigraphic (Site 1236) and biostratigraphic information (Site 1239) (Mix, Tiedemann, Blum, et al., 2003). In a second step, we matched the benthic $\delta^{18}O$ and $\delta^{13}C$ isotope records from Site 1236 and Hole 1239A with those from Site 1241 by visual identification of oxygen and carbon isotope stages. This procedure indirectly resulted in orbitally tuned age models for Sites 1236 and 1239, spanning the intervals from 2.5 to 5.3 Ma and 2.7 to 5 Ma, respectively. The comparison between benthic $\delta^{18}O$ and $\delta^{13}C$ records is shown in Figures **F11** and **F12** and the age-depth control points for Site 1236 and Hole 1239A are given in Tables **T5** and **T6.** The age model for Hole 1239A is regarded as very preliminary, as our stratigraphic correlation to Site 1241 suggests significant gaps at core breaks. The detailed age model for Site 1236 could have never been achieved without using its $\delta^{13}C$ record as a tool for chronostratigraphic correlation with Site 1241. Although the $\delta^{13}C$ record from Site 1236 is indicative of isotope changes at the Pacific intermediate water level, it clearly resembles the general $\delta^{13}C$ structure of the Pacific central and deepwater sites. In contrast, the intermediate water $\delta^{18}O$ signal shows a relatively weak correlation to the "globally correlative" oxygen isotope stratigraphy, represented by Site 1241 in Figure **F11.** This again demonstrates the utility of early Pliocene benthic $\delta^{13}C$ records for stratigraphic correlations.

CONCLUSIONS

Here we present two consistent high-resolution orbitally tuned age models for Leg 202 Sites 1237 and 1241 as well as benthic isotope stratigraphies for Sites 1236, 1237, 1239, and 1241 that cover the time interval from 2.5 to 6 Ma. The age models for Sites 1237 and 1241 were generated by correlating the high-frequency variations in GRA density, percent sand of the carbonate fraction, and benthic $\delta^{13}C$ to the orbital solution of Laskar et al., (1993). Cross-spectral analyses revealed highly significant coherencies between their astronomically related frequency components and orbital obliquity and precession. The age models for Sites 1236 and 1239 were constructed by transferring ages from Site 1241 via correlation of isotope records. The establishment of astronomically calibrated isotope stratigraphies at Sites 1237 and 1241 with an average sampling interval of <3 k.y. along with the excellent paleomagnetic stratigraphy at Site 1237 with clear definitions of all Pliocene chrons allowed a direct comparison with previously published astronomical age models. The excellent correlation of benthic $\delta^{18}O$ and $\delta^{13}C$ stratigraphies between Pacific Site 1241 and Atlantic Site 925/926 (Ceara Rise) confirms the age model constructed at sediment sequences from Atlantic Leg 154. Furthermore, the most ages of the Pliocene polarity reversals at Site 1237 agree well with those of the generally accepted astronomical polarity timescale as summarized in Lourens et al. (2004; ATNTS2004). Hence, our work places the late Miocene to middle Pliocene sediment records from Leg 202 into a high-resolution, globally correlative, and astronomically calibrated stratigraphic framework and provides an excellent basis for further paleoceanographic studies.

The Atlantic-Pacific comparison of benthic $\delta^{18}O$ and $\delta^{13}C$ records indicates that the late Miocene and early Pliocene $\delta^{13}C$ signal is globally

F11. Comparison of benthic $\delta^{18}O$ and $\delta^{13}C$ records, Sites 1241 and 1236, p. 32.

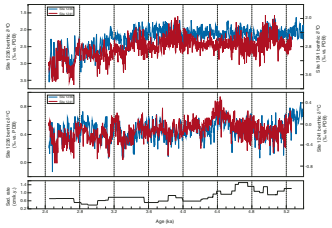

F12. Comparison of benthic $\delta^{18}O$ and $\delta^{13}C$ records, Sites 1241 and 1239, p. 33.

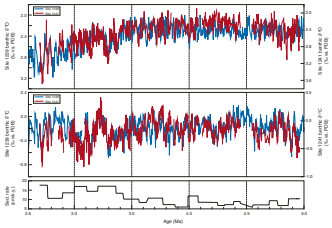

T5. Age model for Site 1236, p. 38.

T6. Age model for Site 1239, p. 39.

correlative and better structured than the $\delta^{18}O$ signal. Although the spectral variability of both parameters is dominated by 41-k.y. cycles with relatively constant phase relationships, the clarity and correlative nature of the 41-k.y. cycle is generally better developed in $\delta^{13}C$ records. This demonstrates that the benthic $\delta^{13}C$ records are not only a powerful medium for orbital tuning, but also a valuable tool for chronostratigraphic correlations that could assist the late Miocene and early Pliocene benthic oxygen isotope stratigraphy. This opportunity may primarily become important when extending the isotope stratigraphy further back in time, particularly for those intervals where the $\delta^{13}C$ response to cyclic changes in global climate is more clearly developed than in the oxygen isotope signal.

In summary, our results from Site 1237 and 1241 demonstrate the potential for expanding both the isotope stratigraphy and the astronomical polarity timescale to the base of the Neogene, as the composite depth of the APC-cored sequence at Site 1237 suggests a complete recovery of the last 30 m.y. along with an excellent magnetic stratigraphy.

ACKNOWLEDGMENTS

We are grateful to the Deutsche Forschungsgemeinschaft (DFG). The establishment of such a high-resolution stratigraphic framework for Leg 202 sediment records would have been impossible without the support of the DFG grants Ti240/12 and Ti240/13. This work also provided an excellent stratigraphic basis for ongoing studies within the DFG supported Research Unit "Impact of Gateways on ocean circulation, climate, and evolution." We thank the crew of the *JOIDES Resolution* and the Leg 202 science party for an exceptionally successful expedition. We especially would like to acknowledge the quick aid of Pieter Grootes and Nils Andersen from the Leibniz-Labor für Altersbestimmung und Isotopenforschung for measuring the benthic isotopes from Site 1236 during a time when our isotope laboratory faced severe mass spectrometer problems. Stimulating discussions with Jeroen Groeneveld, Dirk Nürnberg, and Joachim Schönfeld at different stages of this study were greatly appreciated. We thank Nicole Gau, Lulzim Haxhiaj, Agnes Heinemann, Anna Jesußek, Ulrike Nielsen, Janne Reppschläger, and Kerrin Wittmaack for a great deal of help in sample preparation and isotope measurements. The manuscript significantly benefited from reviews by Lorraine Lisiecki, Torsten Bickert, William Ruddiman, and Nick Shackleton.

This research used samples and/or data provided by the Ocean Drilling Program (ODP). ODP is sponsored by the U.S. National Science Foundation (NSF) and participating countries under management of Joint Oceanographic Institutions (JOI), Inc.

REFERENCES

Berger, A., and Loutre, M.F., 1991. Insolation values for the climate of the last 10 million years. *Quat. Sci. Rev.,* 10(4):297–317. **doi:10.1016/0277-3791(91)90033-Q**

Bickert, T., Curry, W.B., and Wefer, G., 1997. Late Pliocene to Holocene (2.6–0 Ma) western equatorial Atlantic deep-water circulation: inferences from benthic stable isotopes. *In* Shackleton, N.J., Curry, W.B., Richter, C., and Bralower, T.J. (Eds.), *Proc. ODP, Sci. Results,* 154: College Station, TX (Ocean Drilling Program), 239–253. **doi:10.2973/odp.proc.sr.154.110.1997**

Bickert, T., and Wefer, G., 1996. Late Quaternary deep-water circulation in the South Atlantic: reconstruction from carbonate dissolution and benthic stable isotopes. *In* Wefer, G., Berger, W.H., Siedler, G. (Eds.), *The South Atlantic: Present and Past Circulation:* Berlin (Springer), 599–620.

Billups, K., Ravelo, A.C., and Zachos, J.C., 1997. Early Pliocene deep-water circulation: stable isotope evidence for enhanced northern component deep water. *In* Shackleton, N.J., Curry, W.B., Richter, C., and Bralower, T.J. (Eds.), *Proc. ODP, Sci. Results,* 154: College Station, TX (Ocean Drilling Program), 319–330. **doi:10.2973/odp.proc.sr.154.115.1997**

Blackman, R.B., and Tukey, J.H., 1958. *The Measurement of Power Spectra from the Point of View of Communication Engineering:* Mineok, NY (Dover).

Brüggemann, W., 1992. A minimal cost function method for optimizing the age-depth relation of deep-sea sediment cores. *Paleoceanography,* 7(4):467–487.

Cande, S.C., and Kent, D.V., 1995. Revised calibration of the geomagnetic polarity timescale for the Late Cretaceous and Cenozoic. *J. Geophys. Res.,* 100(B4):6093–6095. **doi:10.1029/94JB03098**

Chen, J., Farrell, J.W., Murray, D.W., and Prell, W.L., 1995. Timescale and paleoceanographic implications of a 3.6 m.y. oxygen isotope record from the northeast Indian Ocean (Ocean Drilling Program Site 758). *Paleoceanography,* 10(1):21–48. **doi:10.1029/94PA02290**

Clemens, S.C., 1999. An astronomical tuning strategy for Pliocene sections: implications for global-scale correlation and phase relationships. *In* Shackleton N.J., McCave, I.N., and Graham, P.W. (Eds.), *Astronomical (Milankovitch) Calibration of the Geological Time-Scale*. Philos. Trans. R. Soc., Ser. A., 357(1757):1949–1973. **doi:10.1098/rsta.1999.0409**

Farrell, J.W., and Prell, W.L., 1991. Pacific $CaCO_3$ preservation and $\delta^{18}O$ since 4 Ma: paleoceanic and paleoclimatic implications. *Paleoceanography,* 6:485–498.

Haug, G.H., and Tiedemann, R., 1998. Effect of the formation of the Isthmus of Panama on Atlantic Ocean thermohaline circulation. *Nature (London, U. K.),* 393(6686):673–676. **doi:10.1038/31447**

Haug, G.H., Tiedemann, R., Zahn, R., and Ravelo, A.C., 2001. Role of Panama uplift on oceanic freshwater balance. *Geology,* 29(3):207–210. **doi:10.1130/0091-7613(2001)029<0207:ROPUOO>2.0.CO;2**

Hilgen, F.J., 1991a. Astronomical calibration of Gauss to Matuyama sapropels in the Mediterranean and implication for the geomagnetic polarity time scale. *Earth Planet. Sci. Lett.,* 104(2–4):226–244. **doi:10.1016/0012-821X(91)90206-W**

Hilgen, F.J., 1991b. Extension of the astronomically calibrated (polarity) time scale to the Miocene/Pliocene boundary. *Earth Planet. Sci. Lett.,* 107(2):349–368. **doi:10.1016/0012-821X(91)90082-S**

Hilgen, F.J., Aziz, H.A., Krijgsman, W., Langereis, C.G., Lourens, L.J., Meulenkamp, J.E., Raffi, I., Steenbrink, J., Turco, E., and van Vugt, N., 1999. Present status of the astronomical (polarity) time-scale for the Mediterranean Late Neogene. *In* Shackleton N.J., McCave, I.N., and Graham, P.W. (Eds.), *Astronomical (Milankovitch) Calibration of the Geological Time-Scale*. Philos. Trans. R. Soc., Ser. A., 357(1757):1931–1947. **doi:10.1098/rsta.1999.0408**

Hilgen, F.J., Aziz, H.A., Krijgsman, W., Raffi, I., and Turco, E., 2003. Integrated stratigraphy and astronomical tuning of the Serravallian and lower Tortonian at Monte dei Corvi (middle–upper Miocene, northern Italy). *Palaeogeogr., Palaeoclimatol., Palaeoecol.,* 199(3–4):229–264. **doi:10.1016/S0031-0182(03)00505-4**

Hilgen, F.J., Krijgsman, W., Langereis, C.G., Lourens, L.J., Santarelli, A., and Zachariasse, W.J., 1995. Extending the astronomical (polarity) time scale into the Miocene. *Earth Planet. Sci. Lett.,* 136(3–4):495–510. **doi:10.1016/0012-821X(95)00207-S**

Imbrie, J., Hays, J.D., Martinson, D.G., McIntyre, A., Mix, A.C., Morley, J.J., Pisias, N.G., Prell, W.L., and Shackleton, N.J., 1984. The orbital theory of Pleistocene climate: support from a revised chronology of the marine $\delta^{18}O$ record. *In* Berger, A., Imbrie, J., Hays, J., Kukla, G., and Saltzman, B. (Eds.), *Milankovitch and Climate* (Pt. 1): Hingman, MA (D. Riedel Publ. Co.), 269–305.

Imbrie, J., and Imbrie, J.Z., 1980. Modeling the climatic response to orbital variations. *Science,* 207(4434):943–953. **doi:10.1126/science.207.4434.943**

Kent, D.V., 1999. Orbital tuning of geomagnetic polarity time-scales. *In* Shackleton N.J., McCave, I.N., and Graham, P.W. (Eds.), *Astronomical (Milankovitch) Calibration of the Geological Time-Scale*. Philos. Trans. R. Soc., Ser. A., 357(1757):1995–2007. **doi:10.1098/rsta.1999.0411**

Krijgsman, W., Hilgen, F.J., Raffi, I., Sierro, F.J., and Wilson, D.S., 1999. Chronology, causes and progression of the Messinian salinity crisis. *Nature (London, U. K.),* 400(6745):652–655. **doi:10.1038/23231**

Laskar, J., 1999. The limits of Earth orbital calculations for geological time-scale use. *In* Shackleton N.J., McCave, I.N., and Graham, P.W. (Eds.), *Astronomical (Milankovitch) Calibration of the Geological Time-Scale*. Philos. Trans. R. Soc., Ser. A., 357(1757):1735–1759. **doi:10.1098/rsta.1999.0399**

Laskar, J., Joutel, F., and Boudin, F., 1993. Orbital, precessional, and insolation quantities for the Earth from –20 Myr to +10 Myr. *Astron. Astrophys.,* 270:522–533.

Laskar, J., Robutel, P., Joutel, F., Gastineau, M., Correia, A.C.M., and Levrard, B., 2004. A long-term numerical solution for the insolation quantities of the Earth. *Astron. Astrophys.,* 428(1):261–285. **doi:10.1051/0004-6361:20041335**

Lisiecki, L.E., and Raymo, M.E., 2005. A Pliocene–Pleistocene stack of 57 globally distributed benthic $\delta^{18}O$ records. *Paleoceanography,* 20(1):PA1003. **doi:10.1029/2004PA001071**

Lourens, L.J., Antonarakou, A., Hilgen, F.J., Van Hoof, A.A.M., Vergnaud-Grazzini, C., and Zachariasse, W.J., 1996. Evaluation of the Plio–Pleistocene astronomical timescale. *Paleoceanography,* 11(4):391–414. **doi:10.1029/96PA01125**

Lourens, L.J., Hilgen, F.J., Laskar, J., Shackleton, N.J., and Wilson, D., 2004. The Neogene period. *In* Gradstein, F.M., Ogg, J., et al. (Eds.), *A Geologic Time Scale 2004:* Cambridge (Cambridge Univ. Press), 409–440.

Mix, A.C., Pisias, N.G., Rugh, W., Wilson, J., Morey, A., and Hagelberg, T.K., 1995. Benthic foraminifer stable isotope record from Site 849 (0–5 Ma): local and global climate changes. *In* Pisias, N.G., Mayer, L.A., Janecek, T.R., Palmer-Julson, A., and van Andel, T.H. (Eds.), *Proc. ODP, Sci. Results,* 138: College Station, TX (Ocean Drilling Program), 371–412. **doi:10.2973/odp.proc.sr.138.120.1995**

Mix, A.C., Tiedemann, R., Blum, P., et al., 2003. *Proc. ODP, Init. Repts.,* 202: College Station, TX (Ocean Drilling Program). **doi:10.2973/odp.proc.ir.202.2003**

Paillard, D., Labeyrie, L., and Yiou, P., 1996. Macintosh program performs time-series analysis. *Eos, Trans. Am. Geophys. Union,* 77:379.

Ruddiman, W.F., Cameron, D., and Clement, B.M., 1987. Sediment disturbance and correlation of offset holes drilled with the hydraulic piston corer: Leg 94. *In* Ruddiman, W.F., Kidd, R.B., Thomas, E., et al., *Init. Repts. DSDP,* 94 (Pt. 2): Washington (U.S. Govt. Printing Office), 615–634.

Shackleton, N.J., 1977. Carbon-13 in *Uvigerina:* tropical rainforest history and the equatorial Pacific carbonate dissolution cycles. *In* Andersen, N.R., and Malahoff, A. (Eds.), *The Fate of Fossil Fuel CO_2 in the Oceans:* New York (Plenum), 401–427.

Shackleton, N.J., and Crowhurst, S., 1997. Sediment fluxes based on an orbitally tuned time scale 5 Ma to 14 Ma, Site 926. *In* Shackleton, N.J., Curry, W.B., Richter, C., and Bralower, T.J. (Eds.), *Proc. ODP, Sci. Results,* 154: College Station, TX (Ocean Drilling Program), 69–82. **doi:10.2973/odp.proc.sr.154.102.1997**

Shackleton, N.J., Crowhurst, S.J., Weedon, G.P., and Laskar, J., 1999. Astronomical calibration of Oligocene–Miocene time. *In* Shackleton N.J., McCave, I.N., and Graham, P.W. (Eds.), *Astronomical (Milankovitch) Calibration of the Geological Time-Scale*. Philos. Trans. R. Soc., Ser. A., 357(1757):1907–1929. **doi:10.1098/rsta.1999.0407**

Shackleton, N.J., Hagelberg, T.K., and Crowhurst, S.J., 1995. Evaluating the success of astronomical tuning: pitfalls of using coherence as a criterion for assessing pre-Pleistocene timescales. *Paleoceanography,* 10(4):693–698. **doi:10.1029/95PA01454**

Shackleton, N.J., and Hall, M.A., 1997. The late Miocene stable isotope record, Site 926. *In* Shackleton, N.J., Curry, W.B., Richter, C., and Bralower, T.J. (Eds.), *Proc. ODP, Sci. Results,* 154: College Station, TX (Ocean Drilling Program), 367–373. **doi:10.2973/odp.proc.sr.154.119.1997**

Tiedemann, R., and Franz, S.O., 1997. Deep-water circulation, chemistry, and terrigenous sediment supply in the equatorial Atlantic during the Pliocene, 3.3–2.6 Ma and 5–4.5 Ma. *In* Shackleton, N.J., Curry, W.B., Richter, C., and Bralower, T.J. (Eds.), *Proc. ODP, Sci. Results,* 154: College Station, TX (Ocean Drilling Program), 299–318. **doi:10.2973/odp.proc.sr.154.120.1997**

Tiedemann, R., Sarnthein, M., and Shackleton, N.J., 1994. Astronomic timescale for the Pliocene Atlantic $\delta^{18}O$ and dust flux records of Ocean Drilling Program Site 659. *Paleoceanography,* 9(4):619–638.

APPENDIX

Benthic oxygen and carbon isotope data of Sites 1236, 1237, 1239, and 1241 are in Tables AT1, AT2, AT3, and AT4, respectively.

Figure F1. Revision of former meters composite depth (mcd) splice at Site 1241. Between-hole correlations using color-a values suggest a new tie point in the mcd splice at 157.77 mcd (black dotted line). The composite depth switches from Section 202-1241C-11H-7, 20 cm, to Section 202-1241A-16H-4, 72 cm. The former tie point switched from Section 202-1241C-11H-7, 20 cm, to Section 202-1241A-16H-4, 7 cm, which is 65 cm upcore from the new tie point (dotted gray line). As a consequence, the former mcd has to be corrected by –65 cm below 157.77 mcd (by deleting the interval from Section 202-1241A-16H-4, 7 cm, to 16H-4, 72 cm).

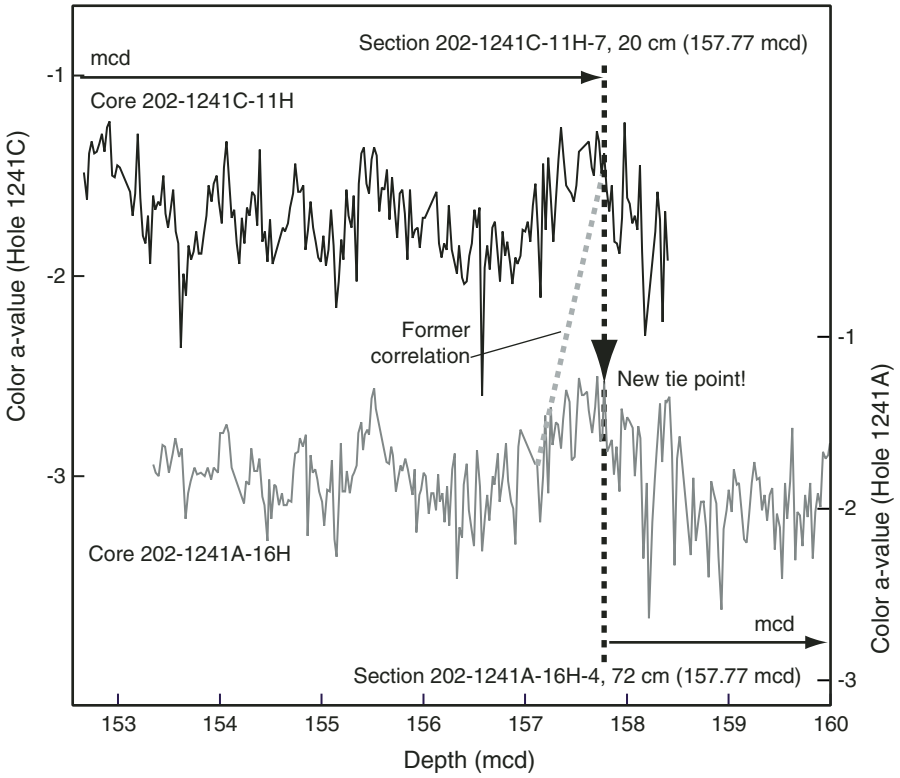

Figure F2. Cyclic variation in gamma ray attenuation (GRA) density and magnetic susceptibility at Site 1237. **A.** Fluctuations in GRA density (red curve) and magnetic susceptibility (blue curve) between 60 and 80 mcd. Each record was detrended by subtraction of the Gaussian weighted smooth (thick lines). The detrended records were subjected to spectral analyses. Ages and depths of magnetic reversal boundaries are indicated. Sedimentation rates were estimated from magnetostratigraphy. **B.** Results from spectral analyses for the intervals from 60–70 mcd and 70–80 mcd. Cycle lengths are given in cm. Considering the sedimentation rates shown in A, cycles of 37–43 cm reflect precession cycles (23 k.y. and 19 k.y.) and cycles of 77–114 cm are related to obliquity cycles (41 k.y.).

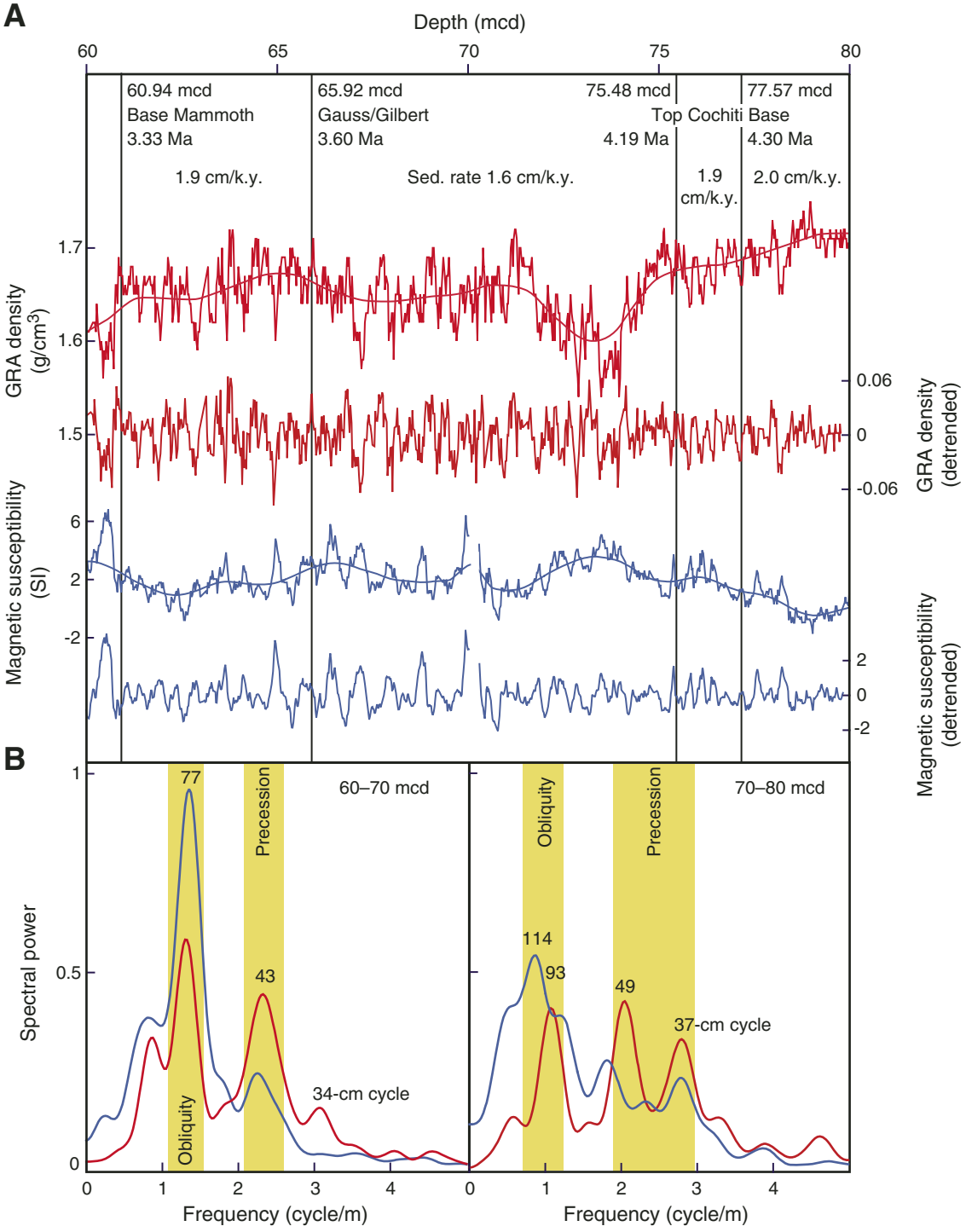

Figure F3. Match between Northern Hemisphere summer insolation (65°N) and gamma ray attenuation (GRA) density (detrended) at Site 1237 from 2.1 to 6.0 Ma. Comparison of orbital precession and obliquity with the 21- and 41-k.y GRA filter outputs, respectively. Sedimentation rates are corrected for ash layers.

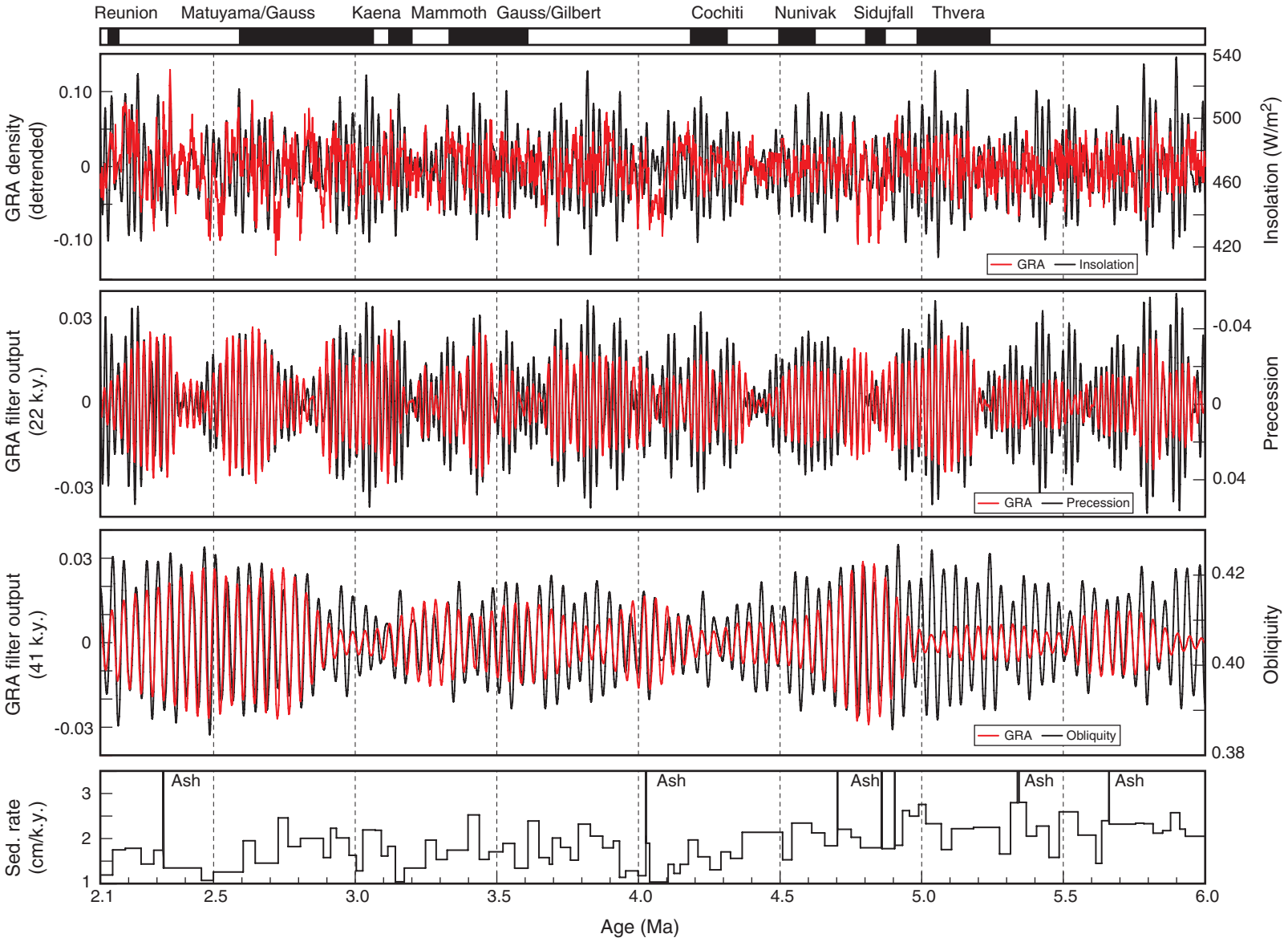

Figure F4. Benthic $\delta^{13}C$ and $\delta^{18}O$ records from Site 1237 for the time interval from 4.2 to 6 Ma and overlays of filtered 41-k.y. components on orbital obliquity. PDB = Peedee belemnite.

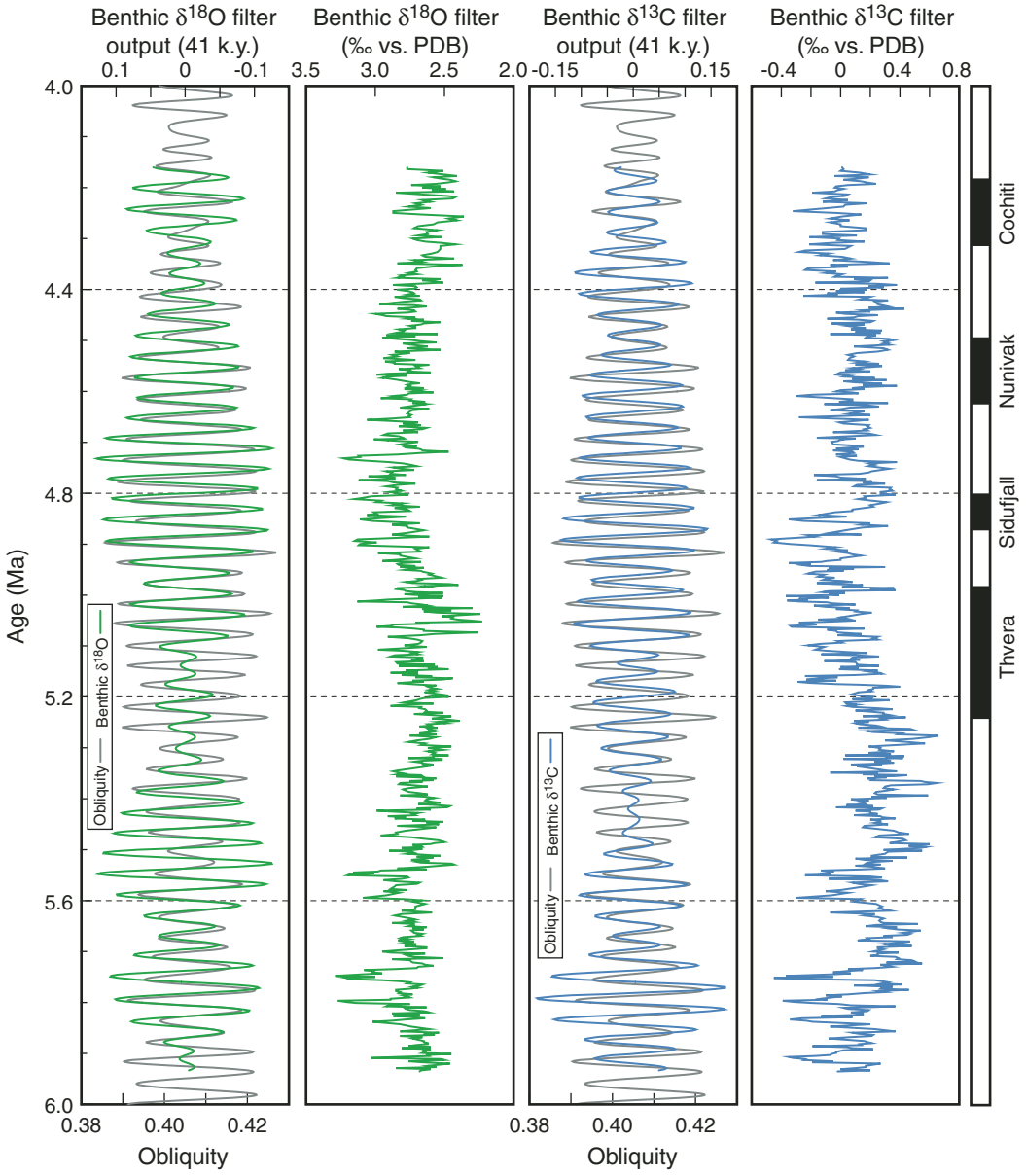

Figure F5. Example of cross-spectral analyses between Northern Hemisphere summer insolation (65°N) and the gamma ray attenuation (GRA) density record from Site 1237 for the time interval from 3 to 4 Ma with power spectra, coherency spectrum, and phase relationships. Both records were interpolated at 2-k.y. steps. The number of lags was set to 50% of the time series (bandwidth = 0.003). All relationships are coherent above the 80% confidence level (nonzero coherency level = 0.52). Positive phases (in k.y.) indicate that GRA density lags insolation forcing.

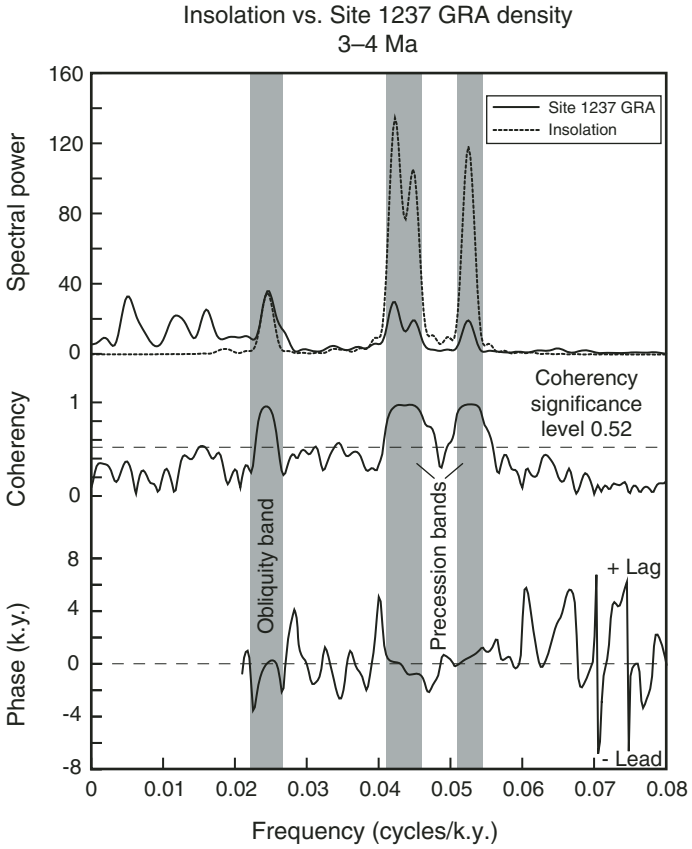

Figure F6. Summary of Site 1241 records for the time interval from 2.4 to 5.8 Ma: percent sand of the carbonate fraction overlain on Northern Hemisphere summer insolation (65°N), benthic $\delta^{13}C$, $\delta^{18}O$, and sedimentation rates; overlays of filtered 21- and 41-k.y. components (percent sand, $\delta^{13}C$, and $\delta^{18}O$) on orbital precession and obliquity, respectively. PDB = Peedee belemnite.

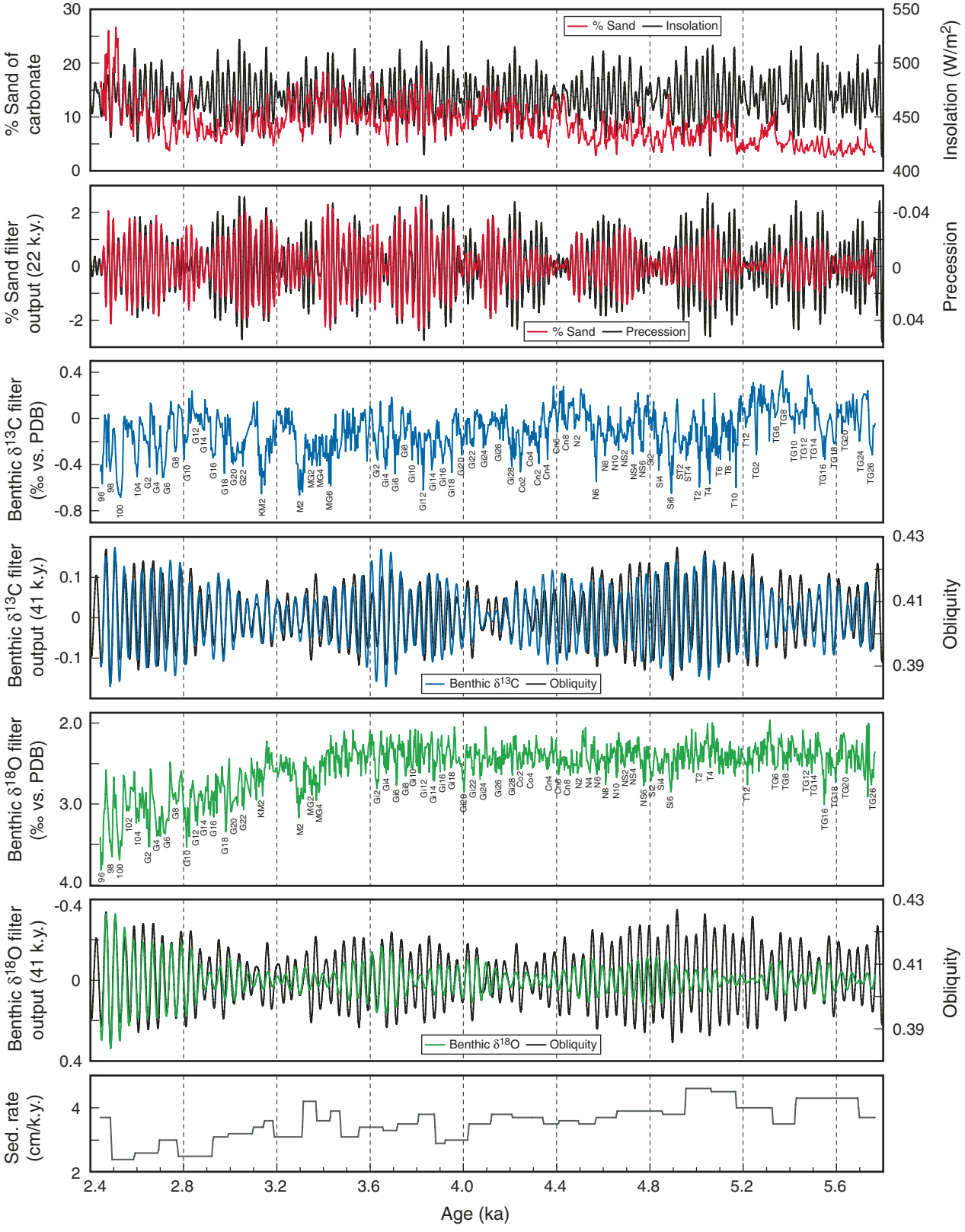

Figure F7. Example of cross-spectral analyses between Northern Hemisphere summer insolation (65°N) and the percent sand record from Site 1241 for the time interval from 3.5 to 4.5 Ma with power spectra, coherency spectrum, and phase relationships. Both records were interpolated at 2-k.y. steps. The number of lags was set to 50% of the time series (bandwidth = 0.003). All relationships are coherent above the 80% confidence level (nonzero coherency level = 0.52). Positive phases (in k.y.) indicate that percent sand lags insolation forcing.

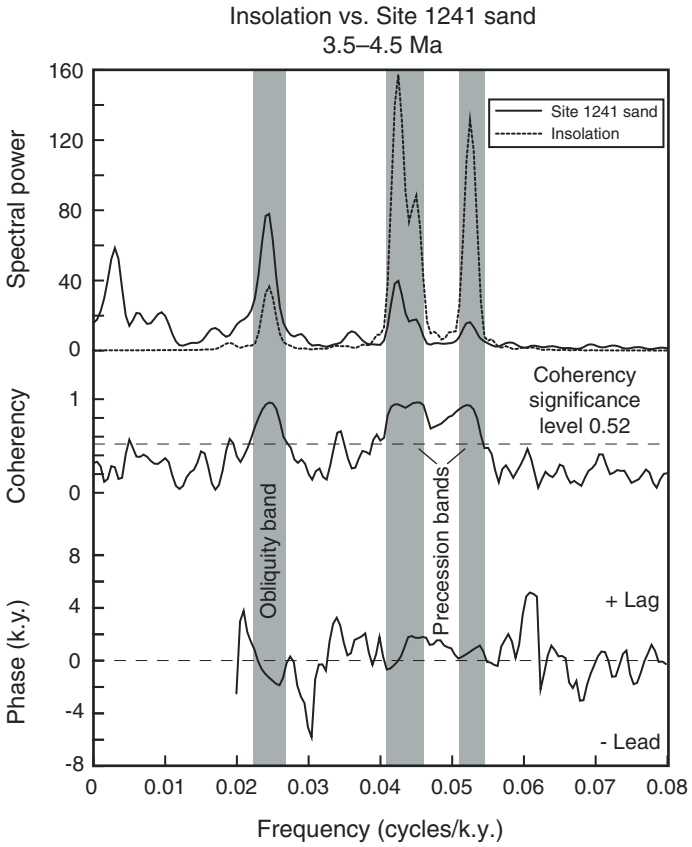

Figure F8. Comparison of benthic $\delta^{18}O$ and $\delta^{13}C$ records from Sites 1237 and 1241 for the time interval from 4 to 6 Ma. Oxygen and carbon isotope stages are numbered following the numbering scheme of Shackleton et al. (1995), which is firmly linked to the underlying 41-k.y. isotope cycles. Even numbers indicate cold stages and odd numbers indicate warm stages. The letters in front of the marine isotope stages identify the magnetic polarity interval. For example, the first cold stage of Sidufjall Chron is called Si2 and the first cold stage occurring in the magnetic interval between Sidufjall and Thvera is called ST2. These signatures indicate the match of isotope stages that correspond to the underlying and continuously numbered orbital obliquity cycles. PDB = Peedee belemnite.

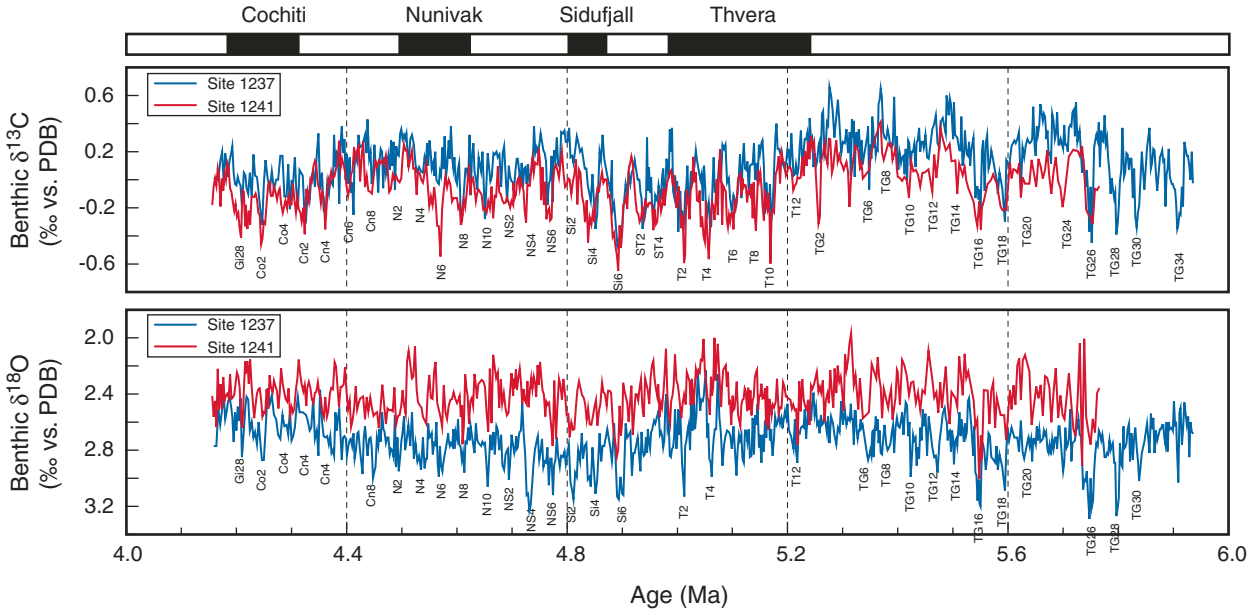

Figure F9. Comparison of benthic $\delta^{18}O$ and $\delta^{13}C$ records from Sites 1241 (this study) and 925/926 (Tiedemann and Franz, 1997; Billups et al., 1997; Shackleton and Hall, 1997) for the time interval from 2.4 to 5.7 Ma. PDB = Peedee belemnite.

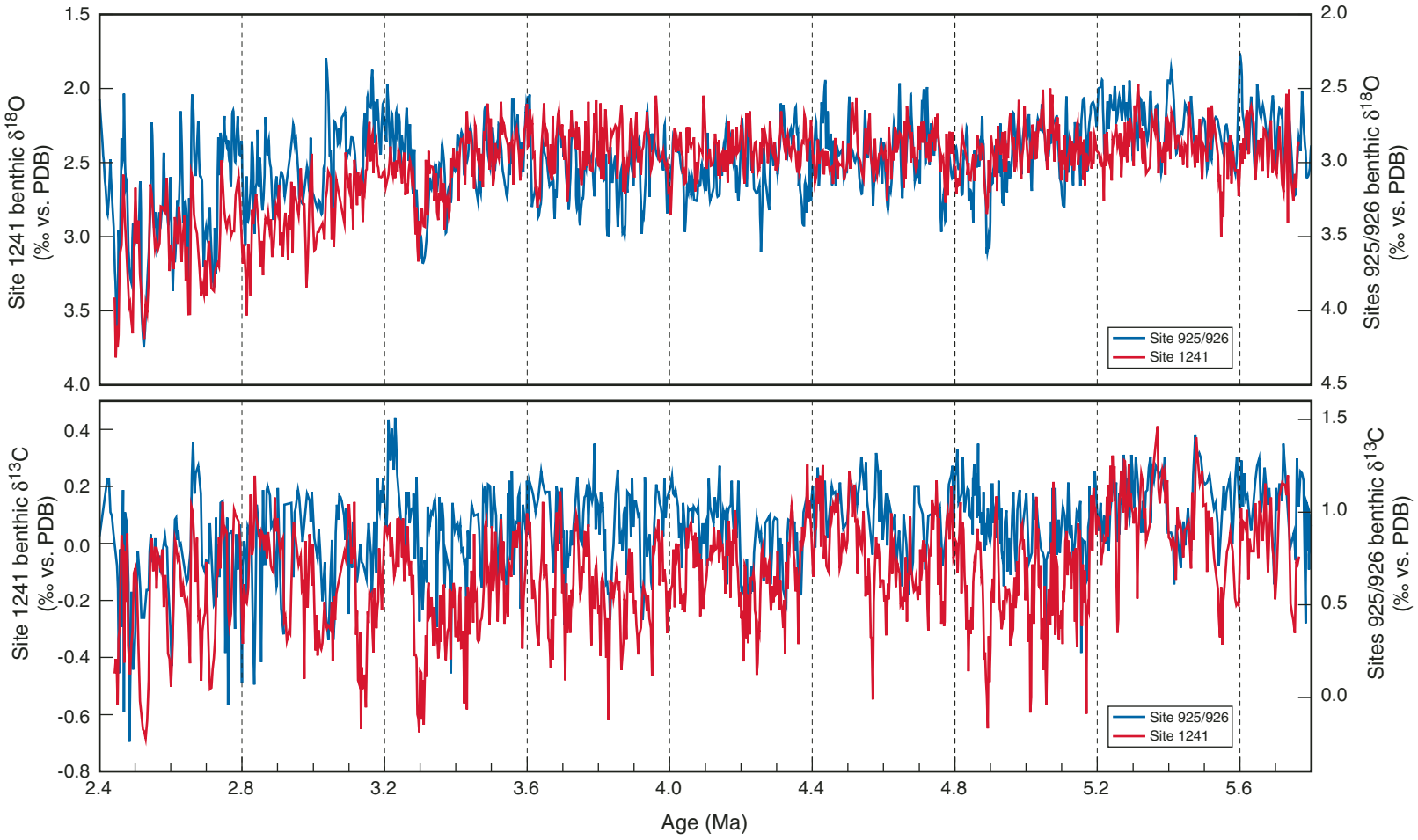

Figure F10. Cross-spectral analyses between benthic $\delta^{18}O$ and between $\delta^{13}C$ records from Sites 1241 and 925/926 for the time intervals from 2.5 to 4 Ma and 4 to 5.7 Ma with power and coherency spectra. Records were interpolated at 2-k.y. steps. The number of lags was set to 50% of the time series. All relationships are coherent above the 80% confidence level (nonzero coherency level = 0.52).

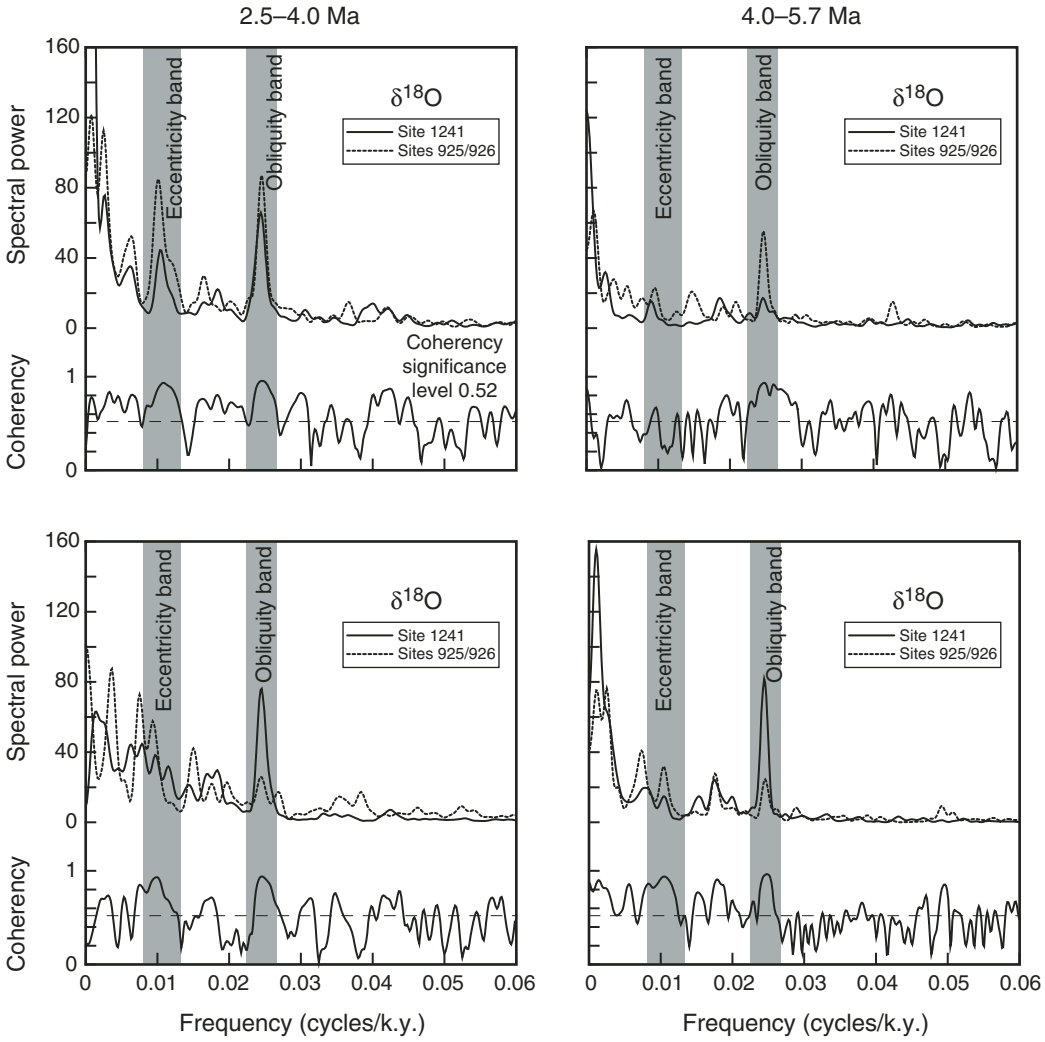

Figure F11. Comparison of benthic $\delta^{18}O$ and $\delta^{13}C$ records from Sites 1241 and 1236 for the time interval from 2.4 to 5.3 Ma. PDB = Peedee belemnite.

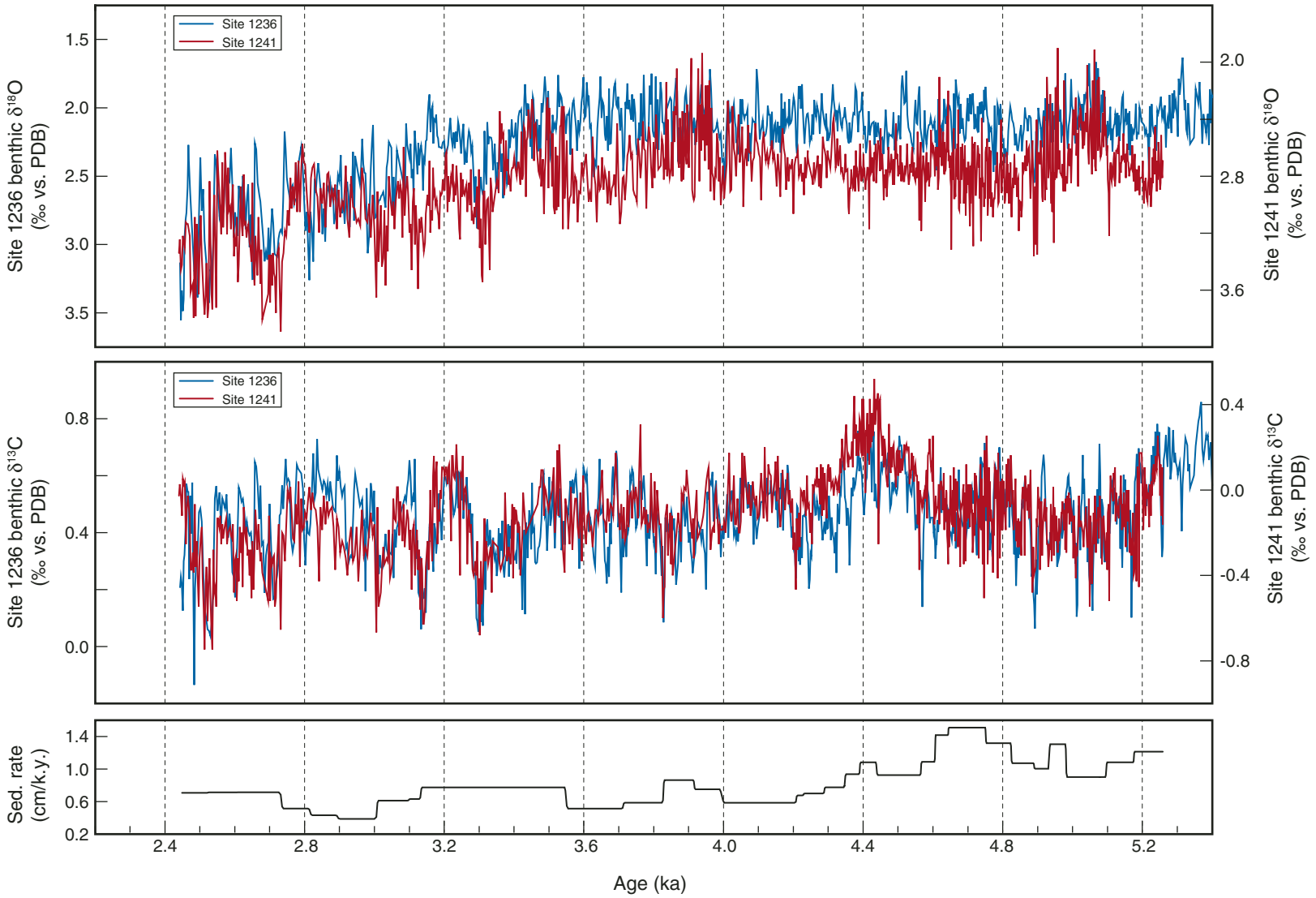

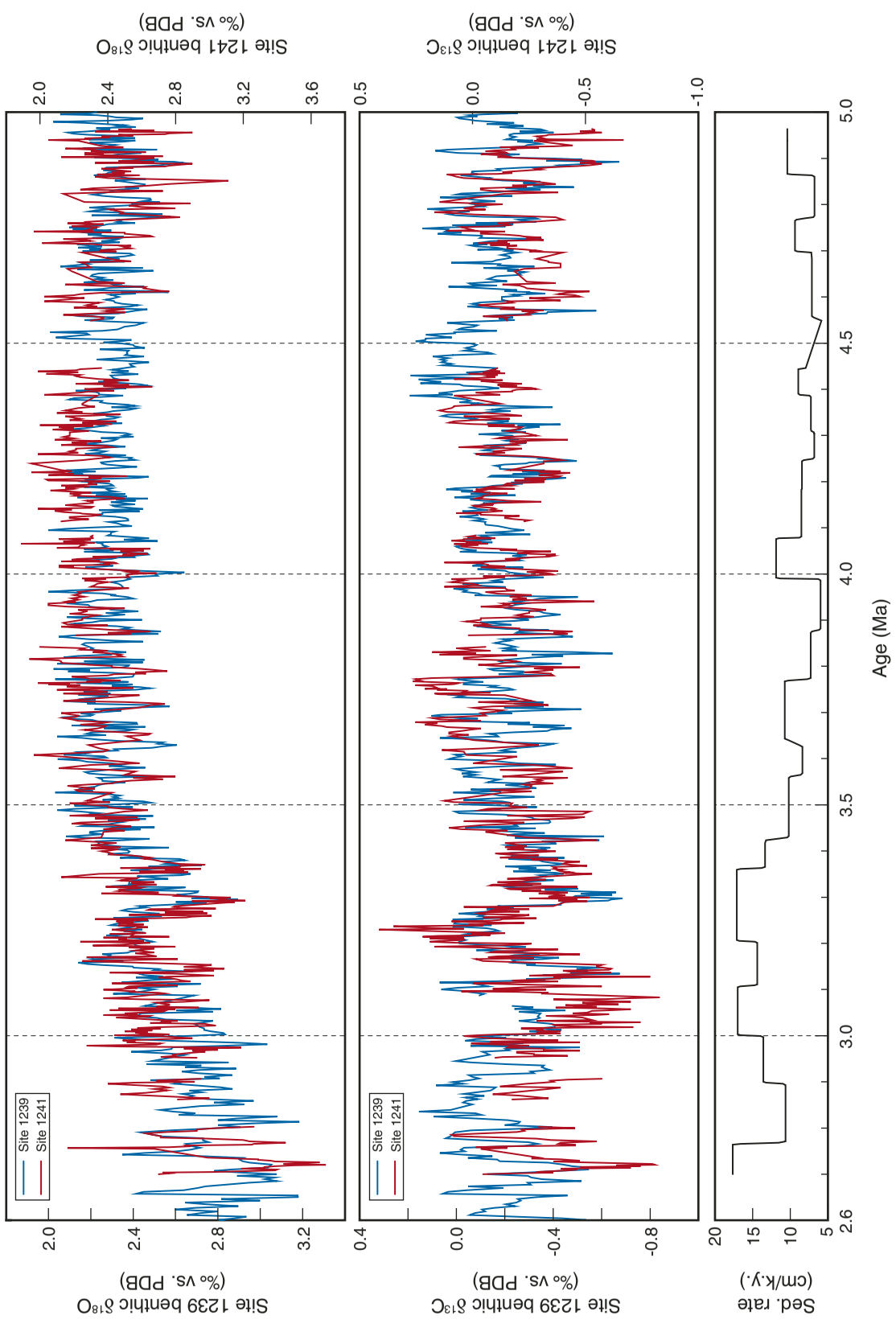

Figure F12. Comparison of benthic $\delta^{18}O$ and $\delta^{13}C$ records from Sites 1241 and 1239 for the time interval from 2.7 to 5 Ma. PDB = Peedee belemnite.

Table T1. Age model for Site 1237.

Age (ka)	Depth (mcd)
2071	40.55
2144	41.42
2188	42.19
2244	43.19
2290	43.85
2321	44.39
2323	44.51
2458	46.33
2500	46.78
2605	48.10
2648	48.94
2729	50.12
2764	50.98
2807	51.76
2888	53.39
2913	53.79
2934	54.26
2978	55.14
3004	55.56
3027	55.86
3070	56.81
3093	57.31
3116	57.67
3142	58.16
3174	58.49
3248	59.49
3286	60.23
3325	60.83
3398	62.10
3439	63.14
3472	63.65
3522	64.50
3563	65.28
3610	65.92
3649	66.84
3685	67.42
3695	67.56
3726	68.17
3760	68.79
3788	69.21
3830	70.19
3874	71.09
3912	71.78
3933	72.20
3955	72.44
3998	73.00
*4026	73.32
*4027	73.45
4039	73.68
4105	74.360
4126	74.66
4148	74.93
4176	75.33
4210	76.00
4252	76.67
4291	77.18
4325	77.76
4366	78.40
4508	81.44
4542	81.96
4611	83.58
4658	84.58
*4702	85.39
*4703	85.57
4751	86.63
4784	87.30
*4858	88.63
*4859	88.76
4904	89.56
4905	89.71
4932	90.21
4956	90.84
4990	91.69
5015	92.38
5069	93.64
5106	94.29
5183	96.00
5275	98.07
5313	98.70
*5338	99.40
*5343	99.90
5369	100.63
5406	101.39
5449	102.37
5485	102.94
5552	104.68
5615	105.99
5635	106.28
*5660	106.88
*5662	107.03
5755	109.19
5784	109.87
5817	110.64
5850	111.34
5878	111.95
5911	112.80
5930	113.22
6005	114.76

Note: Paired asterisks indicate the occurrence and thickness of ash layers.

Table T2. Cross-spectral coherencies and phase relationships between different proxies from Sites 1237, 1241, 925/926, and Northern Hemisphere summer insolation.

Spectral cross correlation	Time interval (Ma)	41 k.y.		23 k.y.		19 k.y.	
		Coh.	Phase	Coh.	Phase	Coh.	Phase
Insol. vs. GRA density (Site 1237)	2.2–3.0	0.94	1.7	0.95	0.3	0.77	–0.3
	3.0–4.0	0.96	0.1	0.97	0.0	0.98	0.5
	4.0–5.0	0.97	1.8	0.97	0.5	0.92	0.0
	5.0–6.0	0.91	–3.2	0.95	–0.3	0.98	–0.5
Insol. vs. benthic $\delta^{13}C$ (Site 1237)	4.2–5.0	0.97	5.1	0.83	6.7		
	5.0–5.9	0.89	2.5	0.65	5.1		
Benthic $\delta^{18}O$ (reversed) vs. benthic $\delta^{13}C$ (Site 1237)	4.2–5.0	0.94	1.7	0.84	6.9		
	5.0–5.9	0.91	2.2	0.67	3.0		
Insol. vs. benthic $\delta^{13}C$ (Site 1241)	2.5–3.5	0.98	4.5	0.82	0.6		
	3.5–4.5	0.96	5.0	0.80	7.0		
	4.5–5.5	0.95	6.0				
Insol. vs. percent sand (Site 1241)	2.5–3.5	0.95	–3.0	0.94	–1.4	0.83	–0.9
	3.5–4.5	0.96	–1.3	0.94	0.0	0.93	0.6
	4.5–5.5	0.96	–1.5	0.94	0.0	0.93	–1.2
Benthic $\delta^{18}O$ (reversed) vs. benthic $\delta^{13}C$ (Site 1241)	2.5–3.5	0.94	3.3	0.82	2.9		
	3.5–4.5	0.96	3.0	0.68	4.8		
	4.5–5.5	0.92	3.2				
Benthic $\delta^{13}C$ (Site 1241) vs. benthic $\delta^{13}C$ (Site 1237)	4.2–5.5	0.98	–2.6	0.77	–2.2		
Benthic $\delta^{18}O$ (Site 1241) vs. benthic $\delta^{18}O$ (Site 1237)	4.2–5.5	0.92	–0.7	0.75	–3.6		
Benthic $\delta^{13}C$ (Site 1241) vs. benthic $\delta^{13}C$ (Site 925/926)	2.5–4.0	0.95	–1.2				
	4.0–5.7	0.96	2.5				
Benthic $\delta^{18}O$ (Site 1241) vs. benthic $\delta^{18}O$ (Site 925/926)	2.5–4.0	0.97	0.8	0.88	2.3		
	4.0–5.7	0.93	–3.5				

Notes: For cross-spectral analysis, all records were interpolated at 2-k.y. steps. The number of lags was set to 50% of the time series (bandwidth = 0.003 for 1-m.y. intervals). All relationships are coherent above the 80% confidence level (nonzero coherency level = 0.52). For example: At the obliquity band, benthic $\delta^{13}C$ maxima (Site 1241) lag insolation maxima by 4.5 k.y. in the time interval from 2.5 to 3.5 Ma or benthic $\delta^{13}C$ maxima (Site 1241) lag $\delta^{18}O$ minima by 3.3 k.y. GRA = gamma ray attenuation.

Table T3. Age model for Site 1241.

Age (ka)	Depth (mcd)
2443	58.21
2489	59.92
2589	62.35
2693	65.05
2753	66.76
2795	67.77
2924	71.25
2991	73.31
3107	76.87
3185	79.76
3211	80.46
3287	82.87
3361	85.65
3429	88.16
3463	89.53
3587	93.42
3666	96.02
3716	97.72
3912	104.72
4021	107.84
4136	111.76
4252	116.42
4313	118.74
4430	123.03
4496	125.13
4567	127.62
4600	128.72
4639	130.34
4657	130.94
4702	132.55
4774	135.69
4880	139.51
4954	142.50
5058	147.00
5104	149.26
5173	152.67
5307	157.68
5347	159.07
5404	161.18
5449	162.84
5508	165.40
5551	167.34
5627	170.74
5691	173.18

Table T4. Ages of the magnetic reversals between 2.1 and 6 Ma.

Geomagnetic reversal boundary		Site 1237 range (mcd)	Site 1237 this study	ATNTS2004	SCHPS95	CK95
Reunion (Base)	Top	41.35	2142	2148		2150
	Mean	41.81	2166			
	Base	42.36	2198			
Gauss/Matuyama	Top	47.82	2583	2581	2600	2600
	Mean	47.93	2591			
	Base	48.04	2600			
Kaena (Top)	Top*	56.61	3061	3032	3046	3040
	Mean*	56.70	3065			
	Base*	56.80	3070			
Kaena (Base)	Top*	57.60	3111	3116	3131	3110
	Mean*	57.73	3119			
	Base*	57.86	3126			
Mammoth (Top)	Top*	58.80	3197	3207	3233	3220
	Mean*	58.85	3201			
	Base*	58.99	3211			
Mammoth (Base)	Top	60.60	3310	3330	3331	3330
	Mean	60.94	3331			
	Base	61.28	3351			
Gilbert/Gauss	Top	65.53	3582	3596	3594	3580
	Mean	65.92	3611			
	Base	66.31	3627			
Cochiti (Top)	Top	75.13	4162	4187	4199	4180
	Mean	75.48	4184			
	Base	75.83	4201			
Cochiti (Base)	Top	77.37	4302	4300	4316	4290
	Mean	77.57	4314			
	Base	77.76	4325			
Nunivak (Top)	Top	81.00	4487	4493	4479	4480
	Mean	81.17	4495			
	Base	81.34	4503			
Nunivak (Base)	Top	83.68	4616	4631	4623	4620
	Mean	83.86	4624			
	Base	84.04	4633			
Sidufjall (Top)	Top	87.37	4787	4799	4781	4800
	Mean	87.65	4802			
	Base	87.93	4817			
Sidufjall (Base)	Top*	88.77	4860	4896	4878	4890
	Mean*	89.07	4876			
	Base	89.27	4888			
Thvera (Top)	Top	90.83	4956	4997	4977	4980
	Mean	91.50	4983			
	Base	92.17	5008			
Thvera (Base)	Top	96.64	5211	5235	5232	5230
	Mean	97.32	5242			
	Base	98.00	5272			

Notes: * = depth ranges of reversals at Site 1237 are different from those published in Mix, Tiedemann, Blum, et al. (2003). Ages according to ATNTS2004 (Lourens et al., 2004), SCHPS95 (Shackleton et al., 1995), CK95 (Cande and Kent, 1995), and this study. The reversals were determined at sections that did not belong to the mcd splice. Using core logging data, we more precisely matched these sections to the mcd splice.

Table T5. Age model for Site 1236.

Age (ka)	Depth (mcd)
2446	10.28
2522	10.82
2606	11.42
2732	12.32
2814	12.74
2892	13.08
3006	13.52
3097	14.08
3132	14.30
3548	17.52
3711	18.36
3827	19.04
3915	19.80
3992	20.38
4207	21.64
4228	21.78
4288	22.20
4347	22.66
4390	23.06
4438	23.58
4565	24.76
4605	25.20
4644	25.74
4751	27.36
4824	28.32
4889	29.02
4933	29.46
4980	30.08
5096	31.12
5175	31.98
5244	32.82

Table T6. Age model for Site 1239.

Age (ka)	Depth (mcd)
2700	150.73
2766	162.29
2896	176.15
2999	190.18
3107	208.51
3204	222.41
3361	249.34
3424	257.70
3561	271.77
3630	277.48
3769	292.48
3876	300.24
3989	307.04
4077	317.52
4183	326.56
4247	331.92
4307	336.03
4386	341.78
4446	347.11
4553	352.34
4696	362.60
4767	369.23
4863	375.77
4956	385.43

Appendix Table AT1. Benthic oxygen and carbon isotope data of Site 1236. (Continued on next eight pages.)

Core, section, interval (cm)	Depth (mcd)	*Cibicidoides mundulus* $\delta^{13}C$ (‰)	*Cibicidoides mundulus* $\delta^{18}O$ (‰)
202-1236A-			
4H-2, 20–21	29.44	0.28	3.21
4H-2, 22–23	29.46		
4H-2, 24–25	29.48	0.36	3.10
4H-2, 26–27	29.50	0.34	2.72
4H-2, 28–29	29.52	0.50	3.28
4H-2, 30–31	29.54	0.44	3.36
4H-2, 32–33	29.56	0.30	3.18
4H-2, 34–35	29.58	0.46	3.41
4H-2, 36–37	29.60	0.41	2.82
4H-2, 38–39	29.62	0.56	3.19
4H-2, 40–41	29.64	0.32	3.59
4H-2, 42–43	29.66	0.49	3.18
4H-2, 44–45	29.68	0.46	3.22
4H-2, 46–47	29.70	0.37	2.68
4H-2, 48–49	29.72	0.46	3.16
4H-2, 50–51	29.74	0.41	3.21
4H-2, 52–53	29.76	0.39	3.16
4H-2, 54–55	29.78	0.33	2.45
4H-2, 56–57	29.80	0.36	3.12
4H-2, 58–59	29.82	0.45	3.16
4H-2, 60–61	29.84	0.37	3.14
4H-2, 62–63	29.86	0.40	3.05
4H-2, 64–65	29.88	0.40	3.18
4H-2, 66–67	29.90		
4H-2, 68–69	29.92		
4H-2, 70–71	29.94	0.47	3.20
4H-2, 72–73	29.96	0.51	3.13
4H-2, 74–75	29.98	0.48	3.27
4H-2, 76–77	30.00	0.43	3.29
4H-2, 78–79	30.02	0.41	2.64
4H-2, 80–81	30.04	0.48	3.16
4H-2, 82–83	30.06	0.34	3.29
4H-2, 84–85	30.08	0.52	3.20
4H-2, 86–87	30.10	0.33	3.24
4H-2, 88–89	30.12	0.53	3.24
4H-2, 90–91	30.14	0.47	3.07
4H-2, 92–93	30.16	0.54	3.01
4H-2, 94–95	30.18	0.43	3.14
4H-2, 96–97	30.20	0.52	3.04
4H-2, 98–99	30.22	0.44	3.24
4H-2, 100–101	30.24		
4H-2, 102–103	30.26	0.45	2.87
4H-2, 104–105	30.28	0.31	2.81
4H-2, 106–107	30.30	0.46	2.96
4H-2, 108–109	30.32	0.35	2.86
4H-2, 110–111	30.34	0.24	2.74
4H-2, 112–113	30.36	0.34	3.08
4H-2, 114–115	30.38	0.33	2.95
4H-2, 116–117	30.40	0.39	3.26
4H-2, 118–119	30.42	0.53	2.87
4H-2, 120–121	30.44	0.42	2.89
4H-2, 122–123	30.46	0.44	2.80
4H-2, 124–125	30.48	0.44	2.82
4H-2, 126–127	30.50	0.42	2.92
4H-2, 128–129	30.52	0.40	3.04
4H-2, 130–131	30.54	0.35	2.88
4H-2, 132–133	30.56	0.41	3.02
4H-2, 134–135	30.58	0.43	2.92
4H-2, 136–137	30.60	0.49	2.83
4H-2, 138–139	30.62	0.39	2.94
4H-2, 140–141	30.64	0.35	2.55
4H-2, 142–143	30.66	0.35	3.05
4H-2, 144–145	30.68	0.52	3.13
4H-2, 146–147	30.70	0.14	2.91
4H-2, 148–149	30.72	0.46	2.80
4H-3, 0–1	30.76	0.22	3.19
4H-3, 2–3	30.78	0.34	2.64
4H-3, 4–5	30.80	0.47	3.10
4H-3, 6–7	30.82	0.36	2.46
4H-3, 8–9	30.84	0.53	3.14
4H-3, 10–11	30.86	0.33	3.17
4H-3, 12–13	30.88	0.44	2.76
4H-3, 14–15	30.90	0.45	2.64
4H-3, 16–17	30.92	0.49	3.05
4H-3, 18–19	30.94	0.38	2.62
4H-3, 20–21	30.96	0.53	3.01
4H-3, 22–23	30.98	0.46	3.09
4H-3, 24–25	31.00	0.45	3.07
4H-3, 26–27	31.02	0.29	2.98
4H-3, 28–29	31.04	0.44	2.83
4H-3, 30–31	31.06	0.46	3.03
4H-3, 32–33	31.08	0.39	2.70
4H-3, 34–35	31.10	0.34	2.94
4H-3, 36–37	31.12	0.30	2.93
4H-3, 38–39	31.14	0.40	3.08
4H-3, 40–41	31.16	0.27	3.02
4H-3, 42–43	31.18	0.47	3.22
4H-3, 44–45	31.20	0.50	3.30
4H-3, 46–47	31.22	0.16	3.55
4H-3, 48–49	31.24	0.45	3.17
4H-3, 50–51	31.26	0.60	3.12
4H-3, 52–53	31.28	0.56	3.21
4H-3, 54–55	31.30	0.55	3.23
4H-3, 56–57	31.32	0.54	3.16
4H-3, 58–59	31.34	0.51	3.19
4H-3, 60–61	31.36	0.61	3.10
4H-3, 62–63	31.38	0.59	3.06
4H-3, 64–65	31.40	0.63	3.26
4H-3, 66–67	31.42	0.44	3.21
4H-3, 68–69	31.44	0.54	3.05
4H-3, 70–71	31.46	0.50	3.05
4H-3, 72–73	31.48	0.47	3.04
4H-3, 74–75	31.50	0.48	3.07
4H-3, 76–77	31.52	0.45	2.97
4H-3, 78–79	31.54	0.52	3.24
4H-3, 80–81	31.56	0.50	3.12
4H-3, 82–83	31.58	0.60	3.18
4H-3, 84–85	31.60	0.50	3.08
4H-3, 86–87	31.62	0.41	3.11
4H-3, 88–89	31.64	0.50	3.10
4H-3, 90–91	31.66	0.42	2.95
4H-3, 92–93	31.68	0.54	3.08
4H-3, 94–95	31.70	0.49	3.12
4H-3, 96–97	31.72	0.42	3.07
4H-3, 98–99	31.74	0.35	3.21
4H-3, 100–101	31.76	0.55	3.09
4H-3, 102–103	31.78	0.46	3.01
4H-3, 104–105	31.80	0.44	3.11
4H-3, 106–107	31.82	0.55	3.12
4H-3, 108–109	31.84	0.43	3.20
4H-3, 110–111	31.86	0.33	3.17
4H-3, 112–113	31.88	0.40	3.16
4H-3, 114–115	31.90	0.32	3.14
4H-3, 116–117	31.92	0.38	3.15
4H-3, 118–119	31.94	0.32	3.02
4H-3, 120–121	31.96	0.47	3.17
4H-3, 122–123	31.98	0.25	3.23
4H-3, 124–125	32.00	0.26	3.14
4H-3, 126–127	32.02	0.29	3.07
4H-3, 128–129	32.04	0.44	3.29
4H-3, 130–131	32.06	0.50	3.23
4H-3, 132–133	32.08	0.23	3.16
4H-3, 134–135	32.10	0.46	3.28
4H-3, 136–137	32.12	0.63	3.28
4H-3, 138–139	32.14	0.56	3.19
4H-3, 140–141	32.16	0.21	3.14
4H-3, 142–143	32.18	0.68	3.31

Appendix Table AT1 (continued).

Core, section, interval (cm)	Depth (mcd)	*Cibicidoides mundulus* $\delta^{13}C$ (‰)	*Cibicidoides mundulus* $\delta^{18}O$ (‰)
4H-3, 144–145	32.20	0.68	3.21
4H-4, 0–1	32.26	0.68	3.21
4H-4, 2–3	32.28	0.60	3.20
4H-4, 4–5	32.30	0.50	3.11
4H-4, 6–7	32.32	0.41	3.28
4H-4, 8–9	32.34	0.51	3.36
4H-4, 10–11	32.36	0.63	3.23
4H-4, 12–13	32.38	0.57	3.25
4H-4, 14–15	32.40	0.46	3.21
4H-4, 16–17	32.42	0.57	3.32
4H-4, 18–19	32.44		
4H-4, 20–21	32.46	0.52	3.35
4H-4, 22–23	32.48	0.54	3.24
4H-4, 24–25	32.50	0.48	3.21
4H-4, 26–27	32.52	0.42	3.03
4H-4, 28–29	32.54	0.57	3.31
4H-4, 30–31	32.56	0.54	3.21
4H-4, 32–33	32.58	0.46	3.38
4H-4, 34–35	32.60	0.58	3.30
4H-4, 36–37	32.62	0.53	3.26
4H-4, 38–39	32.64	0.61	3.09
4H-4, 40–41	32.66	0.60	3.24
4H-4, 42–43	32.68	0.64	3.04
4H-4, 44–45	32.70	0.58	3.19
4H-4, 46–47	32.72	0.59	2.91
4H-4, 48–49	32.74	0.67	3.12
4H-4, 50–51	32.76	0.63	3.16
4H-4, 52–53	32.78	0.62	3.29
4H-4, 54–55	32.80	0.68	3.11
4H-4, 56–57	32.82	0.74	3.22
4H-4, 58–59	32.84	0.68	3.00
4H-4, 60–61	32.86	0.67	3.07
4H-4, 62–63	32.88	0.65	3.19
4H-4, 64–65	32.90	0.53	3.28
4H-4, 66–67	32.92	0.64	3.24
4H-4, 68–69	32.94	0.46	2.96
4H-4, 70–71	32.96	0.54	3.17
4H-4, 72–73	32.98	0.63	3.21
4H-4, 74–75	33.00	0.43	3.11
202-1236B-			
2H-3, 33–34	12.42	0.55	3.40
2H-3, 35–36	12.44	0.52	3.49
2H-3, 37–38	12.46	0.56	3.21
2H-3, 39–40	12.48	0.48	3.39
2H-3, 41–42	12.50	0.38	3.26
2H-3, 43–44	12.52	0.37	3.37
2H-3, 45–46	12.54	0.50	3.12
2H-3, 47–48	12.56	0.43	3.41
2H-3, 49–50	12.58	0.58	3.11
2H-3, 51–52	12.60	0.28	3.41
2H-3, 53–54	12.62	0.52	3.16
2H-3, 55–56	12.64	0.41	3.01
2H-3, 57–58	12.66	0.42	3.12
2H-3, 59–60	12.68	0.47	3.13
2H-3, 61–62	12.70	0.45	3.28
2H-3, 63–64	12.72	0.51	3.41
2H-3, 65–66	12.74	0.56	3.53
2H-3, 67–68	12.76	0.48	3.21
2H-3, 69–70	12.78	0.54	3.15
2H-3, 71–72	12.80	0.49	3.13
2H-3, 73–74	12.82	0.48	3.28
2H-3, 75–76	12.84	0.42	3.32
2H-3, 77–78	12.86	0.23	3.53
2H-3, 79–80	12.88	0.49	3.27
2H-3, 81–82	12.90	0.41	3.36
2H-3, 83–84	12.92	0.53	3.24
2H-3, 85–86	12.94	0.43	3.50
2H-3, 87–88	12.96	0.51	3.19
2H-3, 89–90	12.98	0.46	3.18
2H-3, 91–92	13.00	0.48	3.38
2H-3, 93–94	13.02	0.49	3.28
2H-3, 95–96	13.04	0.42	3.34
2H-3, 97–98	13.06	0.27	3.25
2H-3, 99–100	13.08	0.45	3.51
2H-3, 101–102	13.10	0.42	3.28
2H-3, 103–104	13.12	0.33	3.44
2H-3, 105–106	13.14	0.37	3.35
2H-3, 107–108	13.16	0.35	3.39
2H-3, 109–110	13.18	0.31	3.14
2H-3, 111–112	13.20	0.25	3.45
2H-3, 113–114	13.22	0.37	3.56
2H-3, 115–116	13.24	0.42	3.20
2H-3, 117–118	13.26	0.30	3.38
2H-3, 119–120	13.28	0.32	3.39
2H-3, 121–122	13.30	0.42	3.47
2H-3, 123–124	13.32	0.23	3.45
2H-3, 125–126	13.34	0.36	3.49
2H-3, 127–128	13.36	0.48	3.15
2H-3, 129–130	13.38	0.32	3.25
2H-3, 131–132	13.40	0.35	3.45
2H-3, 133–134	13.42	0.32	3.47
2H-3, 135–136	13.44	0.41	3.36
2H-3, 137–138	13.46	0.47	3.56
2H-3, 139–140	13.48	0.39	3.31
2H-3, 141–142	13.50	0.43	3.52
2H-3, 143–144	13.52	0.05	3.91
2H-3, 145–146	13.54	0.49	3.29
2H-3, 147–148	13.56	0.14	3.70
2H-4, 0–1	13.60	0.19	3.37
2H-4, 2–3	13.62	0.27	3.73
2H-4, 4–5	13.64	0.35	3.68
2H-4, 6–7	13.66	0.29	3.40
2H-4, 8–9	13.68		3.84
2H-4, 10–11	13.70	0.31	3.49
2H-4, 12–13	13.72	0.30	3.64
2H-4, 14–15	13.74	0.41	3.20
2H-4, 16–17	13.76	0.24	3.30
2H-4, 18–19	13.78	0.26	3.37
2H-4, 20–21	13.80	0.29	3.43
2H-4, 22–23	13.82	0.52	3.35
2H-4, 24–25	13.84	0.45	3.51
2H-4, 26–27	13.86	0.44	3.34
2H-4, 28–29	13.88	0.56	3.28
2H-4, 30–31	13.90	0.56	3.23
2H-4, 32–33	13.92	0.39	3.33
2H-4, 34–35	13.94	0.51	3.25
2H-4, 36–37	13.96	0.44	3.29
2H-4, 38–39	13.98	0.37	3.56
2H-4, 40–41	14.00	0.50	3.03
2H-4, 42–43	14.02	0.35	3.43
2H-4, 44–45	14.04	0.41	3.29
2H-4, 46–47	14.06	0.48	3.20
2H-4, 48–49	14.08	0.45	3.32
2H-4, 50–51	14.10	0.34	3.53
2H-4, 52–53	14.12	0.41	3.48
2H-4, 54–55	14.14	0.20	3.75
2H-4, 56–57	14.16	0.41	3.35
2H-4, 58–59	14.18	0.43	3.27
2H-4, 60–61	14.20	0.25	3.60
2H-4, 62–63	14.22	0.34	3.37
2H-4, 64–65	14.24	0.41	3.53
2H-4, 66–67	14.26	0.27	3.86
2H-4, 68–69	14.28	0.34	3.45
2H-4, 70–71	14.30	0.13	3.53
2H-4, 72–73	14.32	0.31	3.44
2H-4, 74–75	14.34	0.27	3.50
2H-4, 76–77	14.36	0.08	3.58
2H-4, 78–79	14.38	0.08	3.64

Appendix Table AT1 (continued).

Core, section, interval (cm)	Depth (mcd)	*Cibicidoides mundulus* $\delta^{13}C$ (‰)	*Cibicidoides mundulus* $\delta^{18}O$ (‰)
2H-4, 80–81	14.40	0.14	3.59
2H-4, 82–83	14.42	0.28	3.42
2H-4, 84–85	14.44		
2H-4, 86–87	14.46	0.37	3.31
2H-4, 88–89	14.48	0.27	3.37
2H-4, 90–91	14.50	0.37	3.11
2H-4, 92–93	14.52	0.55	3.53
2H-4, 94–95	14.54	0.42	3.40
2H-4, 96–97	14.56	0.30	3.46
2H-4, 98–99	14.58	0.60	3.15
2H-4, 100–101	14.60	0.67	3.31
2H-4, 102–103	14.62	0.49	3.29
2H-4, 104–105	14.64	0.60	3.37
2H-4, 106–107	14.66	0.65	3.34
2H-4, 108–109	14.68	0.36	3.40
2H-4, 110–111	14.70	0.48	3.43
2H-4, 112–113	14.72	0.44	3.51
2H-4, 114–115	14.74	0.55	3.30
2H-4, 116–117	14.76	0.52	3.31
2H-4, 118–119	14.78	0.63	3.30
2H-4, 120–121	14.80	0.63	3.22
2H-4, 122–123	14.82	0.62	3.28
2H-4, 124–125	14.84	0.60	3.28
2H-4, 126–127	14.86	0.63	3.08
2H-4, 128–129	14.88	0.63	3.06
2H-4, 130–131	14.90	0.57	3.41
2H-4, 132–133	14.92	0.63	3.20
2H-4, 134–135	14.94	0.64	3.35
2H-4, 136–137	14.96	0.56	3.30
2H-4, 138–139	14.98	0.37	3.20
2H-4, 140–141	15.00	0.67	3.23
2H-4, 142–143	15.02	0.67	3.13
2H-4, 144–145	15.04	0.60	3.35
2H-4, 146–147	15.06	0.59	3.27
2H-4, 148–149	15.08	0.62	3.31
2H-5, 0–1	15.10	0.71	3.14
2H-5, 2–3	15.12	0.63	3.23
2H-5, 4–5	15.14	0.57	3.38
2H-5, 6–7	15.16	0.46	3.51
2H-5, 8–9	15.18	0.25	3.57
2H-5, 10–11	15.20	0.61	3.18
2H-5, 12–13	15.22	0.60	3.32
2H-5, 14–15	15.24	0.67	3.22
2H-5, 16–17	15.26	0.48	3.30
2H-5, 18–19	15.28	0.55	3.31
2H-5, 20–21	15.30	0.56	3.27
2H-5, 22–23	15.32	0.53	3.25
2H-5, 24–25	15.34	0.29	3.41
2H-5, 26–27	15.36	0.43	3.31
2H-5, 28–29	15.38	0.48	3.24
2H-5, 30–31	15.40	0.40	3.37
2H-5, 32–33	15.42	0.43	3.16
2H-5, 34–35	15.44		
2H-5, 36–37	15.46	0.27	3.43
2H-5, 38–39	15.48	0.25	3.48
2H-5, 40–41	15.50		
2H-5, 42–43	15.52	0.30	3.44
2H-5, 44–45	15.54	0.25	3.35
2H-5, 46–47	15.56	0.37	3.26
2H-5, 48–49	15.58	0.15	3.51
2H-5, 50–51	15.60	0.24	3.16
2H-5, 52–53	15.62	0.04	3.62
2H-5, 54–55	15.64	0.30	3.45
2H-5, 56–57	15.66	0.15	3.78
2H-5, 58–59	15.68	0.19	3.82
2H-5, 60–61	15.70	0.29	3.29
2H-5, 62–63	15.72	0.45	3.29
2H-5, 64–65	15.74	0.30	3.60
2H-5, 66–67	15.76	0.37	3.44
2H-5, 68–69	15.78	0.34	3.34
2H-5, 70–71	15.80	0.29	3.33
2H-5, 72–73	15.82	0.31	3.54
2H-5, 74–75	15.84		
2H-5, 76–77	15.86	0.35	3.21
2H-5, 78–79	15.88	0.19	3.29
2H-5, 80–81	15.90	0.37	3.41
3H-2, 23–24	20.96	0.50	2.89
3H-2, 25–26	20.98	0.53	2.99
3H-2, 27–28	21.00	0.45	3.01
3H-2, 29–30	21.02	0.46	3.07
3H-2, 31–32	21.04	0.54	3.09
3H-2, 33–34	21.06	0.61	3.34
3H-2, 35–36	21.08	0.53	3.01
3H-2, 37–38	21.10	0.45	2.94
3H-2, 39–40	21.12	0.70	3.05
3H-2, 41–42	21.14	0.49	3.11
3H-2, 43–44	21.16	0.44	3.06
3H-2, 45–46	21.18	0.64	3.13
3H-2, 47–48	21.20	0.61	3.09
3H-2, 49–50	21.22	0.60	3.04
3H-2, 51–52	21.24	0.47	2.99
3H-2, 53–54	21.26	0.53	3.10
3H-2, 55–56	21.28	0.56	3.07
3H-2, 57–58	21.30	0.65	3.15
3H-2, 59–60	21.32	0.51	3.26
3H-2, 61–62	21.34	0.67	3.07
3H-2, 63–64	21.36	0.48	3.18
3H-2, 65–66	21.38	0.42	3.32
3H-2, 67–68	21.40	0.47	3.04
3H-2, 69–70	21.42	0.62	2.92
3H-2, 71–72	21.44	0.53	3.04
3H-2, 73–74	21.46	0.48	3.08
3H-2, 75–76	21.48	0.54	3.28
3H-2, 77–78	21.50	0.61	3.09
3H-2, 79–80	21.52	0.50	3.23
3H-2, 81–82	21.54	0.55	3.14
3H-2, 83–84	21.56	0.47	3.15
3H-2, 85–86	21.58	0.52	3.10
3H-2, 87–88	21.60	0.34	3.42
3H-2, 89–90	21.62	0.40	3.14
3H-2, 91–92	21.64	0.20	3.09
3H-2, 93–94	21.66	0.45	3.09
3H-2, 95–96	21.68	0.34	3.05
3H-2, 97–98	21.70	0.47	3.20
3H-2, 99–100	21.72	0.35	3.18
3H-2, 101–102	21.74	0.55	3.13
3H-2, 103–104	21.76	0.54	3.23
3H-2, 105–106	21.78	0.51	3.18
3H-2, 107–108	21.80	0.55	3.31
3H-2, 109–110	21.82	0.50	3.09
3H-2, 111–112	21.84	0.46	3.21
3H-2, 113–114	21.86	0.60	3.14
3H-2, 115–116	21.88	0.49	3.05
3H-2, 117–118	21.90	0.50	3.13
3H-2, 119–120	21.92	0.40	3.16
3H-2, 121–122	21.94	0.47	3.18
3H-2, 123–124	21.96	0.36	3.21
3H-2, 125–126	21.98	0.57	3.25
3H-2, 127–128	22.00	0.55	3.12
3H-2, 129–130	22.02	0.58	3.21
3H-2, 131–132	22.04	0.57	3.18
3H-2, 133–134	22.06	0.63	3.12
3H-2, 135–136	22.08	0.56	3.08
3H-2, 137–138	22.10	0.59	3.26
3H-2, 139–140	22.12	0.50	3.13
3H-2, 141–142	22.14	0.64	3.27
3H-2, 143–144	22.16	0.46	3.14
3H-2, 145–146	22.18	0.63	2.97

Appendix Table AT1 (continued).

Core, section, interval (cm)	Depth (mcd)	*Cibicidoides mundulus* $\delta^{13}C$ (‰)	*Cibicidoides mundulus* $\delta^{18}O$ (‰)
3H-2, 147–148	22.20	0.48	3.03
3H-2, 149–150	22.22	0.61	3.05
3H-3, 0–1	22.24	0.54	3.08
3H-3, 2–3	22.26	0.45	3.21
3H-3, 4–5	22.28	0.62	3.05
3H-3, 6–7	22.30	0.64	3.09
3H-3, 8–9	22.32	0.58	3.11
3H-3, 10–11	22.34	0.63	3.15
3H-3, 12–13	22.36	0.56	3.08
3H-3, 14–15	22.38	0.57	2.99
3H-3, 16–17	22.40	0.58	2.89
3H-3, 18–19	22.42	0.53	2.86
3H-3, 20–21	22.44	0.57	3.03
3H-3, 22–23	22.46	0.59	3.15
3H-3, 24–25	22.48	0.58	3.13
3H-3, 26–27	22.50	0.55	2.98
3H-3, 28–29	22.52	0.58	3.14
3H-3, 30–31	22.54	0.54	3.07
3H-3, 32–33	22.56	0.66	3.02
3H-3, 34–35	22.58	0.61	3.17
3H-3, 36–37	22.60	0.73	3.15
3H-3, 38–39	22.62	0.68	3.20
3H-3, 40–41	22.64	0.64	3.22
3H-3, 42–43	22.66	0.62	3.18
3H-3, 44–45	22.68	0.74	3.07
3H-3, 46–47	22.70	0.78	3.17
3H-3, 48–49	22.72		
3H-3, 50–51	22.74	0.65	3.16
3H-3, 52–53	22.76	0.63	3.38
3H-3, 54–55	22.78	0.67	3.42
3H-3, 56–57	22.80	0.66	3.27
3H-3, 58–59	22.82	0.66	3.27
3H-3, 60–61	22.84	0.67	3.16
3H-3, 62–63	22.86	0.72	3.21
3H-3, 64–65	22.88	0.63	3.27
3H-3, 66–67	22.90	0.78	3.26
3H-3, 68–69	22.92	0.88	3.14
3H-3, 70–71	22.94	0.73	3.29
3H-3, 72–73	22.96	0.78	3.05
3H-3, 74–75	22.98	0.67	3.19
3H-3, 76–77	23.00	0.75	3.17
3H-3, 78–79	23.02	0.72	3.24
3H-3, 80–81	23.04	0.67	3.29
3H-3, 82–83	23.06	0.80	3.11
3H-3, 84–85	23.08	0.79	3.01
3H-3, 86–87	23.10	0.69	3.19
3H-3, 88–89	23.12	0.68	3.23
3H-3, 90–91	23.14	0.87	3.18
3H-3, 92–93	23.16	0.67	3.21
3H-3, 94–95	23.18	0.87	3.07
3H-3, 96–97	23.20	0.78	3.18
3H-3, 98–99	23.22	0.72	3.17
3H-3, 100–101	23.24	0.54	3.28
3H-3, 102–103	23.26	0.76	3.23
3H-3, 104–105	23.28	0.74	3.22
3H-3, 106–107	23.30	0.82	3.15
3H-3, 108–109	23.32	0.68	3.15
3H-3, 110–111	23.34	0.78	3.17
3H-3, 112–113	23.36	0.64	3.51
3H-3, 114–115	23.38	0.87	2.99
3H-3, 116–117	23.40	0.70	3.03
3H-3, 118–119	23.42	0.82	3.18
3H-3, 120–121	23.44	0.72	3.17
3H-3, 122–123	23.46	0.82	3.09
3H-3, 124–125	23.48	0.74	3.15
3H-3, 126–127	23.50	0.84	3.23
3H-3, 128–129	23.52	0.94	3.06
3H-3, 130–131	23.54	0.78	3.10
3H-3, 132–133	23.56	0.80	3.01
3H-3, 134–135	23.58	0.87	3.24
3H-3, 136–137	23.60	0.85	3.13
3H-3, 138–139	23.62	0.89	2.99
3H-3, 140–141	23.64		
3H-3, 142–143	23.66	0.86	3.04
3H-3, 144–145	23.68	0.87	3.17
3H-3, 146–147	23.70	0.77	2.92
3H-3, 148–149	23.72	0.73	3.16
3H-3, 150–151	23.74	0.67	3.07
3H-4, 1–2	23.76	0.74	3.20
3H-4, 3–4	23.78	0.63	3.34
3H-4, 5–6	23.80	0.73	3.19
3H-4, 7–8	23.82	0.69	3.27
3H-4, 9–10	23.84	0.61	3.16
3H-4, 11–12	23.86	0.58	3.32
3H-4, 13–14	23.88	0.56	3.21
3H-4, 15–16	23.90	0.67	3.03
3H-4, 17–18	23.92	0.78	3.10
3H-4, 19–20	23.94	0.65	3.18
3H-4, 21–22	23.96	0.61	3.16
3H-4, 23–24	23.98	0.70	3.07
3H-4, 25–26	24.00	0.63	3.12
3H-4, 27–28	24.02	0.70	3.25
3H-4, 29–30	24.04	0.71	3.10
3H-4, 31–32	24.06	0.64	3.25
3H-4, 33–34	24.08	0.61	3.06
3H-4, 35–36	24.10	0.56	2.89
3H-4, 37–38	24.12	0.68	3.10
3H-4, 39–40	24.14	0.69	3.07
3H-4, 41–42	24.16	0.60	3.20
3H-4, 43–44	24.18	0.67	3.14
3H-4, 45–46	24.20	0.69	3.19
3H-4, 47–48	24.22	0.61	3.02
3H-4, 49–50	24.24	0.66	3.23
3H-4, 51–52	24.26	0.62	3.12
3H-4, 53–54	24.27	0.62	3.14
3H-4, 55–56	24.30	0.67	3.23
3H-4, 57–58	24.32	0.71	3.23
3H-4, 59–60	24.34	0.68	3.14
3H-4, 61–62	24.36	0.70	3.17
3H-4, 63–64	24.38	0.71	3.12
3H-4, 65–66	24.40	0.69	3.01
3H-4, 67–68	24.42	0.70	3.18
3H-4, 69–70	24.44	0.70	3.25
3H-4, 71–72	24.46	0.57	3.21
3H-4, 73–74	24.48	0.61	3.13
3H-4, 75–76	24.50	0.60	3.18
3H-4, 77–78	24.52	0.68	3.07
3H-4, 79–80	24.54	0.62	3.03
3H-4, 81–82	24.56	0.67	3.20
3H-4, 83–84	24.58	0.58	3.12
3H-4, 85–86	24.60	0.62	3.21
3H-4, 87–88	24.62	0.64	3.23
3H-4, 89–90	24.64	0.60	3.15
3H-4, 91–92	24.66	0.60	3.21
3H-4, 93–94	24.68	0.43	2.94
3H-4, 95–96	24.70	0.58	3.11
3H-4, 97–98	24.72	0.27	3.46
3H-4, 99–100	24.74	0.55	3.12
3H-4, 101–102	24.76	0.53	3.00
3H-4, 103–104	24.78		
3H-4, 105–106	24.80	0.49	3.21
3H-4, 107–108	24.82	0.51	3.15
3H-4, 109–110	24.84	0.50	3.08
3H-4, 111–112	24.86	0.54	3.14
3H-4, 113–114	24.88	0.55	3.20
3H-4, 115–116	24.90	0.52	3.35
3H-4, 117–118	24.92	0.58	3.12
3H-4, 119–120	24.94	0.62	3.06

Appendix Table AT1 (continued).

Core, section, interval (cm)	Depth (mcd)	*Cibicidoides mundulus* $\delta^{13}C$ (‰)	*Cibicidoides mundulus* $\delta^{18}O$ (‰)
3H-4, 121–122	24.96	0.45	3.22
3H-4, 123–124	24.98	0.67	3.21
3H-4, 125–126	25.00	0.68	3.12
3H-4, 127–128	25.02	0.68	3.26
3H-4, 129–130	25.04	0.73	3.21
3H-4, 131–132	25.06	0.66	3.20
3H-4, 133–134	25.08	0.63	2.93
3H-4, 135–136	25.10	0.64	3.02
3H-4, 137–138	25.12	0.58	3.06
3H-4, 139–140	25.14	0.74	3.02
3H-4, 141–142	25.16	0.56	3.03
3H-4, 143–144	25.18	0.43	3.09
3H-4, 145–146	25.20	0.49	3.20
3H-4, 147–148	25.22	0.50	3.10
3H-4, 149–150	25.24	0.53	3.03
3H-5, 0–1	25.26	0.47	3.14
3H-5, 2–3	25.28	0.48	3.06
3H-5, 4–5	25.30	0.49	3.03
3H-5, 6–7	25.32	0.49	3.28
3H-5, 8–9	25.34		
3H-5, 10–11	25.36	0.57	3.21
3H-5, 12–13	25.38	0.43	2.62
3H-5, 14–15	25.40	0.56	3.05
3H-5, 16–17	25.42	0.55	3.09
3H-5, 18–19	25.44	0.58	2.92
3H-5, 20–21	25.46	0.58	3.03
3H-5, 22–23	25.48	0.55	3.14
3H-5, 24–25	25.50	0.56	3.01
3H-5, 26–27	25.52	0.48	3.03
3H-5, 28–29	25.54	0.53	2.94
3H-5, 30–31	25.56	0.61	3.14
3H-5, 32–33	25.58	0.41	3.19
3H-5, 34–35	25.60	0.52	3.00
3H-5, 36–37	25.62	0.44	3.17
3H-5, 38–39	25.64	0.47	3.16
3H-5, 40–41	25.66	0.55	3.06
3H-5, 42–43	25.68	0.54	3.03
3H-5, 44–45	25.70	0.39	2.85
3H-5, 46–47	25.72	0.36	3.06
3H-5, 48–49	25.74	0.29	2.70
3H-5, 50–51	25.76	0.48	3.11
3H-5, 52–53	25.78	0.35	3.09
202-1236C-			
1H-5, 0–1	9.40	0.28	3.69
1H-5, 2–3	9.42	0.18	3.88
1H-5, 4–5	9.44	0.41	3.54
1H-5, 6–7	9.46	0.36	3.46
1H-5, 8–9	9.48	0.45	3.47
1H-5, 10–11	9.50	0.31	3.49
1H-5, 12–13	9.52	0.23	3.64
1H-5, 14–15	9.54	0.12	3.64
1H-5, 16–17	9.56	0.15	3.77
1H-5, 18–19	9.58	0.39	3.38
1H-5, 20–21	9.60	0.32	3.40
1H-5, 22–23	9.62	0.35	3.19
1H-5, 24–25	9.64	0.39	3.52
1H-5, 26–27	9.66	0.32	3.38
1H-5, 28–29	9.68	0.20	3.40
1H-5, 30–31	9.70	0.29	3.61
1H-5, 32–33	9.72	0.25	3.58
1H-5, 34–35	9.74	0.32	3.44
1H-5, 36–37	9.76	0.34	3.61
1H-5, 38–39	9.78	0.34	3.54
1H-5, 40–41	9.80	0.25	3.54
1H-5, 42–43	9.82	0.35	3.33
1H-5, 44–45	9.84	0.08	3.83
1H-5, 46–47	9.86	0.35	3.37
1H-5, 48–49	9.88	0.40	3.64
1H-5, 50–51	9.90	0.47	3.34
1H-5, 52–53	9.92	0.32	3.56
1H-5, 54–55	9.94	0.29	3.37
1H-5, 56–57	9.96	0.43	3.39
1H-5, 58–59	9.98	0.54	3.42
1H-5, 60–61	10.00	0.38	3.42
1H-5, 62–63	10.02	0.30	3.39
1H-5, 64–65	10.04	0.39	3.34
1H-5, 66–67	10.06	0.40	3.40
1H-5, 68–69	10.08	0.43	3.48
1H-5, 70–71	10.10	0.64	3.52
1H-5, 72–73	10.12	0.48	3.59
1H-5, 74–75	10.14	0.62	3.43
1H-5, 76–77	10.16	0.43	3.75
1H-5, 78–79	10.18	0.64	3.44
1H-5, 80–81	10.20	0.63	3.60
1H-5, 82–83	10.22	0.54	3.32
1H-5, 84–85	10.24	0.53	3.65
1H-5, 86–87	10.26	0.57	3.57
1H-5, 88–89	10.28	0.53	3.75
1H-5, 90–91	10.30	0.46	3.72
1H-5, 92–93	10.32	0.59	3.55
1H-5, 94–95	10.34	0.57	3.59
1H-5, 96–97	10.36	0.58	3.62
1H-5, 98–99	10.38	0.36	3.47
1H-5, 100–101	10.40	0.48	3.48
1H-5, 102–103	10.42	0.53	3.48
1H-5, 104–105	10.44		
1H-5, 106–107	10.46	0.45	3.55
1H-5, 108–109	10.48	0.27	3.88
1H-5, 110–111	10.50	0.27	3.85
1H-5, 112–113	10.52	0.33	3.83
1H-5, 114–115	10.54	0.26	4.03
1H-5, 116–117	10.56	0.50	3.44
1H-5, 118–119	10.58	0.28	4.02
1H-5, 120–121	10.60	0.37	3.48
1H-5, 122–123	10.62	0.25	3.59
1H-5, 124–125	10.64	0.14	3.89
1H-5, 126–127	10.66	0.31	3.66
1H-5, 128–129	10.68	0.38	3.43
1H-5, 130–131	10.70	0.42	3.67
1H-5, 132–133	10.72	0.24	3.78
1H-5, 134–135	10.74	0.13	3.92
1H-5, 136–137	10.76	–0.01	4.01
1H-5, 138–139	10.78	0.22	3.89
1H-5, 140–141	10.80	0.28	3.71
1H-5, 142–143	10.82	0.09	4.03
1H-5, 144–145	10.84	0.22	3.97
1H-5, 146–147	10.86	0.31	3.23
1H-5, 148–149	10.88	0.18	3.53
1H-5, 150–151	10.90	0.05	3.89
1H-6, 1–2	10.92	–0.01	3.98
1H-6, 3–4	10.94	0.34	3.52
1H-6, 5–6	10.96	0.19	3.31
1H-6, 7–8	10.98	0.21	3.67
1H-6, 9–10	11.00	0.14	3.97
1H-6, 11–12	11.02	0.45	3.05
1H-6, 13–14	11.04	0.45	3.17
1H-6, 15–16	11.06	0.42	3.29
1H-6, 17–18	11.08	0.46	3.43
1H-6, 19–20	11.10	0.36	3.54
1H-6, 21–22	11.12	0.43	3.12
1H-6, 23–24	11.14	0.38	3.50
1H-6, 25–26	11.16	0.41	3.30
1H-6, 27–28	11.18	0.43	3.06
1H-6, 29–30	11.20	0.45	3.21
1H-6, 31–32	11.22	0.36	3.54
1H-6, 33–34	11.24	0.40	3.15
1H-6, 35–36	11.26	0.41	3.40
1H-6, 37–38	11.28	0.42	3.38

Appendix Table AT1 (continued).

Core, section, interval (cm)	Depth (mcd)	*Cibicidoides mundulus* $\delta^{13}C$ (‰)	*Cibicidoides mundulus* $\delta^{18}O$ (‰)
1H-6, 39–40	11.30	0.39	3.51
1H-6, 41–42	11.32	0.38	3.34
1H-6, 43–44	11.34	0.43	3.25
1H-6, 45–46	11.36	0.19	3.67
1H-6, 47–48	11.38	0.30	3.57
1H-6, 49–50	11.40	0.32	3.61
1H-6, 51–52	11.42	0.16	3.44
1H-6, 53–54	11.44	0.31	3.82
1H-6, 55–56	11.46	0.23	3.72
1H-6, 57–58	11.48	0.42	3.46
1H-6, 59–60	11.50	0.33	3.26
1H-6, 61–62	11.52	0.40	3.49
1H-6, 63–64	11.54	0.21	3.55
1H-6, 65–66	11.56	0.49	3.19
1H-6, 67–68	11.58	0.41	3.48
1H-6, 69–70	11.60	0.38	3.47
1H-6, 71–72	11.62	0.42	3.56
1H-6, 73–74	11.64	0.32	3.50
1H-6, 75–76	11.66	0.34	3.48
1H-6, 77–78	11.68	0.25	3.59
1H-6, 79–80	11.70	0.34	3.62
1H-6, 81–82	11.72	0.17	3.70
1H-6, 83–84	11.74	0.37	3.24
1H-6, 85–86	11.76	0.20	3.74
1H-6, 87–88	11.78	0.34	3.84
1H-6, 89–90	11.80	0.48	3.55
1H-6, 91–92	11.82		
1H-6, 93–94	11.84	0.34	3.78
1H-6, 95–96	11.86	0.43	3.44
1H-6, 97–98	11.88		
1H-6, 99–100	11.90	0.30	3.83
1H-6, 101–102	11.92	0.33	3.63
1H-6, 103–104	11.94	0.26	4.04
1H-6, 105–106	11.96		
1H-6, 107–108	11.98		
1H-6, 109–110	12.00		
1H-6, 111–112	12.02		
1H-6, 113–114	12.04		
1H-6, 115–116	12.06	0.16	3.89
1H-6, 117–118	12.08	0.46	3.66
1H-6, 119–120	12.10	0.16	3.94
1H-6, 121–122	12.12	0.31	3.66
1H-6, 123–124	12.14	0.29	3.84
1H-6, 125–126	12.16	0.31	3.65
1H-6, 127–128	12.18	0.32	3.77
1H-6, 129–130	12.20	0.14	3.79
1H-6, 131–132	12.22	0.17	4.00
1H-6, 133–134	12.24	0.28	3.67
1H-6, 135–136	12.26		
1H-6, 137–138	12.28	0.43	3.62
1H-6, 139–140	12.30		
1H-6, 141–142	12.32	0.06	4.11
1H-6, 143–144	12.34	0.40	3.70
1H-6, 145–146	12.36	0.39	3.65
1H-6, 147–148	12.38	0.30	3.52
1H-6, 149–150	12.40	0.43	3.55
2H-3, 11–12	16.00		3.22
2H-3, 13–14	16.02	0.35	3.24
2H-3, 15–16	16.04	0.31	3.30
2H-3, 17–18	16.06		2.82
2H-3, 19–20	16.08	0.27	3.01
2H-3, 21–22	16.10		2.89
2H-3, 23–24	16.12		2.97
2H-3, 25–26	16.14		2.95
2H-3, 27–28	16.16	0.32	3.31
2H-3, 29–30	16.18	0.54	3.22
2H-3, 31–32	16.20		2.99
2H-3, 33–34	16.22	0.30	3.17
2H-3, 35–36	16.24	0.32	3.10
2H-3, 37–38	16.26	0.35	3.25
2H-3, 39–40	16.28	0.32	3.22
2H-3, 41–42	16.30	0.29	3.29
2H-3, 43–44	16.32	0.37	3.17
2H-3, 45–46	16.34	0.50	3.15
2H-3, 47–48	16.36	0.24	3.15
2H-3, 49–50	16.38	0.49	3.09
2H-3, 51–52	16.40	0.43	3.14
2H-3, 53–54	16.42	0.48	3.17
2H-3, 55–56	16.44	0.46	3.20
2H-3, 57–58	16.46	0.40	3.12
2H-3, 59–60	16.48	0.43	3.12
2H-3, 61–62	16.50	0.42	3.19
2H-3, 63–64	16.52	0.25	3.25
2H-3, 65–66	16.54		2.94
2H-3, 67–68	16.56	0.39	3.22
2H-3, 69–70	16.58	0.54	3.19
2H-3, 71–72	16.60		2.91
2H-3, 73–74	16.62		2.94
2H-3, 75–76	16.64	0.40	3.32
2H-3, 77–78	16.66		2.99
2H-3, 79–80	16.68		2.97
2H-3, 81–82	16.70		2.81
2H-3, 83–84	16.72		
2H-3, 85–86	16.74		2.98
2H-3, 87–88	16.76		2.85
2H-3, 89–90	16.78		2.75
2H-3, 91–92	16.80		2.82
2H-3, 93–94	16.82		3.11
2H-3, 95–96	16.84		2.90
2H-3, 97–98	16.86		2.89
2H-3, 99–100	16.88		3.03
2H-3, 101–102	16.90	0.50	3.10
2H-3, 103–104	16.92	0.53	3.17
2H-3, 105–106	16.94	0.56	3.19
2H-3, 107–108	16.96	0.56	3.04
2H-3, 109–110	16.98	0.62	3.26
2H-3, 111–112	17.00	0.62	3.20
2H-3, 113–114	17.02	0.62	3.10
2H-3, 115–116	17.04	0.46	3.42
2H-3, 117–118	17.06	0.56	3.17
2H-3, 119–120	17.08	0.55	3.09
2H-3, 121–122	17.10		2.80
2H-3, 123–124	17.12		2.74
2H-3, 125–126	17.14	0.48	3.27
2H-3, 127–128	17.16		2.80
2H-3, 129–130	17.18		2.93
2H-3, 131–132	17.20		2.96
2H-3, 133–134	17.22	0.55	3.26
2H-3, 135–136	17.24		2.95
2H-3, 137–138	17.26	0.63	3.38
2H-3, 139–140	17.28	0.40	3.42
2H-3, 141–142	17.30		3.03
2H-3, 143–144	17.32	0.55	3.40
2H-3, 145–146	17.34	0.69	3.08
2H-3, 147–148	17.36	0.46	3.38
2H-3, 149–150	17.38	0.71	3.21
2H-4, 0–1	17.40		2.91
2H-4, 2–3	17.42		2.90
2H-4, 4–5	17.44		2.79
2H-4, 6–7	17.46	0.34	3.51
2H-4, 8–9	17.48		2.79
2H-4, 10–11	17.50	0.26	3.33
2H-4, 12–13	17.52	0.52	3.26
2H-4, 14–15	17.54		2.99
2H-4, 16–17	17.56	0.43	3.51
2H-4, 18–19	17.58	0.36	3.33
2H-4, 20–21	17.60	0.56	3.31
2H-4, 22–23	17.62	0.34	3.04

Appendix Table AT1 (continued).

Core, section, interval (cm)	Depth (mcd)	*Cibicidoides mundulus* $\delta^{13}C$ (‰)	*Cibicidoides mundulus* $\delta^{18}O$ (‰)
2H-4, 24–25	17.64	0.45	3.36
2H-4, 26–27	17.66	0.52	3.20
2H-4, 28–29	17.68	0.52	3.23
2H-4, 30–31	17.70	0.42	3.47
2H-4, 32–33	17.72	0.38	3.29
2H-4, 34–35	17.74	0.54	3.30
2H-4, 36–37	17.76	0.30	3.12
2H-4, 38–39	17.78	0.60	3.20
2H-4, 40–41	17.80	0.42	3.13
2H-4, 42–43	17.82	0.36	3.07
2H-4, 44–45	17.84	0.46	3.21
2H-4, 46–47	17.86	0.47	3.35
2H-4, 48–49	17.88	0.41	3.30
2H-4, 50–51	17.90	0.42	3.35
2H-4, 52–53	17.92	0.35	2.97
2H-4, 54–55	17.94	0.42	3.18
2H-4, 56–57	17.96	0.48	3.25
2H-4, 58–59	17.98	0.48	3.47
2H-4, 60–61	18.00	0.44	3.14
2H-4, 62–63	18.02	0.50	3.28
2H-4, 64–65	18.04	0.56	3.26
2H-4, 66–67	18.06	0.62	3.09
2H-4, 68–69	18.08	0.45	3.28
2H-4, 70–71	18.10	0.44	3.17
2H-4, 72–73	18.12	0.40	3.22
2H-4, 74–75	18.14	0.52	3.36
2H-4, 76–77	18.16	0.44	3.17
2H-4, 78–79	18.18	0.50	3.37
2H-4, 80–81	18.20	0.49	3.27
2H-4, 82–83	18.22	0.46	3.25
2H-4, 84–85	18.24	0.54	3.19
2H-4, 86–87	18.26	0.68	3.32
2H-4, 88–89	18.28	0.56	2.89
2H-4, 90–91	18.30	0.47	3.23
2H-4, 92–93	18.32	0.41	3.48
2H-4, 94–95	18.34	0.50	3.41
2H-4, 96–97	18.36	0.38	3.21
2H-4, 98–99	18.38	0.49	3.20
2H-4, 100–101	18.40	0.37	3.34
2H-4, 102–103	18.42	0.39	3.23
2H-4, 104–105	18.44	0.55	3.08
2H-4, 106–107	18.46	0.42	3.05
2H-4, 108–109	18.48	0.53	2.96
2H-4, 110–111	18.50	0.54	3.09
2H-4, 112–113	18.52	0.45	3.07
2H-4, 114–115	18.54	0.55	3.28
2H-4, 116–117	18.56	0.52	3.31
2H-4, 118–119	18.58	0.56	3.32
2H-4, 120–121	18.60	0.52	3.35
2H-4, 122–123	18.62	0.45	2.98
2H-4, 124–125	18.64	0.64	3.08
2H-4, 126–127	18.66	0.78	3.21
2H-4, 128–129	18.68	0.43	3.12
2H-4, 130–131	18.70	0.45	2.88
2H-4, 132–133	18.72	0.49	3.04
2H-4, 134–135	18.74	0.43	3.05
2H-4, 136–137	18.76	0.48	3.39
2H-4, 138–139	18.78	0.40	3.06
2H-4, 140–141	18.80	0.43	2.91
2H-4, 142–143	18.82	0.42	2.97
2H-4, 144–145	18.84	0.61	3.14
2H-4, 146–147	18.86	0.45	3.27
2H-4, 148–149	18.88	0.40	3.00
2H-4, 150–151	18.90	0.58	3.21
2H-5, 1–2	18.92	0.33	2.84
2H-5, 3–4	18.94	0.55	2.95
2H-5, 5–6	18.96	0.49	3.16
2H-5, 7–8	18.98	0.43	3.15
2H-5, 9–10	19.00	0.43	3.14
2H-5, 11–12	19.02	0.34	2.98
2H-5, 13–14	19.04	0.10	3.02
2H-5, 15–16	19.06	0.20	3.22
2H-5, 17–18	19.08	0.21	3.13
2H-5, 19–20	19.10	0.46	3.16
2H-5, 21–22	19.12		2.65
2H-5, 23–24	19.14	0.50	3.20
2H-5, 25–26	19.16	0.32	2.87
2H-5, 27–28	19.18	0.38	3.15
2H-5, 29–30	19.20	0.41	3.21
2H-5, 31–32	19.22	0.47	3.19
2H-5, 33–34	19.24	0.29	3.15
2H-5, 35–36	19.26	0.46	3.00
2H-5, 37–38	19.28	0.25	3.20
2H-5, 39–40	19.30		2.82
2H-5, 41–42	19.32		3.00
2H-5, 43–44	19.34		2.79
2H-5, 45–46	19.36		2.84
2H-5, 47–48	19.38		2.57
2H-5, 49–50	19.40		2.96
2H-5, 51–52	19.42	0.47	3.12
2H-5, 53–54	19.44		3.15
2H-5, 55–56	19.46		2.86
2H-5, 57–58	19.48	0.37	3.08
2H-5, 59–60	19.50	0.54	3.23
2H-5, 61–62	19.52		2.82
2H-5, 63–64	19.54	0.51	3.22
2H-5, 65–66	19.56	0.56	3.12
2H-5, 67–68	19.58		2.83
2H-5, 69–70	19.60	0.55	3.08
2H-5, 71–72	19.62	0.62	3.13
2H-5, 73–74	19.64		2.78
2H-5, 75–76	19.66		3.00
2H-5, 77–78	19.68		3.15
2H-5, 79–80	19.70		2.91
2H-5, 81–82	19.72		2.76
2H-5, 83–84	19.74		2.51
2H-5, 85–86	19.76	0.38	3.28
2H-5, 87–88	19.78	0.45	3.32
2H-5, 89–90	19.80	0.31	3.34
2H-5, 91–92	19.82	0.44	3.32
2H-5, 93–94	19.84		2.92
2H-5, 95–96	19.86	0.55	3.00
2H-5, 97–98	19.88	0.38	2.80
2H-5, 99–100	19.90		2.57
2H-5, 101–102	19.92	0.40	3.23
2H-5, 103–104	19.94		2.78
2H-5, 105–106	19.96	0.42	3.05
2H-5, 107–108	19.98		2.48
2H-5, 109–110	20.00		2.99
2H-5, 111–112	20.02		2.84
2H-5, 113–114	20.04	0.52	3.11
2H-5, 115–116	20.06		2.67
2H-5, 117–118	20.08	0.59	3.02
2H-5, 119–120	20.10		2.67
2H-5, 121–122	20.12	0.63	3.16
2H-5, 123–124	20.14		2.64
2H-5, 125–126	20.16	0.34	3.29
2H-5, 127–128	20.18		2.80
2H-5, 129–130	20.20	0.41	3.18
2H-5, 131–132	20.22	0.42	3.21
2H-5, 133–134	20.24	0.40	3.34
2H-5, 135–136	20.26	0.53	3.17
2H-5, 137–138	20.28	0.55	3.19
2H-5, 139–140	20.30		2.95
2H-5, 141–142	20.32		3.01
2H-5, 143–144	20.34	0.36	3.23
2H-5, 145–146	20.36	0.43	3.09
2H-5, 147–148	20.38	0.41	3.37

Appendix Table AT1 (continued).

Core, section, interval (cm)	Depth (mcd)	*Cibicidoides mundulus* $\delta^{13}C$ (‰)	*Cibicidoides mundulus* $\delta^{18}O$ (‰)
2H-6, 0–1	20.42	0.41	3.14
2H-6, 2–3	20.44	0.44	3.33
2H-6, 4–5	20.46	0.40	3.22
2H-6, 6–7	20.48	0.47	3.13
2H-6, 8–9	20.50	0.54	2.76
2H-6, 10–11	20.52	0.68	2.97
2H-6, 12–13	20.54	0.48	3.29
2H-6, 14–15	20.56	0.44	3.28
2H-6, 16–17	20.58	0.48	2.79
2H-6, 18–19	20.60	0.60	3.04
2H-6, 20–21	20.62	0.43	3.08
2H-6, 22–23	20.64	0.43	3.20
2H-6, 24–25	20.66	0.52	2.97
2H-6, 26–27	20.68	0.40	2.84
2H-6, 28–29	20.70	0.40	3.12
2H-6, 30–31	20.72	0.44	3.07
2H-6, 32–33	20.74	0.68	2.91
2H-6, 34–35	20.76	0.47	3.38
2H-6, 36–37	20.78	0.67	3.11
2H-6, 38–39	20.80	0.59	3.04
2H-6, 40–41	20.82	0.53	3.14
2H-6, 42–43	20.84	0.50	2.90
2H-6, 44–45	20.86	0.57	3.06
2H-6, 46–47	20.88	0.46	3.06
2H-6, 48–49	20.90	0.49	3.23
2H-6, 50–51	20.92	0.58	3.11
2H-6, 52–53	20.94	0.52	3.09
3H-2, 65–66	25.80	0.48	3.15
3H-2, 67–68	25.82	0.48	3.08
3H-2, 69–70	25.84	0.60	3.22
3H-2, 71–72	25.86	0.51	3.26
3H-2, 73–74	25.88	0.44	3.63
3H-2, 75–76	25.90	0.43	3.17
3H-2, 77–78	25.92	0.43	3.06
3H-2, 79–80	25.94	0.55	3.22
3H-2, 81–82	25.96	0.42	3.06
3H-2, 83–84	25.98	0.63	2.92
3H-2, 85–86	26.00	0.52	3.33
3H-2, 87–88	26.02	0.50	3.33
3H-2, 89–90	26.04	0.37	3.29
3H-2, 91–92	26.06	0.59	3.32
3H-2, 93–94	26.08	0.48	3.12
3H-2, 95–96	26.10	0.48	3.04
3H-2, 97–98	26.12	0.49	3.20
3H-2, 99–100	26.14	0.58	3.01
3H-2, 101–102	26.16	0.35	3.22
3H-2, 103–104	26.18	0.39	2.81
3H-2, 105–106	26.20	0.45	3.39
3H-2, 107–108	26.22	0.44	3.40
3H-2, 109–110	26.24	0.45	3.23
3H-2, 111–112	26.26	0.28	3.36
3H-2, 113–114	26.28	0.50	3.03
3H-2, 115–116	26.30		
3H-2, 117–118	26.32	0.49	3.22
3H-2, 119–120	26.34	0.50	3.14
3H-2, 121–122	26.36	0.50	3.01
3H-2, 123–124	26.38	0.55	3.12
3H-2, 125–126	26.40	0.57	3.10
3H-2, 127–128	26.42	0.29	3.36
3H-2, 129–130	26.44	0.54	3.21
3H-2, 131–132	26.46	0.51	3.02
3H-2, 133–134	26.48	0.46	3.15
3H-2, 135–136	26.50	0.30	3.43
3H-2, 137–138	26.52	0.64	3.15
3H-2, 139–140	26.54	0.44	3.30
3H-2, 141–142	26.56	0.50	3.16
3H-2, 143–144	26.58	0.52	3.25
3H-2, 145–146	26.60	0.45	3.12
3H-2, 147–148	26.62	0.57	3.12
3H-2, 149–150	26.64	0.47	3.26
3H-3, 0–1	26.66	0.53	3.34
3H-3, 2–3	26.68	0.42	3.49
3H-3, 4–5	26.70	0.57	3.14
3H-3, 6–7	26.72	0.54	3.36
3H-3, 8–9	26.74	0.55	3.15
3H-3, 10–11	26.76	0.47	3.11
3H-3, 12–13	26.78	0.48	2.97
3H-3, 14–15	26.80	0.33	3.35
3H-3, 16–17	26.82	0.37	3.61
3H-3, 18–19	26.84	0.47	3.16
3H-3, 20–21	26.86	0.46	3.01
3H-3, 22–23	26.88	0.39	3.04
3H-3, 24–25	26.90	0.61	3.00
3H-3, 26–27	26.92	0.43	3.31
3H-3, 28–29	26.94	0.60	3.31
3H-3, 36–37	27.02	0.49	3.02
3H-3, 38–39	27.04	0.44	3.04
3H-3, 40–41	27.06	0.31	3.15
3H-3, 42–43	27.08	0.52	3.07
3H-3, 44–45	27.10	0.43	3.33
3H-3, 46–47	27.12	0.44	3.21
3H-3, 48–49	27.14	0.64	3.32
3H-3, 50–51	27.16	0.41	3.58
3H-3, 52–53	27.18	0.59	3.31
3H-3, 54–55	27.20	0.48	2.86
3H-3, 56–57	27.22	0.44	3.20
3H-3, 58–59	27.24	0.29	3.21
3H-3, 60–61	27.26	0.47	3.26
3H-3, 62–63	27.28	0.53	3.26
3H-3, 64–65	27.30	0.17	3.38
3H-3, 66–67	27.32	0.69	3.24
3H-3, 68–69	27.34	0.57	3.33
3H-3, 70–71	27.36	0.49	3.06
3H-3, 72–73	27.38	0.62	3.03
3H-3, 74–75	27.40	0.74	3.11
3H-3, 76–77	27.42	0.65	2.98
3H-3, 78–79	27.44	0.29	3.43
3H-3, 80–81	27.46	0.38	3.36
3H-3, 82–83	27.48	0.63	3.11
3H-3, 84–85	27.50	0.46	3.03
3H-3, 86–87	27.52	0.58	3.33
3H-3, 88–89	27.54	0.44	3.05
3H-3, 90–91	27.56	0.48	3.38
3H-3, 92–93	27.58	0.47	3.30
3H-3, 94–95	27.60	0.42	3.30
3H-3, 96–97	27.62	0.38	3.35
3H-3, 98–99	27.64	0.26	3.44
3H-3, 100–101	27.66	0.45	3.36
3H-3, 102–103	27.68	0.39	3.33
3H-3, 104–105	27.70	0.63	3.33
3H-3, 106–107	27.72	0.62	3.23
3H-3, 108–109	27.74	0.52	3.23
3H-3, 110–111	27.76	0.62	3.14
3H-3, 112–113	27.78	0.54	3.24
3H-3, 114–115	27.80	0.48	3.06
3H-3, 116–117	27.82	0.24	3.25
3H-3, 118–119	27.84	0.68	3.36
3H-3, 120–121	27.86	0.54	3.35
3H-3, 122–123	27.88	0.54	3.20
3H-3, 124–125	27.90	0.31	3.13
3H-3, 126–127	27.92	0.58	3.12
3H-3, 128–129	27.94	0.52	2.87
3H-3, 130–131	27.96	0.41	3.30
3H-3, 132–133	27.98	0.59	3.19
3H-3, 134–135	28.00	0.41	3.17
3H-3, 136–137	28.02	0.49	3.21
3H-3, 138–139	28.04	0.58	3.09
3H-3, 140–141	28.06	0.47	3.07

Appendix Table AT1 (continued).

Core, section, interval (cm)	Depth (mcd)	*Cibicidoides mundulus* $\delta^{13}C$ (‰)	*Cibicidoides mundulus* $\delta^{18}O$ (‰)
3H-3, 142–143	28.08	0.47	3.36
3H-3, 144–145	28.10	0.45	3.34
3H-3, 146–147	28.12	0.41	3.26
3H-3, 148–149	28.14	0.64	3.19
3H-3, 150–151	28.16	0.49	3.06
3H-4, 1–2	28.18	0.53	3.30
3H-4, 3–4	28.20	0.61	3.13
3H-4, 5–6	28.22	0.66	3.25
3H-4, 7–8	28.24	0.51	3.36
3H-4, 9–10	28.26	0.53	3.18
3H-4, 11–12	28.28	0.49	3.36
3H-4, 13–14	28.30	0.67	3.12
3H-4, 15–16	28.32	0.67	3.36
3H-4, 17–18	28.34	0.59	3.44
3H-4, 19–20	28.36	0.50	3.27
3H-4, 21–22	28.38	0.55	3.21
3H-4, 23–24	28.40	0.41	3.27
3H-4, 25–26	28.42	0.44	3.07
3H-4, 27–28	28.44	0.52	3.22
3H-4, 29–30	28.46	0.59	3.25
3H-4, 31–32	28.48	0.37	3.15
3H-4, 33–34	28.50	0.44	3.32
3H-4, 35–36	28.52	0.35	3.23
3H-4, 37–38	28.54	0.45	3.21
3H-4, 39–40	28.56	0.35	3.52
3H-4, 41–42	28.58	0.40	3.34
3H-4, 43–44	28.60	0.44	3.40
3H-4, 45–46	28.62	0.37	3.35
3H-4, 47–48	28.64	0.32	3.44
3H-4, 49–50	28.66	0.53	3.37
3H-4, 51–52	28.68	0.56	3.12
3H-4, 53–54	28.70	0.52	3.18
3H-4, 55–56	28.72	0.56	3.16
3H-4, 57–58	28.74	0.32	3.12
3H-4, 59–60	28.76	0.60	3.08
3H-4, 61–62	28.78	0.53	3.17
3H-4, 63–64	28.80	0.54	2.99
3H-4, 65–66	28.82	0.48	3.14
3H-4, 67–68	28.84	0.48	3.11
3H-4, 69–70	28.86	0.57	3.04
3H-4, 71–72	28.88	0.45	3.03
3H-4, 73–75	28.90		
3H-4, 75–76	28.92	0.62	3.33
3H-4, 77–78	28.94		
3H-4, 79–80	28.96		
3H-4, 81–82	28.98	0.19	2.99
3H-4, 83–84	29.00	0.35	3.26
3H-4, 85–86	29.02	0.25	3.67
3H-4, 87–88	29.04	0.26	3.51
3H-4, 89–90	29.06	0.27	3.26
3H-4, 91–92	29.08	0.28	3.60
3H-4, 93–94	29.10	0.45	2.87
3H-4, 95–96	29.12	0.42	3.66
3H-4, 97–98	29.14	0.56	3.13
3H-4, 99–100	29.16	0.50	3.06
3H-4, 101–102	29.18	0.51	3.11
3H-4, 103–104	29.20	0.27	3.13
3H-4, 105–106	29.22	0.46	2.99
3H-4, 107–108	29.24	0.51	3.09
3H-4, 109–110	29.26	0.32	3.32
3H-4, 111–112	29.28	0.40	3.35
3H-4, 113–114	29.30	0.46	3.05
3H-4, 115–116	29.32	0.49	2.85
3H-4, 117–118	29.34	0.52	3.34
3H-4, 119–120	29.36	0.44	3.23
3H-4, 121–122	29.38	0.49	3.28
3H-4, 123–124	29.40	0.36	2.62
3H-4, 125–126	29.42	0.36	2.81

Appendix Table AT2. Benthic oxygen and carbon isotope data of Site 1237. (Continued on next five pages.)

Core, section, interval (cm)	Depth (mcd)	*Cibicidoides mundulus* $\delta^{13}C$ (‰)	*Cibicidoides mundulus* $\delta^{18}O$ (‰)
202-1237C-			
8H-3, 10–12	75.10	0.01	2.77
8H-3, 15–17	75.15	0.02	2.77
8H-3, 20–22	75.20	0.00	2.51
8H-3, 25–27	75.25	0.13	2.62
8H-3, 30–32	75.30	0.20	2.51
8H-3, 35–37	75.35	–0.04	2.41
8H-3, 40–42	75.40	0.19	2.58
8H-3, 45–47	75.45	0.12	2.53
8H-3, 50–52	75.50	0.02	2.46
8H-3, 55–57	75.55	0.14	2.42
8H-3, 60–62	75.60	0.18	2.48
8H-3, 65–67	75.65	0.24	2.56
8H-3, 70–72	75.70	0.05	2.74
8H-3, 75–77	75.75	–0.03	2.53
8H-3, 80–82	75.80	–0.04	2.66
8H-3, 85–87	75.85	0.02	2.49
8H-3, 90–92	75.90	–0.02	2.59
8H-3, 95–97	75.95	–0.04	2.43
8H-3, 100–102	76.00	–0.19	2.85
8H-3, 105–107	76.05	0.05	2.66
8H-3, 110–112	76.10	0.03	2.48
8H-3, 115–117	76.15	0.10	2.63
8H-3, 120–122	76.20	–0.02	2.80
8H-3, 125–127	76.25	0.00	2.42
8H-3, 130–132	76.30	0.04	2.77
8H-3, 135–137	76.35	0.04	2.63
8H-3, 140–142	76.40	–0.05	2.78
8H-3, 145–147	76.45	0.13	2.46
9H-1, 95–97	82.92	0.13	2.65
9H-1, 100–102	82.97	0.28	2.73
9H-1, 105–107	83.02	0.15	2.77
9H-1, 110–112	83.07	0.38	2.75
9H-1, 115–117	83.12	0.15	2.77
9H-1, 120–122	83.17	0.08	2.65
9H-1, 125–127	83.22	0.16	2.79
9H-1, 130–132	83.27	0.00	2.67
9H-1, 135–137	83.32	–0.03	2.72
9H-1, 140–142	83.37	0.08	2.58
9H-1, 145–147	83.42	0.12	2.76
9H-2, 0–2	83.48	–0.19	2.77
9H-2, 5–7	83.53	–0.30	2.87
9H-2, 10–12	83.58	–0.18	2.82
9H-2, 15–17	83.63	–0.04	2.96
9H-2, 20–22	83.68	0.08	2.74
9H-2, 25–27	83.73	0.08	2.75
9H-2, 30–32	83.78	–0.01	2.64
9H-2, 35–37	83.83	0.32	2.73
9H-2, 40–42	83.88	–0.11	2.63
9H-2, 45–47	83.93	0.18	2.70
9H-2, 50–52	83.98	0.26	2.77
9H-2, 55–57	84.03	0.06	2.82
9H-2, 60–62	84.08	0.01	2.61
9H-2, 65–67	84.13	–0.07	2.73
9H-2, 70–72	84.18	0.16	2.75
9H-2, 75–77	84.23		
9H-2, 80–82	84.28	0.06	2.77
9H-2, 85–87	84.33	0.20	2.74
9H-2, 90–92	84.38	–0.05	2.76
9H-2, 95–97	84.43	–0.28	2.75
9H-2, 100–102	84.48	–0.05	2.88
9H-2, 105–107	84.53	0.19	3.06
9H-2, 110–112	84.58		
9H-2, 115–117	84.63	–0.01	2.69
9H-2, 120–122	84.68	0.02	2.80
9H-2, 125–127	84.73	0.19	2.67
9H-2, 130–132	84.78	0.18	2.83
9H-2, 135–137	84.83	0.20	2.63
9H-2, 140–142	84.88	0.16	2.66
9H-2, 145–147	84.93	0.18	2.80
9H-3, 0–2	84.99	–0.05	2.69
9H-3, 5–7	85.04	0.19	2.91
9H-3, 10–12	85.09	0.24	2.94
9H-3, 15–17	85.14	0.05	2.83
9H-3, 20–22	85.19	–0.16	2.80
9H-3, 25–27	85.24	0.10	2.79
9H-3, 30–32	85.29	0.02	3.01
9H-3, 35–37	85.34	–0.01	2.91
9H-3, 40–42	85.39	–0.02	2.81
9H-3, 45–47	85.44	–0.06	2.69
9H-3, 60–62	85.59	–0.05	2.82
9H-3, 65–67	85.64	0.06	2.78
9H-3, 70–72	85.69	0.15	2.70
9H-3, 75–77	85.74	0.15	2.79
9H-3, 80–82	85.79	0.06	2.78
9H-3, 85–87	85.84	–0.03	2.69
9H-3, 90–92	85.89	0.12	2.67
9H-3, 95–97	85.94	–0.05	2.66
9H-3, 100–102	85.99	0.08	2.47
9H-3, 105–107	86.04	0.09	2.67
9H-3, 110–112	86.09	–0.03	2.84
9H-3, 115–117	86.14	0.11	3.12
9H-3, 120–122	86.19	0.00	3.11
9H-3, 125–127	86.24	–0.78	3.23
9H-3, 130–132	86.29	0.06	3.19
9H-3, 135–137	86.34	0.12	3.05
9H-3, 140–142	86.39	0.38	2.90
9H-3, 145–147	86.44	0.19	2.80
9H-4, 0–2	86.50	0.23	2.74
9H-4, 5–7	86.55	0.19	2.70
9H-4, 10–12	86.60	0.26	2.87
9H-4, 15–17	86.65	0.33	2.81
9H-4, 20–22	86.70	0.27	2.72
9H-4, 25–27	86.75	0.21	2.92
9H-4, 30–32	86.80	0.19	2.88
9H-4, 35–37	86.85	0.13	2.89
9H-4, 40–42	86.90	–0.18	2.78
9H-4, 45–47	86.95	–0.03	3.05
9H-4, 50–52	87.00	0.00	2.86
9H-4, 55–57	87.05	0.17	2.86
9H-4, 60–62	87.10	–0.16	3.12
9H-4, 65–67	87.15	0.21	2.91
9H-4, 70–72	87.20	0.15	2.87
9H-4, 75–77	87.25	0.30	2.71
9H-4, 80–82	87.30	0.11	2.84
9H-4, 85–87	87.35	0.09	2.92
9H-4, 90–92	87.40	0.34	2.84
9H-4, 95–97	87.45	0.33	2.85
9H-4, 100–102	87.50	0.35	2.81
9H-4, 105–107	87.55	0.27	2.90
9H-4, 110–112	87.60	0.27	2.82
9H-4, 115–117	87.65	0.37	2.76
9H-4, 120–122	87.70	0.16	3.03
9H-4, 125–127	87.75	0.17	3.09
9H-4, 130–132	87.80	0.12	3.15
9H-4, 135–137	87.85	0.21	2.96
9H-4, 140–142	87.90	0.31	2.99
9H-4, 145–147	87.95	0.27	2.80
9H-5, 0–2	88.01	0.20	2.88
9H-5, 5–7	88.06	0.22	2.68
9H-5, 10–12	88.11	0.16	2.86
9H-5, 15–17	88.16	0.08	2.77
9H-5, 20–22	88.21	0.08	2.75
9H-5, 25–27	88.26	–0.04	3.01
9H-5, 30–32	88.31	–0.10	2.99
9H-5, 35–37	88.36	–0.15	3.06

Appendix Table AT2 (continued).

Core, section, interval (cm)	Depth (mcd)	*Cibicidoides mundulus* $\delta^{13}C$ (‰)	*Cibicidoides mundulus* $\delta^{18}O$ (‰)
9H-5, 40–42	88.41	0.04	2.78
9H-5, 45–47	88.46		
9H-5, 50–52	88.51	–0.35	3.11
9H-5, 55–57	88.56	–0.25	3.02
9H-5, 60–62	88.61		
9H-5, 65–67	88.66	0.18	2.37
9H-5, 75–77	88.76	0.20	2.68
9H-5, 80–82	88.81	0.14	2.88
9H-5, 85–87	88.86	0.32	2.77
9H-5, 90–92	88.91	0.15	2.77
9H-5, 95–97	88.96		
9H-5, 100–102	89.01	0.03	2.65
9H-5, 105–107	89.06		
9H-5, 110–112	89.11	–0.08	2.78
9H-5, 115–117	89.16	0.14	2.88
10H-3, 0–2	95.53		
10H-3, 5–7	95.58		
10H-3, 10–12	95.63		
10H-3, 15–17	95.68	–0.07	2.73
10H-3, 20–22	95.73	–0.27	2.74
10H-3, 25–27	95.78	–0.18	2.84
10H-3, 30–32	95.83	0.06	2.71
10H-3, 35–37	95.88	0.26	2.56
10H-3, 40–42	95.93	0.40	2.62
10H-3, 45–47	95.98	0.22	2.60
10H-3, 50–52	96.03	0.22	2.55
10H-3, 55–57	96.08	0.19	2.61
10H-3, 60–62	96.13	0.21	2.57
10H-3, 65–67	96.18	0.12	2.64
10H-3, 70–72	96.23		
10H-3, 75–77	96.28	0.07	2.52
10H-3, 80–82	96.33	0.14	2.57
10H-3, 85–87	96.38	0.22	2.47
10H-3, 90–92	96.43	0.21	2.65
10H-3, 95–97	96.48	0.08	2.68
10H-3, 100–102	96.53	0.33	2.70
10H-3, 105–107	96.58		
10H-3, 110–112	96.63	0.03	2.79
10H-3, 115–117	96.68	0.04	2.58
10H-3, 120–122	96.73	0.11	2.80
10H-3, 125–127	96.78	0.04	2.89
10H-3, 130–132	96.83	0.08	2.67
10H-3, 135–137	96.88	0.25	2.68
10H-3, 140–142	96.93	0.35	2.64
10H-3, 145–147	96.98	0.10	2.63
10H-4, 0–2	97.04	0.21	2.64
10H-4, 5–7	97.09	0.29	2.51
10H-4, 10–12	97.14	0.29	2.72
10H-4, 15–17	97.19	0.33	2.60
10H-4, 20–22	97.24	0.15	2.45
10H-4, 25–27	97.29	0.44	2.51
10H-4, 30–32	97.34	0.28	2.59
10H-4, 35–37	97.39	0.30	2.47
10H-4, 40–42	97.44	0.09	2.39
10H-4, 45–47	97.49	0.19	2.55
10H-4, 50–52	97.54	0.10	2.49
10H-4, 55–57	97.59	0.13	2.62
10H-4, 60–62	97.64	0.24	2.60
10H-4, 65–67	97.69	0.27	2.68
10H-4, 70–72	97.74	0.12	2.55
10H-4, 75–77	97.79	0.47	2.62
10H-4, 80–82	97.84	0.49	2.61
10H-4, 85–87	97.89	0.18	2.56
10H-4, 90–92	97.94	0.22	2.61
10H-4, 95–97	97.99	0.41	2.68
10H-4, 100–102	98.04	0.39	2.56
10H-4, 105–107	98.09	0.66	2.75
10H-4, 110–112	98.14	0.60	2.56
10H-4, 115–117	98.19	0.49	2.61
10H-4, 120–122	98.24	0.30	2.70
10H-4, 125–127	98.29	0.45	2.76
10H-4, 130–132	98.34	0.57	2.64
10H-4, 135–137	98.39	0.38	2.67
10H-4, 140–142	98.44	0.19	2.45
10H-4, 145–147	98.49	0.27	2.62
10H-5, 0–2	98.55	0.26	2.51
10H-5, 5–7	98.60	0.36	2.62
10H-5, 10–12	98.65	0.19	2.57
10H-5, 15–17	98.70	0.34	2.59
10H-5, 20–22	98.75	0.03	2.47
10H-5, 25–27	98.80	0.43	2.58
10H-5, 30–32	98.85	0.30	2.58
10H-5, 35–37	98.90	0.42	2.76
10H-5, 40–42	98.95	0.02	2.52
10H-5, 45–47	99.00	0.28	2.52
10H-5, 50–52	99.05	0.34	2.66
10H-5, 55–57	99.10	0.23	2.72
10H-5, 60–62	99.15	0.36	2.66
10H-5, 65–67	99.20	0.28	2.66
10H-5, 70–72	99.25	0.07	2.58
10H-5, 75–77	99.30	0.28	2.64
10H-5, 80–82	99.35	0.11	2.62
10H-5, 85–87	99.40	–0.04	2.57
10H-5, 90–92	99.45	0.21	2.55
10H-5, 128–130	99.85	–0.12	2.70
10H-5, 135–137	99.90	0.07	2.78
10H-5, 140–142	99.95	0.31	2.84
10H-5, 145–147	100.00	0.38	2.87
10H-6, 0–2	100.06	–0.07	2.83
10H-6, 5–7	100.11	0.25	2.80
10H-6, 10–12	100.16	0.15	2.84
10H-6, 15–17	100.21	0.45	2.67
10H-6, 20–22	100.26	0.36	2.66
11H-3, 15–17	106.15	0.13	2.94
11H-3, 20–22	106.20	0.16	2.86
11H-3, 25–27	106.25	0.25	2.80
11H-3, 30–32	106.30	0.29	2.74
11H-3, 35–37	106.35	0.27	2.71
11H-3, 40–42	106.40	0.26	2.77
11H-3, 45–47	106.45	0.27	2.72
11H-3, 50–52	106.50	0.29	2.88
11H-3, 55–57	106.55	0.52	2.72
11H-3, 60–62	106.60	0.24	2.72
11H-3, 65–67	106.65	0.17	2.76
11H-3, 70–72	106.70	0.38	2.63
11H-3, 75–77	106.75	0.32	2.73
11H-3, 80–82	106.80	0.39	2.65
11H-3, 85–87	106.85	0.54	2.74
11H-3, 90–92	106.90		
11H-3, 100–102	107.00	0.36	2.77
11H-3, 105–107	107.05	0.42	2.72
11H-3, 110–112	107.10	0.47	2.66
11H-3, 115–117	107.15	0.45	2.69
11H-3, 120–122	107.20	0.29	2.67
11H-3, 125–127	107.25	0.35	2.80
11H-3, 130–132	107.30	0.18	2.82
11H-3, 135–137	107.35	0.19	2.76
11H-3, 140–142	107.40	0.12	2.83
11H-3, 145–147	107.45	0.47	2.72
11H-4, 0–2	107.51	0.42	2.79
11H-4, 5–7	107.56	0.29	2.71
11H-4, 10–12	107.61	0.33	2.71
11H-4, 15–17	107.66	0.48	2.79
11H-4, 20–22	107.71	0.25	2.63
11H-4, 25–27	107.76	0.25	2.63
11H-4, 30–32	107.81	0.29	2.73

Appendix Table AT2 (continued).

Core, section, interval (cm)	Depth (mcd)	*Cibicidoides mundulus* $\delta^{13}C$ (‰)	*Cibicidoides mundulus* $\delta^{18}O$ (‰)
11H-4, 35–37	107.86		
11H-4, 40–42	107.91	0.22	2.95
11H-4, 45–47	107.96	0.39	2.89
11H-4, 50–52	108.01	0.25	2.64
11H-4, 55–57	108.06	0.25	2.78
11H-4, 60–62	108.11	0.20	2.76
11H-4, 65–67	108.16	0.37	2.72
11H-4, 70–72	108.21	0.39	2.51
11H-4, 75–77	108.26	0.38	2.88
11H-4, 80–82	108.31	0.48	2.75
11H-4, 85–87	108.36	0.50	2.74
11H-4, 90–92	108.41	0.31	2.73
11H-4, 95–97	108.46	0.55	2.66
11H-4, 100–102	108.51	0.27	2.64
11H-4, 105–107	108.56	0.31	2.58
11H-4, 110–112	108.61	0.35	2.69
11H-4, 115–117	108.66	0.23	2.70
11H-4, 120–122	108.71	0.05	2.86
11H-4, 125–127	108.76	0.15	3.08
11H-4, 130–132	108.81	0.04	3.01
11H-4, 135–137	108.86	–0.05	3.02
11H-4, 140–142	108.91	0.07	2.95
11H-4, 145–147	108.96	–0.06	3.10
11H-5, 0–2	109.02	–0.37	3.29
11H-5, 5–7	109.07	–0.05	3.00
11H-5, 10–12	109.12	–0.45	3.21
11H-5, 15–17	109.17	–0.21	3.16
11H-5, 20–22	109.22	0.23	2.95
11H-5, 25–27	109.27	0.28	2.83
11H-5, 30–32	109.32	0.32	2.75
11H-5, 35–37	109.37	0.28	2.77
11H-5, 40–42	109.42	0.41	2.66
11H-5, 45–47	109.47	0.09	2.68
11H-5, 50–52	109.52	0.35	2.73
11H-5, 55–57	109.57	0.28	2.69
11H-5, 60–62	109.62	0.27	2.75
11H-5, 65–67	109.67	0.46	2.85
11H-5, 70–72	109.72	0.26	2.85
11H-5, 75–77	109.77	0.30	2.82
11H-5, 80–82	109.82	0.16	2.83
11H-5, 85–87	109.87	0.05	2.73
11H-5, 90–92	109.92	–0.10	2.80
11H-5, 95–97	109.97	0.01	2.77
11H-5, 100–102	110.02	–0.06	2.75
11H-5, 105–107	110.07	–0.13	2.89
11H-5, 110–112	110.12	–0.09	2.89
11H-5, 115–117	110.17	–0.39	3.27
11H-5, 120–122	110.22	–0.31	3.21
11H-5, 125–127	110.27	–0.19	3.14
11H-5, 130–132	110.32	–0.01	2.75
11H-5, 135–137	110.37	0.07	2.90
11H-5, 140–142	110.42	0.37	2.92
11H-5, 145–147	110.47	0.16	2.63
202-1237D-			
5H-1, 60–62	76.08	–0.03	2.83
5H-1, 65–67	76.13	–0.06	2.42
5H-1, 70–72	76.18	–0.10	2.44
5H-1, 75–77	76.23	0.05	2.66
5H-1, 80–82	76.28	–0.12	2.60
5H-1, 85–87	76.33	0.18	2.71
5H-1, 90–92	76.38	0.03	2.67
5H-1, 95–97	76.43	0.02	2.76
5H-1, 100–102	76.48	–0.09	2.60
5H-1, 105–107	76.53	–0.21	2.74
5H-1, 110–112	76.58	–0.32	2.87
5H-1, 115–117	76.63	–0.03	2.87
5H-1, 120–122	76.68	0.14	2.67
5H-1, 125–127	76.73	0.01	2.36
5H-1, 130–132	76.78	–0.07	2.47
5H-1, 135–137	76.83	0.06	2.41
5H-1, 140–142	76.88	–0.07	2.55
5H-1, 145–147	76.93	0.00	2.58
5H-2, 0–2	76.98	0.00	2.69
5H-2, 5–7	77.03	0.17	2.72
5H-2, 10–12	77.08	0.17	2.55
5H-2, 15–17	77.13	–0.12	2.63
5H-2, 20–22	77.18	–0.12	2.62
5H-2, 25–27	77.23	0.11	2.69
5H-2, 30–32	77.28	–0.21	2.52
5H-2, 35–37	77.33	–0.01	2.73
5H-2, 40–42	77.38	–0.02	2.70
5H-2, 45–47	77.43	0.16	2.64
5H-2, 50–52	77.48	–0.06	2.52
5H-2, 55–57	77.53	–0.21	2.42
5H-2, 60–62	77.58	0.07	2.53
5H-2, 65–67	77.63		
5H-2, 70–72	77.68	0.03	2.53
5H-2, 75–77	77.73	–0.24	3.38
5H-2, 80–82	77.78	–0.28	2.55
5H-2, 85–87	77.83	–0.08	2.59
5H-2, 90–92	77.88	–0.14	2.66
5H-2, 95–97	77.93	0.01	2.64
5H-2, 100–102	77.98	0.07	2.43
5H-2, 105–107	78.03	–0.05	2.72
5H-2, 110–112	78.08	0.18	2.66
5H-2, 115–117	78.13	0.33	2.84
5H-2, 120–122	78.18	–0.07	2.37
5H-2, 125–127	78.23	0.05	2.59
5H-2, 130–132	78.28	–0.22	2.70
5H-2, 135–137	78.33	–0.24	2.71
5H-2, 140–142	78.38	–0.03	2.70
5H-2, 145–147	78.43	–0.10	2.76
5H-3, 0–2	78.49	0.01	2.70
5H-3, 5–7	78.54	–0.02	2.82
5H-3, 10–12	78.59	–0.04	2.80
5H-3, 15–17	78.64	0.32	2.84
5H-3, 20–22	78.69	0.09	2.53
5H-3, 25–27	78.74	0.20	2.66
5H-3, 30–32	78.79	0.19	2.57
5H-3, 35–37	78.84	–0.17	2.51
5H-3, 40–42	78.89	0.26	2.71
5H-3, 45–47	78.94	0.38	2.87
5H-3, 50–52	78.99	0.19	2.71
5H-3, 55–57	79.04	0.29	2.70
5H-3, 60–62	79.09	0.00	2.72
5H-3, 65–67	79.14	0.18	2.84
5H-3, 70–72	79.19	–0.03	2.77
5H-3, 75–77	79.24	0.16	2.73
5H-3, 80–82	79.29	–0.09	2.72
5H-3, 85–87	79.34	–0.02	2.77
5H-3, 90–92	79.39	–0.25	2.68
5H-3, 95–97	79.44	0.20	2.86
5H-3, 100–102	79.49	0.17	2.80
5H-3, 105–107	79.54	0.13	2.68
5H-3, 110–112	79.59	0.32	2.67
5H-3, 115–117	79.64	0.23	2.79
5H-3, 120–122	79.69		
5H-3, 125–127	79.74	0.25	2.97
5H-3, 130–132	79.79	0.28	2.72
5H-3, 135–137	79.84	0.32	2.63
5H-3, 140–142	79.89	0.19	2.75
5H-3, 145–147	79.94	0.43	2.84
5H-4, 0–2	80.00	0.15	2.72
5H-4, 5–7	80.05	0.20	2.71
5H-4, 10–12	80.10	–0.03	2.77
5H-4, 15–17	80.15	0.03	3.00

Appendix Table AT2 (continued).

Core, section, interval (cm)	Depth (mcd)	*Cibicidoides mundulus* $\delta^{13}C$ (‰)	*Cibicidoides mundulus* $\delta^{18}O$ (‰)
5H-4, 20–22	80.20	0.25	2.95
5H-4, 25–27	80.25	0.12	2.92
5H-4, 30–32	80.30	0.09	2.71
5H-4, 35–37	80.35	–0.09	2.77
5H-4, 40–42	80.40	0.12	2.65
5H-4, 45–47	80.45	0.22	2.74
5H-4, 50–52	80.50	0.20	2.53
5H-4, 55–57	80.55	–0.06	2.65
5H-4, 60–62	80.60	0.16	2.67
5H-4, 65–67	80.65	0.04	2.75
5H-4, 70–72	80.70	0.10	2.71
5H-4, 75–77	80.75	0.17	2.71
5H-4, 80–82	80.80	0.07	2.83
5H-4, 85–87	80.85	0.28	2.79
5H-4, 90–92	80.90	0.10	2.80
5H-4, 95–97	80.95	0.27	2.85
5H-4, 100–102	81.00	–0.07	2.55
5H-4, 105–107	81.05	0.24	2.92
5H-4, 110–112	81.10	0.18	2.71
5H-4, 115–117	81.15	0.17	2.95
5H-4, 120–122	81.20	0.33	2.85
5H-4, 125–127	81.25	0.36	2.74
5H-4, 130–132	81.30	0.29	2.67
5H-4, 135–137	81.35	0.32	2.56
5H-4, 140–142	81.40	0.29	2.80
5H-4, 145–147	81.45	0.33	2.74
5H-5, 0–2	81.50	0.09	2.62
5H-5, 5–7	81.55	0.29	2.77
5H-5, 10–12	81.60	0.32	2.53
5H-5, 15–17	81.65	0.25	2.86
5H-5, 20–22	81.70	0.11	2.75
5H-5, 25–27	81.75	0.05	2.88
5H-5, 30–32	81.80	0.09	2.84
5H-5, 35–37	81.85	0.06	2.94
5H-5, 40–42	81.90	0.05	2.71
5H-5, 45–47	81.95	0.16	2.93
5H-5, 50–52	82.00	0.11	2.86
5H-5, 55–57	82.05	0.26	2.86
5H-5, 60–62	82.10	0.10	2.61
5H-5, 65–67	82.15	0.28	2.71
5H-5, 70–72	82.20	0.20	2.70
5H-5, 75–77	82.25	0.08	2.68
5H-5, 80–82	82.30	0.12	2.83
5H-5, 85–87	82.35	0.03	2.75
5H-5, 90–92	82.40	0.20	2.76
5H-5, 95–97	82.45	0.00	2.60
5H-5, 100–102	82.50	–0.02	2.91
5H-5, 105–107	82.55	–0.03	2.99
5H-5, 110–112	82.60	0.06	2.77
5H-5, 115–117	82.65	0.03	2.91
5H-5, 120–122	82.70	0.23	2.95
5H-5, 125–127	82.75	0.08	2.88
5H-5, 130–132	82.80	0.31	2.83
5H-5, 135–137	82.85	0.02	2.79
5H-5, 140–142	82.90	0.09	2.73
5H-5, 145–147	82.95	0.22	2.68
6H-2, 25–27	89.13	–0.10	2.79
6H-2, 30–32	89.18	–0.22	2.83
6H-2, 35–37	89.23	–0.17	2.61
6H-2, 40–42	89.28		
6H-2, 45–47	89.33	–0.47	3.13
6H-2, 50–52	89.38	–0.43	3.59
6H-2, 55–57	89.43	–0.45	2.99
6H-2, 60–62	89.48	–0.34	3.11
6H-2, 65–67	89.53	–0.21	3.12
6H-2, 70–72	89.58	–0.08	2.97
6H-2, 75–77	89.63	–0.18	3.13
6H-2, 80–82	89.68		
6H-2, 85–87	89.73	–0.03	2.61
6H-2, 90–92	89.78	–0.10	2.31
6H-2, 95–97	89.83	0.05	2.20
6H-2, 100–102	89.88	–0.03	2.67
6H-2, 105–107	89.93	0.05	2.98
6H-2, 110–112	89.98	0.08	2.82
6H-2, 115–117	90.03	0.14	2.82
6H-2, 120–122	90.08		
6H-2, 125–127	90.13	0.00	2.71
6H-2, 130–132	90.18	0.00	2.86
6H-2, 135–137	90.23	–0.09	2.95
6H-2, 140–142	90.28	–0.13	2.67
6H-2, 145–147	90.33	–0.35	2.80
6H-3, 0–2	90.39	–0.20	2.84
6H-3, 5–7	90.44	–0.26	2.83
6H-3, 10–12	90.49	–0.21	2.71
6H-3, 15–17	90.54	0.30	2.82
6H-3, 20–22	90.59	–0.08	2.65
6H-3, 25–27	90.64	0.09	2.74
6H-3, 30–32	90.69	–0.09	2.79
6H-3, 35–37	90.74	0.02	2.67
6H-3, 40–42	90.79	–0.17	2.66
6H-3, 45–47	90.84		
6H-3, 50–52	90.89	–0.22	2.59
6H-3, 55–57	90.94	–0.11	2.61
6H-3, 60–62	90.99		
6H-3, 65–67	91.04	–0.15	2.55
6H-3, 70–72	91.09	–0.04	2.52
6H-3, 75–77	91.14	–0.10	2.69
6H-3, 80–82	91.19	–0.12	2.67
6H-3, 85–87	91.24	0.02	2.70
6H-3, 90–92	91.29	0.08	2.78
6H-3, 95–97	91.34	–0.16	2.73
6H-3, 100–102	91.39	–0.04	2.46
6H-3, 105–107	91.44	0.15	2.40
6H-3, 110–112	91.49	0.09	2.65
6H-3, 115–117	91.54	0.01	2.61
6H-3, 120–122	91.59	0.36	2.84
6H-3, 125–127	91.64	0.20	2.85
6H-3, 130–132	91.69	0.37	2.79
6H-3, 135–137	91.74	–0.08	2.78
6H-3, 140–142	91.79	–0.12	2.70
6H-3, 145–147	91.84	0.03	2.51
6H-4, 0–2	91.90	–0.08	2.79
6H-4, 5–7	91.95	–0.01	2.72
6H-4, 10–12	92.00	–0.37	2.51
6H-4, 15–17	92.05	–0.18	2.69
6H-4, 20–22	92.10	–0.08	2.52
6H-4, 25–27	92.15	–0.28	2.74
6H-4, 30–32	92.20	–0.22	2.90
6H-4, 35–37	92.25	–0.36	3.00
6H-4, 40–42	92.30	–0.28	3.13
6H-4, 45–47	92.35	–0.09	2.77
6H-4, 50–52	92.40	–0.06	2.74
6H-4, 55–57	92.45	0.10	2.66
6H-4, 60–62	92.50	–0.18	2.62
6H-4, 65–67	92.55	–0.10	2.80
6H-4, 70–72	92.60	0.06	2.30
6H-4, 75–77	92.65	–0.03	2.66
6H-4, 80–82	92.70	0.11	2.45
6H-4, 85–87	92.75	0.10	2.65
6H-4, 90–92	92.80	0.21	2.55
6H-4, 95–97	92.85	0.14	2.24
6H-4, 100–102	92.90		
6H-4, 105–107	92.95	0.05	2.52
6H-4, 110–112	93.00	0.00	2.44
6H-4, 115–117	93.05	0.04	2.45
6H-4, 120–122	93.10	–0.15	2.41

Appendix Table AT2 (continued).

Core, section, interval (cm)	Depth (mcd)	*Cibicidoides mundulus* $\delta^{13}C$ (‰)	*Cibicidoides mundulus* $\delta^{18}O$ (‰)
6H-4, 125–127	93.15	0.10	2.31
6H-4, 130–132	93.20	–0.05	2.23
6H-4, 135–137	93.25	–0.28	2.71
6H-4, 140–142	93.30	–0.21	2.61
6H-4, 145–147	93.35	–0.16	2.86
6H-5, 0–2	93.41	–0.34	2.89
6H-5, 5–7	93.46	–0.33	2.99
6H-5, 10–12	93.51	–0.08	2.82
6H-5, 15–17	93.56	0.16	2.72
6H-5, 20–22	93.61	–0.09	2.65
6H-5, 25–27	93.66	–0.03	2.65
6H-5, 30–32	93.71	–0.02	2.26
6H-5, 35–37	93.76	0.14	2.57
6H-5, 40–42	93.81	–0.02	2.67
6H-5, 45–47	93.86	0.25	2.91
6H-5, 50–52	93.91	0.22	2.76
6H-5, 55–57	93.96	0.25	2.70
6H-5, 60–62	94.01	–0.02	2.66
6H-5, 65–67	94.06	0.01	2.67
6H-5, 70–72	94.11	–0.14	2.69
6H-5, 75–77	94.16	–0.22	2.79
6H-5, 80–82	94.21	–0.11	2.63
6H-5, 85–87	94.26		
6H-5, 90–92	94.31	–0.17	2.98
6H-5, 95–97	94.36	–0.10	2.81
6H-5, 100–102	94.41	0.04	2.69
6H-5, 105–107	94.46	0.18	2.73
6H-5, 110–112	94.51	–0.13	2.69
6H-5, 115–117	94.56	0.10	2.86
6H-5, 120–122	94.61	0.26	2.89
6H-5, 125–127	94.66	0.08	2.66
6H-5, 130–132	94.71	0.07	2.66
6H-5, 135–137	94.76	0.13	2.74
6H-5, 140–142	94.81	–0.11	2.65
6H-5, 145–147	94.86	0.10	2.85
6H-6, 0–2	94.92	0.11	2.84
6H-6, 5–7	94.97	0.11	2.57
6H-6, 10–12	95.02	0.26	2.83
6H-6, 15–17	95.07	0.00	2.55
6H-6, 20–22	95.12	0.12	2.62
6H-6, 25–27	95.17	–0.01	2.47
6H-6, 30–32	95.22	0.25	2.78
6H-6, 35–37	95.27	0.19	2.69
6H-6, 40–42	95.32	0.26	2.89
6H-6, 45–47	95.37	0.28	2.69
6H-6, 50–52	95.42	0.10	2.81
6H-6, 55–57	95.47	–0.24	2.59
6H-6, 60–62	95.52	–0.02	2.71
6H-6, 65–67	95.57	–0.13	2.44
6H-6, 70–72	95.62	–0.23	2.52
6H-6, 75–77	95.67	–0.03	2.73
6H-6, 80–82	95.72	–0.29	2.65
7H-2, 95–97	100.28	0.23	2.85
7H-2, 100–102	100.33	0.31	2.68
7H-2, 105–107	100.38	0.18	2.56
7H-2, 110–112	100.43	0.22	2.66
7H-2, 115–117	100.48	0.21	2.58
7H-2, 120–122	100.53	0.54	2.75
7H-2, 125–127	100.58	0.57	2.66
7H-2, 130–132	100.63	0.65	2.82
7H-2, 135–137	100.68	0.59	2.83
7H-2, 140–142	100.73	0.34	2.72
7H-2, 145–147	100.78	0.30	2.62
7H-3, 0–2	100.84	0.29	2.76
7H-3, 5–7	100.89	0.36	2.80
7H-3, 10–12	100.94	0.31	2.78
7H-3, 15–17	100.99	0.24	2.76
7H-3, 20–22	101.04	0.23	2.68
7H-3, 25–27	101.09	0.25	2.62
7H-3, 30–32	101.14	0.59	2.82
7H-3, 35–37	101.19	0.21	2.64
7H-3, 40–42	101.24	0.31	2.57
7H-3, 45–47	101.29	0.07	2.63
7H-3, 50–52	101.34	0.19	2.64
7H-3, 55–57	101.39	0.12	2.59
7H-3, 60–62	101.44	0.16	2.53
7H-3, 65–67	101.49	0.17	2.69
7H-3, 70–72	101.54	0.04	2.56
7H-3, 75–77	101.59	0.22	2.46
7H-3, 80–82	101.64	–0.03	2.48
7H-3, 85–87	101.69	0.28	2.70
7H-3, 90–92	101.74	0.26	2.60
7H-3, 95–97	101.79	0.10	2.99
7H-3, 100–102	101.84	0.20	2.87
7H-3, 105–107	101.89	0.20	2.69
7H-3, 110–112	101.94	0.25	2.73
7H-3, 115–117	101.99	0.09	2.71
7H-3, 120–122	102.04	0.27	2.91
7H-3, 125–127	102.09	0.28	2.78
7H-3, 130–132	102.14	0.37	2.86
7H-3, 135–137	102.19	0.20	2.64
7H-3, 140–142	102.24	0.27	2.73
7H-3, 145–147	102.29	0.27	2.51
7H-4, 0–2	102.34	0.23	2.63
7H-4, 5–7	102.39	0.32	2.54
7H-4, 10–12	102.44	0.16	2.84
7H-4, 15–17	102.49	0.15	2.56
7H-4, 20–22	102.54		
7H-4, 25–27	102.59	0.36	2.78
7H-4, 30–32	102.64	0.39	2.85
7H-4, 35–37	102.69	0.46	2.84
7H-4, 40–42	102.74	0.26	2.96
7H-4, 45–47	102.79	0.23	2.74
7H-4, 50–52	102.84	0.42	2.65
7H-4, 55–57	102.89	0.44	2.54
7H-4, 60–62	102.94	0.37	2.50
7H-4, 65–67	102.99	0.33	2.57
7H-4, 70–72	103.04	0.60	2.60
7H-4, 75–77	103.09	0.54	2.73
7H-4, 80–82	103.14	0.46	2.67
7H-4, 85–87	103.19	0.58	2.66
7H-4, 90–92	103.24	0.54	2.81
7H-4, 95–97	103.29	0.42	2.66
7H-4, 100–102	103.34	0.29	2.72
7H-4, 105–107	103.39	0.55	2.90
7H-4, 110–112	103.44	0.32	2.74
7H-4, 115–117	103.49	0.31	2.72
7H-4, 120–122	103.54	0.30	2.77
7H-4, 125–127	103.59		
7H-4, 130–132	103.64	0.21	2.53
7H-4, 135–137	103.69	0.21	2.70
7H-4, 140–142	103.74	0.45	2.58
7H-4, 145–147	103.79	0.10	2.64
7H-5, 0–2	103.85	0.16	2.74
7H-5, 5–7	103.90	0.35	2.61
7H-5, 10–12	103.95	0.23	2.70
7H-5, 15–17	104.00	0.18	2.67
7H-5, 20–22	104.05	0.17	2.45
7H-5, 25–27	104.10	0.27	2.43
7H-5, 30–32	104.15	0.10	2.53
7H-5, 35–37	104.20	0.21	2.62
7H-5, 40–42	104.25		
7H-5, 45–47	104.30	0.30	2.84
7H-5, 50–52	104.35	0.14	2.63
7H-5, 55–57	104.40	–0.13	2.96
7H-5, 60–62	104.45	–0.05	2.98

Appendix Table AT2 (continued).

Core, section, interval (cm)	Depth (mcd)	*Cibicidoides mundulus* $\delta^{13}C$ (‰)	*Cibicidoides mundulus* $\delta^{18}O$ (‰)
7H-5, 65–67	104.50	–0.05	3.16
7H-5, 70–72	104.55	–0.14	3.01
7H-5, 75–77	104.60	–0.07	3.18
7H-5, 80–82	104.65	–0.24	3.20
7H-5, 85–87	104.70	0.20	2.77
7H-5, 90–92	104.75	0.28	2.76
7H-5, 95–97	104.80	–0.08	2.81
7H-5, 100–102	104.85	0.26	2.94
7H-5, 105–107	104.90	0.32	2.85
7H-5, 110–112	104.95	0.08	2.68
7H-5, 115–117	105.00	0.12	2.70
7H-5, 120–122	105.05	0.21	2.85
7H-5, 125–127	105.10	0.16	2.86
7H-5, 130–132	105.15		
7H-5, 135–137	105.20	0.05	2.89
7H-5, 140–142	105.25	0.00	2.77
7H-5, 145–147	105.30	–0.10	2.94
7H-6, 0–2	105.36	0.05	2.83
7H-6, 5–7	105.41		
7H-6, 10–12	105.46	–0.06	2.92
7H-6, 15–17	105.51		
7H-6, 20–22	105.56	–0.30	3.09
7H-6, 25–27	105.61	0.14	2.79
7H-6, 30–32	105.66	0.12	2.66
7H-6, 35–37	105.71	0.09	2.73
7H-6, 40–42	105.76		
7H-6, 45–47	105.81	0.24	2.64
7H-6, 50–52	105.86		
7H-6, 55–57	105.91	0.28	2.71
7H-6, 60–62	105.96	0.26	2.71
7H-6, 65–67	106.01	0.29	2.71
7H-6, 70–72	106.06	0.34	2.81
7H-6, 75–77	106.11	–0.07	2.59
7H-6, 80–82	106.16	0.23	2.81
8H-3, 0–2	110.39	0.11	2.70
8H-3, 5–7	110.44	0.06	2.74
8H-3, 10–12	110.49	0.02	2.79
8H-3, 15–17	110.54	0.05	2.78
8H-3, 20–22	110.59	0.19	2.75
8H-3, 25–27	110.64	0.18	2.65
8H-3, 30–32	110.69	0.07	2.61
8H-3, 35–37	110.74	0.15	2.88
8H-3, 40–42	110.79	0.15	2.68
8H-3, 45–47	110.84	–0.13	2.87
8H-3, 50–52	110.89	0.08	2.71
8H-3, 55–57	110.94	–0.26	2.64
8H-3, 60–62	110.99	–0.34	2.78
8H-3, 65–67	111.04	–0.23	2.88
8H-3, 70–72	111.09	–0.19	3.02
8H-3, 75–77	111.14		
8H-3, 80–82	111.19	0.20	2.82
8H-3, 85–87	111.24		
8H-3, 90–92	111.29	–0.07	2.74
8H-3, 95–97	111.34		
8H-3, 100–102	111.39	0.23	2.61
8H-3, 105–107	111.44		
8H-3, 110–112	111.49	0.37	2.82
8H-3, 115–117	111.54	0.08	2.54
8H-3, 120–122	111.59	0.12	2.65
8H-3, 125–127	111.64	0.22	2.57
8H-3, 130–132	111.69	0.21	2.82
8H-3, 135–137	111.74	0.05	2.66
8H-3, 140–142	111.79	–0.08	2.73
8H-3, 145–147	111.84		
8H-4, 0–2	111.90	0.16	2.65
8H-4, 5–7	111.95	0.18	2.65
8H-4, 10–12	112.00	0.21	2.62
8H-4, 15–17	112.05	0.13	2.62
8H-4, 20–22	112.10	0.14	2.71
8H-4, 25–27	112.15	–0.19	2.76
8H-4, 30–32	112.20	0.04	2.60
8H-4, 35–37	112.25	0.08	2.81
8H-4, 40–42	112.30	0.22	2.60
8H-4, 45–47	112.35	0.02	2.65
8H-4, 50–52	112.40		
8H-4, 55–57	112.45	–0.03	2.64
8H-4, 60–62	112.50	–0.03	2.66
8H-4, 65–67	112.55	–0.06	2.45
8H-4, 70–72	112.60	–0.07	2.62
8H-4, 75–77	112.65	–0.17	2.61
8H-4, 80–82	112.70	–0.35	2.84
8H-4, 85–87	112.75	–0.32	3.03
8H-4, 90–92	112.80	–0.24	2.53
8H-4, 95–97	112.85	–0.25	2.50
8H-4, 100–102	112.90	–0.05	2.76
8H-4, 105–107	112.95	–0.19	2.66
8H-4, 110–112	113.00	0.27	2.46
8H-4, 115–117	113.05		
8H-4, 120–122	113.10	0.17	2.62
8H-4, 125–127	113.15	0.17	2.56
8H-4, 130–132	113.20	0.10	2.85
8H-4, 135–137	113.25	0.00	2.60
8H-4, 140–142	113.30	0.20	2.67
8H-4, 145–147	113.35	–0.02	2.68

Appendix Table AT3. Benthic oxygen and carbon isotope data of Site 1239. (Continued on next five pages.)

Core, section, interval (cm)	Depth (mcd)	*Cibicidoides wuellerstorfi* $\delta^{13}C$ (‰)	*Cibicidoides wuellerstorfi* $\delta^{18}O$ (‰)
202-1239A-			
16H-2, 2–4	150.73	–0.11	2.52
16H-2, 32–34	151.03	–0.24	2.57
16H-2, 62–64	151.33	–0.40	2.54
16H-2, 92–94	151.63	–0.33	2.78
16H-2, 122–124	151.93		
16H-3, 2–4	152.25	–0.46	3.07
16H-3, 32–34	152.55	–0.50	3.08
16H-3, 62–64	152.85	–0.43	2.91
16H-3, 92–94	153.15	–0.72	3.02
16H-3, 122–124	153.45	–0.51	3.02
16H-4, 2–4	153.76	–0.76	3.07
16H-4, 32–34	154.06	–0.66	3.16
16H-4, 62–64	154.36	–0.82	3.31
16H-4, 92–94	154.66	–0.81	3.11
16H-4, 122–124	154.96		
16H-5, 2–4	155.27	–0.52	3.28
16H-5, 32–34	155.57	–0.40	3.07
16H-5, 62–64	155.87	–0.51	3.05
16H-5, 92–94	156.17	–0.46	2.99
16H-5, 122–124	156.47	–0.43	2.99
16H-6, 2–4	156.79	–0.31	2.87
16H-6, 32–34	157.09	–0.34	2.75
17H-2, 2–4	160.48	–0.10	2.50
17H-2, 32–34	160.78	–0.21	2.09
17H-2, 62–64	161.08	–0.08	2.57
17H-2, 92–94	161.38	–0.20	2.66
17H-2, 122–124	161.68	–0.49	2.65
17H-3, 2–4	161.99	–0.49	2.96
17H-3, 32–34	162.29	–0.42	2.97
17H-3, 62–64	162.59	–0.43	3.12
17H-3, 92–94	162.89	–0.58	2.95
17H-3, 122–124	163.19	–0.39	2.92
17H-4, 2–4	163.51	–0.33	2.75
17H-4, 32–34	163.81	–0.19	2.53
17H-4, 62–64	164.11	0.01	2.53
17H-4, 92–94	164.41	0.02	2.49
17H-4, 122–124	164.71	–0.11	2.46
17H-5, 2–4	165.03	–0.25	2.56
17H-5, 32–34	165.33	–0.28	2.70
17H-5, 62–64	165.63	–0.27	2.70
17H-5, 92–94	165.93	–0.49	2.79
17H-5, 122–124	166.23	–0.34	2.97
18H-2, 62–64	172.53	–0.23	2.61
18H-2, 92–94	172.83	–0.38	2.76
18H-2, 122–124	173.13		
18H-3, 2–4	173.44	–0.26	2.48
18H-3, 32–34	173.74	–0.15	2.34
18H-3, 62–64	174.04	–0.22	2.46
18H-3, 92–94	174.34	–0.26	2.51
18H-3, 122–124	174.64	–0.32	2.56
18H-4, 2–4	174.95	–0.38	2.50
18H-4, 32–34	175.25	–0.43	2.57
18H-4, 62–64	175.55	–0.18	2.54
18H-4, 92–94	175.85		
18H-4, 122–124	176.15	–0.29	2.28
18H-5, 2–4	176.47	–0.36	2.41
18H-5, 32–34	176.77	–0.40	2.69
18H-5, 62–64	177.07	–0.39	2.51
18H-5, 92–94	177.37	–0.46	2.61
18H-5, 122–124	177.67	–0.60	2.72
19H-4, 2–4	183.77	–0.16	2.70
19H-4, 32–34	184.07	–0.19	2.53
19H-4, 62–64	184.37	–0.46	2.60
19H-4, 92–94	184.67	–0.32	2.59
19H-4, 122–124	184.97	–0.32	2.62
19H-5, 2–4	185.28	–0.25	2.67
19H-5, 32–34	185.58	–0.25	2.74
19H-5, 62–64	185.88	–0.51	2.68
19H-5, 92–94	186.18	–0.36	2.80
19H-5, 122–124	186.48	–0.36	2.64
19H-6, 2–4	186.80	–0.21	2.91
19H-6, 32–34	187.10	–0.22	2.34
19H-6, 62–64	187.40	–0.30	2.18
19H-6, 92–94	187.70	–0.17	2.51
19H-6, 122–124	188.00	–0.06	2.53
19H-7, 2–4	188.32	–0.51	2.37
19H-7, 32–34	188.62	–0.14	2.41
19H-7, 62–64	188.92	–0.42	2.35
20X-1, 2–4	189.58	–0.14	2.68
20X-1, 32–34	189.88		
20X-1, 62–64	190.18	–0.03	2.51
20X-1, 92–94	190.48	–0.09	2.31
20X-1, 122–124	190.78	–0.18	2.57
20X-2, 2–4	191.09	–0.43	2.45
20X-2, 32–34	191.39	–0.33	2.41
20X-2, 62–64	191.69	–0.38	2.47
20X-2, 92–94	191.99	–0.43	2.36
20X-2, 122–124	192.29	–0.33	2.49
20X-3, 2–4	192.60	–0.36	2.39
20X-3, 32–34	192.90	–0.27	2.53
20X-3, 62–64	193.20	–0.27	2.42
20X-3, 92–94	193.50	–0.73	2.51
20X-3, 122–124	193.80	–0.49	2.67
20X-4, 2–4	194.10	–0.41	2.79
20X-4, 32–34	194.40	–0.40	2.76
20X-4, 62–64	194.70	–0.60	2.74
20X-4, 92–94	195.00	–0.55	2.48
20X-4, 122–124	195.30	–0.39	2.81
20X-5, 2–4	195.61	–0.57	1.62
20X-5, 32–34	195.91	–0.46	2.86
20X-5, 62–64	196.21		
20X-5, 92–94	196.51	–0.46	2.13
20X-5, 122–124	196.81	–0.58	3.18
20X-6, 2–4	197.12	–0.30	2.95
20X-6, 32–34	197.42	–0.55	2.81
20X-6, 62–64	197.72	–0.50	3.08
20X-6, 92–94	198.02	–0.50	2.81
20X-6, 122–124	198.32	–0.41	2.86
20X-7, 2–4	198.64	–0.33	2.75
20X-7, 32–34	198.94	–0.56	2.58
21X-1, 2–4	195.24	–0.76	2.58
21X-1, 32–34	195.54	–0.55	2.53
21X-1, 62–64	195.84	–0.33	2.61
21X-1, 92–94	196.14	–0.56	2.53
21X-1, 122–124	196.44		
21X-2, 2–4	196.76		
21X-2, 32–34	197.06	–0.52	2.32
21X-2, 62–64	197.36	–0.47	2.47
21X-2, 92–94	197.66	–0.37	2.48
21X-2, 122–124	197.96	–0.57	2.26
21X-3, 2–4	198.27	–0.63	2.42
21X-3, 32–34	198.57	–0.48	2.36
21X-3, 62–64	198.87	–0.54	2.44
21X-3, 92–94	199.17	–0.55	2.54
21X-3, 122–124	199.47	–0.56	2.55
21X-4, 2–4	199.78	–0.65	2.29
21X-4, 32–34	200.08	–0.72	2.60
21X-4, 62–64	200.38	–0.61	2.33
21X-4, 92–94	200.68	–0.41	2.71
21X-4, 122–124	200.98	–0.58	2.51
21X-5, 2–4	201.30		
21X-5, 32–34	201.60	–0.45	2.57
21X-5, 62–64	201.90	–0.67	2.57
21X-5, 92–94	202.20	–0.55	2.53
21X-5, 122–124	202.50	–0.52	2.51
21X-6, 2–4	202.81	–0.72	2.64
21X-6, 32–34	203.11		

Appendix Table AT3 (continued).

Core, section, interval (cm)	Depth (mcd)	*Cibicidoides wuellerstorfi* $\delta^{13}C$ (‰)	*Cibicidoides wuellerstorfi* $\delta^{18}O$ (‰)
21X-6, 62–64	203.41	–0.50	2.76
21X-6, 92–94	203.71	–0.40	2.44
21X-7, 2–4	203.82	–0.62	1.83
21X-7, 32–34	204.12	–0.71	2.26
21X-7, 62–64	204.42	–0.84	2.37
22X-1, 2–4	205.80	–0.35	2.55
22X-1, 32–34	206.10	–0.38	2.52
22X-1, 62–64	206.40	–0.26	2.38
22X-1, 92–94	206.70	–0.02	2.41
22X-1, 122–124	207.00		
22X-2, 2–4	207.31	–0.37	2.26
22X-2, 32–34	207.61	–0.15	2.35
22X-2, 62–64	207.91	–0.22	2.42
22X-2, 92–94	208.21	–0.29	2.37
22X-2, 122–124	208.51	–0.60	2.38
22X-3, 2–4	208.82	–0.41	2.61
22X-3, 32–34	209.12		
22X-3, 62–64	209.42	–0.07	2.30
22X-3, 92–94	209.72		
22X-3, 122–124	210.02	–0.42	2.67
22X-4, 2–4	210.33	–0.23	2.63
22X-4, 32–34	210.63	–0.34	2.61
22X-4, 66–68	210.97	–0.43	2.58
22X-4, 92–94	211.23	–0.40	2.52
22X-4, 122–124	211.53	–0.80	2.56
22X-5, 2–4	211.84	–0.30	2.78
22X-5, 32–34	212.14		
22X-5, 62–64	212.44	–0.53	2.59
22X-5, 92–94	212.74	–0.64	2.29
22X-5, 122–124	213.04	–0.47	2.65
22X-6, 2–4	213.35	–0.44	2.78
22X-6, 32–34	213.65	–0.63	2.64
22X-6, 62–64	213.95	–0.64	2.83
22X-6, 92–94	214.25		
22X-6, 122–124	214.55	–0.58	2.64
22X-7, 2–4	214.86	–0.58	2.73
22X-7, 32–34	215.16	–0.60	2.77
23X-1, 2–4	216.36	–0.11	2.16
23X-1, 32–34	216.66		
23X-1, 62–64	216.96	–0.08	2.61
23X-1, 92–94	217.26	–0.32	1.69
23X-1, 122–124	217.56	–0.13	2.18
23X-2, 2–4	217.88	–0.17	2.51
23X-2, 32–34	218.18		
23X-2, 62–64	218.48	–0.51	2.46
23X-2, 92–94	218.78	–0.37	2.41
23X-2, 122–124	219.08	–0.14	2.50
23X-3, 2–4	219.39	–0.16	2.45
23X-3, 32–34	219.69	–0.30	2.41
23X-3, 62–64	219.99	–0.42	1.19
23X-3, 92–94	220.29	–0.21	2.50
23X-3, 122–124	220.59	–0.11	2.38
23X-4, 2–4	220.90	0.09	2.60
23X-4, 32–34	221.20	–0.15	2.21
23X-4, 62–64	221.50	–0.26	2.34
23X-4, 92–94	221.80	–0.31	1.44
23X-4, 122–124	222.10	0.00	2.48
23X-5, 2–4	222.41	0.11	2.15
23X-5, 32–34	222.71	0.07	2.45
23X-5, 62–64	223.01	–0.03	2.39
23X-5, 92–94	223.31	–0.03	2.33
23X-5, 122–124	223.61	0.11	2.37
23X-6, 2–4	223.92	–0.03	2.26
23X-6, 32–34	224.22	0.14	2.57
23X-6, 62–64	224.52	0.08	2.39
23X-6, 92–94	224.82	–0.14	1.85
23X-6, 122–124	225.12	–0.06	2.40
23X-7, 2–4	225.24	–0.11	2.29
23X-7, 32–34	225.54	–0.20	2.46

Core, section, interval (cm)	Depth (mcd)	*Cibicidoides wuellerstorfi* $\delta^{13}C$ (‰)	*Cibicidoides wuellerstorfi* $\delta^{18}O$ (‰)
24X-1, 2–4	226.92	0.32	2.30
24X-1, 32–34	227.22	–0.03	2.41
24X-1, 62–64	227.52	0.10	2.42
24X-1, 92–94	227.82	0.18	2.47
24X-1, 122–124	228.12	0.26	2.41
24X-2, 2–4	228.42	–0.11	2.33
24X-2, 32–34	228.72	–0.05	2.45
24X-2, 62–64	229.02		
24X-2, 92–94	229.32	–0.28	2.33
24X-2, 122–124	229.62	–0.05	2.40
24X-3, 2–4	229.92	0.02	2.32
24X-3, 32–34	230.22	–0.14	2.40
24X-3, 62–64	230.52	–0.18	2.47
24X-3, 92–94	230.82	–0.19	2.22
24X-3, 122–124	231.12	–0.33	2.50
24X-4, 2–4	231.42	–0.11	2.65
24X-4, 32–34	231.72	–0.20	2.68
24X-4, 62–64	232.02	–0.28	2.77
24X-4, 92–94	232.32	–0.30	2.38
24X-4, 122–124	232.62	–0.11	2.59
24X-5, 2–4	232.92	–0.09	2.75
24X-5, 32–34	233.22	–0.12	2.55
24X-5, 62–64	233.52	–0.26	2.73
24X-5, 92–94	233.82	–0.14	2.58
24X-5, 122–124	234.12	–0.15	2.47
24X-6, 2–4	234.42	–0.30	2.48
24X-6, 32–34	234.72	–0.16	2.79
24X-6, 62–64	235.02	–0.22	2.63
24X-6, 92–94	235.32	–0.03	2.59
24X-6, 122–124	235.62	–0.40	2.60
25X-1, 2–4	237.08	–0.45	2.88
25X-1, 32–34	237.38	–0.54	2.68
25X-1, 62–64	237.68	–0.42	2.93
25X-1, 92–94	237.98	–0.48	2.80
25X-1, 122–124	238.28	–0.50	2.84
25X-2, 2–4	238.48	–0.30	2.76
25X-2, 32–34	238.78	–0.55	2.86
25X-2, 62–64	239.08	–0.38	2.71
25X-2, 92–94	239.38	–0.40	2.60
25X-2, 122–124	239.68	–0.45	2.61
25X-3, 2–4	239.98	–0.41	2.49
25X-3, 32–34	240.28	–0.34	2.25
25X-3, 62–64	240.58	–0.46	2.52
25X-3, 92–94	240.88	–0.40	2.46
25X-3, 122–124	241.18	–0.27	2.33
25X-4, 2–4	241.50	–0.35	2.35
25X-4, 32–34	241.80	–0.22	2.34
25X-4, 62–64	242.10	–0.21	2.42
25X-4, 92–94	242.40	–0.38	2.44
25X-4, 122–124	242.70	–0.50	2.27
25X-5, 2–4	243.00	–0.41	2.42
25X-5, 32–34	243.30	–0.14	2.39
25X-5, 62–64	243.60	–0.15	2.51
25X-5, 92–94	243.90	–0.35	2.43
25X-5, 122–124	244.20	–0.23	2.39
25X-6, 2–4	244.50	–0.17	2.50
25X-6, 32–34	244.80	–0.27	2.40
25X-6, 62–64	245.10	–0.30	2.34
25X-6, 92–94	245.40	–0.37	2.36
25X-6, 122–124	245.70	–0.21	2.41
25X-7, 2–4	246.01	–0.27	2.42
25X-7, 32–34	246.31	–0.33	2.06
26X-1, 2–4	247.54	–0.56	2.24
26X-1, 32–34	247.84	–0.45	2.48
26X-1, 62–64	248.14	–0.47	2.66
26X-1, 92–94	248.44	–0.43	2.43
26X-1, 122–124	248.74	–0.42	2.64
26X-2, 2–4	249.04	–0.44	2.55
26X-2, 32–34	249.34	–0.40	2.72

Appendix Table AT3 (continued).

Core, section, interval (cm)	Depth (mcd)	*Cibicidoides wuellerstorfi* $\delta^{13}C$ (‰)	*Cibicidoides wuellerstorfi* $\delta^{18}O$ (‰)
26X-2, 62–64	249.64	–0.41	2.34
26X-2, 92–94	249.94	–0.40	2.62
26X-2, 122–124	250.24	–0.54	2.62
26X-3, 2–4	250.55	–0.47	2.74
26X-3, 32–34	250.85	–0.44	2.62
26X-3, 62–64	251.15	–0.45	2.58
26X-3, 92–94	251.45	–0.51	2.54
26X-3, 122–124	251.75		
26X-4, 2–4	252.05	–0.31	2.49
26X-4, 32–34	252.35	–0.42	2.45
26X-4, 62–64	252.65	–0.18	2.48
26X-4, 92–94	252.95		
26X-4, 122–124	253.25	–0.34	2.39
26X-5, 2–4	253.56	–0.21	2.29
26X-5, 32–34	253.86	–0.16	2.30
26X-5, 62–64	254.16	–0.32	2.28
26X-5, 92–94	254.46	–0.41	2.25
26X-5, 122–124	254.76	–0.35	2.29
26X-6, 2–4	255.07	–0.21	2.33
26X-6, 32–34	255.37	–0.28	2.20
26X-6, 62–64	255.67	–0.20	2.34
26X-6, 92–94	255.97	–0.29	2.24
26X-6, 122–124	256.27	–0.26	2.20
26X-7, 2–4	256.58		
26X-7, 32–34	256.88	–0.20	2.32
27X-1, 2–4	257.70	–0.58	2.08
27X-1, 32–34	258.00		
27X-1, 62–64	258.30	–0.29	2.25
27X-1, 92–94	258.60		
27X-1, 122–124	258.90		
27X-2, 2–4	259.20		
27X-2, 32–34	259.50	–0.12	2.26
27X-2, 62–64	259.80	–0.21	2.36
27X-2, 92–94	260.10	–0.02	2.26
27X-2, 122–124	260.40	0.03	2.32
27X-3, 2–4	260.71	–0.04	2.39
27X-3, 32–34	261.01	–0.11	2.31
27X-3, 62–64	261.31	–0.24	2.11
27X-3, 92–94	261.61	–0.28	2.15
27X-3, 122–124	261.91	–0.03	2.34
27X-4, 2–4	262.21	–0.30	2.43
27X-4, 32–34	262.51	–0.48	2.22
27X-4, 62–64	262.81	–0.53	2.42
27X-4, 92–94	263.11	–0.21	2.10
27X-4, 122–124	263.41	–0.52	2.26
27X-5, 2–4	263.71		
27X-5, 32–34	264.01	–0.55	2.36
27X-5, 62–64	264.31	–0.10	2.47
27X-5, 92–94	264.61	–0.13	2.35
27X-5, 122–124	264.91	–0.29	2.28
27X-6, 2–4	265.22	–0.22	2.28
27X-6, 32–34	265.52		
27X-6, 62–64	265.82	–0.23	2.10
27X-6, 92–94	266.12	0.01	2.29
27X-6, 122–124	266.42	0.05	2.18
27X-7, 2–4	266.72		
27X-7, 32–34	267.02		
28X-1, 2–4	268.16	–0.19	2.30
28X-1, 32–34	268.46	–0.31	2.14
28X-1, 62–64	268.76	–0.14	2.13
28X-1, 92–94	269.06	–0.30	2.22
28X-1, 122–124	269.36		
28X-2, 2–4	269.66	–0.31	2.09
28X-2, 32–34	269.96	–0.28	2.19
28X-2, 62–64	270.26	–0.40	2.30
28X-2, 92–94	270.56	–0.31	2.32
28X-2, 122–124	270.86	–0.35	2.39
28X-3, 2–4	271.17	–0.33	2.54
28X-3, 32–34	271.47	–0.46	2.40
28X-3, 62–64	271.77	–0.19	2.60
28X-3, 92–94	272.07	–0.29	2.36
28X-3, 122–124	272.37		
28X-4, 2–4	272.68	–0.44	2.41
28X-4, 32–34	272.98	–0.18	2.29
28X-4, 62–64	273.28	–0.48	2.05
28X-4, 92–94	273.58		
28X-4, 122–124	273.88	–0.32	2.20
28X-5, 2–4	274.18	–0.07	2.43
28X-5, 32–34	274.48		
28X-5, 62–64	274.78		
28X-5, 92–94	275.08		
28X-5, 122–124	275.38	–0.25	2.07
28X-6, 2–4	275.68	–0.04	1.93
28X-6, 32–34	275.98		
28X-6, 62–64	276.28	–0.03	2.26
28X-6, 92–94	276.58	0.06	2.28
28X-7, 2–4	276.88	–0.12	2.24
28X-7, 32–34	277.18		
28X-7, 62–64	277.48	–0.34	2.19
29X-1, 2–4	278.62	–0.07	2.43
29X-1, 32–34	278.92		
29X-1, 62–64	279.22		
29X-1, 92–94	279.52	0.02	2.37
29X-1, 122–124	279.82	–0.05	2.47
29X-2, 2–4	280.12	0.03	2.48
29X-2, 32–34	280.42	0.03	2.36
29X-2, 62–64	280.72	–0.02	2.22
29X-2, 92–94	281.02	–0.05	2.17
29X-2, 122–124	281.32	–0.10	2.23
29X-3, 2–4	281.62	0.04	2.26
29X-3, 32–34	281.92	0.06	2.27
29X-3, 62–64	282.22	0.13	2.15
29X-3, 92–94	282.52	0.08	2.25
29X-3, 122–124	282.82	0.17	2.28
29X-4, 2–4	283.14	–0.10	2.14
29X-4, 32–34	283.44	0.07	2.11
29X-4, 62–64	283.74	0.10	2.07
29X-4, 92–94	284.04	0.00	2.13
29X-4, 122–124	284.34	–0.12	2.14
29X-5, 2–4	284.64		
29X-5, 32–34	284.94	–0.10	2.06
29X-5, 62–64	285.24	–0.16	2.24
29X-5, 92–94	285.54	–0.19	2.26
29X-5, 122–124	285.84	–0.11	2.35
29X-6, 2–4	286.15	–0.07	2.42
29X-6, 32–34	286.45	–0.15	2.46
29X-6, 62–64	286.75	–0.38	2.48
29X-6, 92–94	287.05	–0.34	2.55
29X-7, 2–4	287.15	–0.22	2.52
29X-7, 32–34	287.45	–0.09	2.36
29X-7, 62–64	287.75	–0.31	2.07
30X-1, 2–4	289.08	–0.20	2.43
30X-1, 22–24	289.28	0.07	2.20
30X-1, 42–44	289.48	0.09	2.07
30X-1, 62–64	289.68	–0.14	2.22
30X-1, 82–84	289.88	–0.03	2.28
30X-1, 102–104	290.08	–0.04	2.23
30X-1, 122–124	290.28	0.08	2.04
30X-1, 142–144	290.48	0.04	2.12
30X-2, 2–4	290.58	0.13	2.28
30X-2, 22–24	290.78	0.08	2.40
30X-2, 42–44	290.98	0.09	2.09
30X-2, 62–64	291.18	0.10	2.09
30X-2, 82–84	291.38	0.17	2.15
30X-2, 102–104	291.58	0.03	2.00
30X-2, 112–114	291.68	0.01	2.10
30X-2, 132–134	291.88	–0.01	1.95
30X-3, 2–4	292.08	0.09	2.25

Appendix Table AT3 (continued).

Core, section, interval (cm)	Depth (mcd)	*Cibicidoides wuellerstorfi* $\delta^{13}C$ (‰)	*Cibicidoides wuellerstorfi* $\delta^{18}O$ (‰)
30X-3, 22–24	292.28	0.18	2.18
30X-3, 42–44	292.48	0.15	2.34
30X-3, 62–64	292.68	0.17	2.20
30X-3, 82–84	292.88	0.10	2.18
30X-3, 102–104	293.08	–0.16	2.11
30X-3, 122–124	293.28	–0.40	2.28
30X-3, 142–144	293.48	–0.39	2.31
30X-4, 2–4	293.58	–0.39	2.46
30X-4, 22–24	293.78	–0.28	2.41
30X-4, 42–44	293.98	–0.35	2.56
30X-4, 62–64	294.18	–0.40	2.49
30X-4, 82–84	294.38	–0.32	2.41
30X-4, 102–104	294.58	–0.51	2.30
30X-4, 122–124	294.78	–0.16	2.30
30X-4, 142–144	294.98	–0.09	2.19
30X-5, 2–4	295.08	–0.17	2.15
30X-5, 22–24	295.28	–0.20	2.06
30X-5, 42–44	295.48	–0.25	2.06
30X-5, 62–64	295.68	–0.22	2.05
30X-5, 82–84	295.88	–0.03	1.91
30X-5, 102–104	296.08	–0.03	2.17
30X-5, 122–124	296.28	–0.12	2.35
30X-5, 142–144	296.48	–0.25	2.33
30X-6, 2–4	296.58	0.07	2.34
30X-6, 22–24	296.78	–0.08	2.28
30X-6, 42–44	296.98	0.10	2.21
30X-6, 62–64	297.18	–0.14	2.28
30X-6, 82–84	297.38	–0.06	2.15
30X-6, 102–104	297.58	0.00	2.17
30X-6, 122–124	297.78	–0.12	1.96
31X-1, 2–4	299.64	–0.05	2.13
31X-1, 22–24	299.84	–0.46	2.39
31X-1, 42–44	300.04	–0.40	2.28
31X-1, 62–64	300.24	–0.48	2.48
31X-1, 82–84	300.44	–0.26	2.29
31X-1, 102–104	300.64	–0.26	2.20
31X-1, 122–124	300.84	–0.14	2.06
31X-1, 142–144	301.04	–0.07	2.28
31X-2, 2–4	301.14	–0.13	2.09
31X-2, 22–24	301.34	–0.10	2.07
31X-2, 42–44	301.54	–0.04	2.11
31X-2, 62–64	301.74	–0.10	2.16
31X-2, 82–84	301.94	–0.10	2.16
31X-2, 102–104	302.14	–0.32	2.19
31X-2, 122–124	302.34	–0.25	2.23
31X-2, 142–144	302.54	–0.28	2.10
31X-3, 2–4	302.64	–0.30	2.15
31X-3, 22–24	302.84	–0.30	2.18
31X-3, 42–44	303.04	–0.37	2.14
31X-3, 62–64	303.24	–0.29	2.36
31X-3, 68–70	303.30		
31X-3, 82–84	303.44	–0.10	2.09
31X-3, 102–104	303.64	–0.22	2.00
31X-3, 122–124	303.84	–0.19	2.00
31X-3, 142–144	304.04	–0.43	2.13
31X-4, 2–4	304.14	–0.57	2.09
31X-4, 22–24	304.34	–0.23	2.14
31X-4, 42–44	304.54	–0.29	2.11
31X-4, 62–64	304.74	–0.22	2.17
31X-4, 82–84	304.94	–0.31	2.12
31X-4, 102–104	305.14	–0.17	2.15
31X-4, 122–124	305.34	–0.12	2.14
31X-4, 142–144	305.54	–0.24	2.21
31X-5, 2–4	305.64	–0.21	2.26
31X-5, 22–24	305.84	–0.20	2.38
31X-5, 42–44	306.04	0.05	2.20
31X-5, 62–64	306.24	–0.09	2.22
31X-5, 82–84	306.44	–0.07	2.23
31X-5, 102–104	306.64	0.02	2.28
31X-5, 122–124	306.84	–0.03	2.17
31X-5, 142–144	307.04	0.02	2.27
31X-6, 2–4	307.15	–0.11	2.16
31X-6, 22–24	307.35	–0.14	2.28
31X-6, 42–44	307.55	–0.20	2.38
31X-6, 62–64	307.75	–0.11	2.86
31X-6, 82–84	307.95	–0.28	2.37
31X-6, 102–104	308.15	–0.40	2.38
31X-6, 122–124	308.35	–0.39	2.41
31X-6, 142–144	308.55	–0.37	2.51
31X-7, 2–4	308.66	–0.32	2.39
31X-7, 22–24	308.86	–0.29	2.37
31X-7, 42–44	309.06	–0.42	2.43
32X-1, 2–4	310.10	–0.10	2.05
32X-1, 22–24	310.30	–0.20	2.12
32X-1, 42–44	310.50	–0.13	2.05
32X-1, 62–64	310.70	–0.13	2.29
32X-1, 82–84	310.90	–0.11	2.26
32X-1, 102–104	311.10	–0.11	2.32
32X-1, 122–124	311.30	0.05	2.31
32X-1, 142–144	311.50	–0.12	2.22
32X-2, 2–4	311.60	–0.12	2.06
32X-2, 22–24	311.80	–0.23	2.24
32X-2, 42–44	312.00	–0.26	2.11
32X-2, 62–64	312.20	–0.20	2.14
32X-2, 82–84	312.40	–0.27	2.25
32X-2, 102–104	312.60	–0.32	2.32
32X-2, 122–124	312.80	–0.38	2.21
32X-2, 142–144	313.00	–0.40	2.39
32X-3, 2–4	313.12	–0.37	2.40
32X-3, 22–24	313.32	–0.41	2.35
32X-3, 42–44	313.52	–0.31	2.47
32X-3, 62–64	313.72	–0.25	2.40
32X-3, 82–84	313.92	–0.29	2.37
32X-3, 102–104	314.12	–0.39	2.34
32X-3, 122–124	314.32	–0.25	2.45
32X-3, 142–144	314.52	–0.18	2.42
32X-4, 2–4	314.62	–0.25	2.29
32X-4, 22–24	314.82	–0.17	2.48
32X-4, 42–44	315.02	–0.08	2.04
32X-4, 62–64	315.22	–0.06	2.14
32X-4, 82–84	315.42	–0.02	1.66
32X-4, 102–104	315.62	–0.02	2.15
32X-4, 122–124	315.82	–0.09	2.17
32X-4, 142–144	316.02	0.01	2.15
32X-5, 2–4	316.12	–0.13	1.87
32X-5, 22–24	316.32	–0.04	2.22
32X-5, 42–44	316.52	–0.10	2.17
32X-5, 62–64	316.72	–0.04	2.07
32X-5, 82–84	316.92	0.02	2.15
32X-5, 102–104	317.12	–0.03	2.20
32X-5, 122–124	317.32	–0.03	2.05
32X-5, 142–144	317.52	–0.16	2.21
32X-6, 2–4	317.62	–0.10	2.21
32X-6, 22–24	317.82	–0.05	2.20
32X-6, 42–44	318.02	–0.08	2.21
33X-1, 2–4	320.66	–0.28	2.06
33X-1, 22–24	320.86	–0.30	2.11
33X-1, 42–44	321.06	–0.24	2.19
33X-1, 62–64	321.26	–0.20	2.10
33X-1, 82–84	321.46	–0.20	2.10
33X-1, 102–104	321.66	–0.26	2.21
33X-1, 122–124	321.86	–0.10	2.25
33X-1, 142–144	322.06	–0.10	2.16
33X-2, 2–4	322.16	0.00	2.15
33X-2, 22–24	322.36	–0.13	2.07
33X-2, 42–44	322.56	–0.19	2.03
33X-2, 62–64	322.76	–0.14	2.11
33X-2, 82–84	322.96	–0.16	1.95

Appendix Table AT3 (continued).

Core, section, interval (cm)	Depth (mcd)	*Cibicidoides wuellerstorfi* $\delta^{13}C$ (‰)	*Cibicidoides wuellerstorfi* $\delta^{18}O$ (‰)
33X-2, 102–104	323.16	–0.15	2.20
33X-2, 122–124	323.36	–0.08	2.21
33X-2, 142–144	323.56	–0.07	2.12
33X-3, 2–4	323.67	–0.15	2.08
33X-3, 22–24	323.87	–0.12	2.14
33X-3, 42–44	324.07	–0.17	2.21
33X-3, 62–64	324.27	–0.35	2.21
33X-3, 82–84	324.47	–0.21	2.18
33X-3, 102–104	324.67	–0.16	2.25
33X-3, 122–124	324.87	–0.08	2.36
33X-4, 2–4	325.16	–0.11	2.29
33X-4, 22–24	325.36	–0.11	2.12
33X-4, 42–44	325.56	–0.14	2.14
33X-4, 62–64	325.76	–0.21	2.10
33X-4, 82–84	325.96	–0.13	2.20
33X-4, 102–104	326.16	–0.08	2.11
33X-4, 122–124	326.36	–0.11	2.01
33X-4, 142–144	326.56	–0.08	2.10
33X-5, 2–4	326.66	–0.24	2.12
33X-5, 22–24	326.86	–0.12	2.08
33X-5, 42–44	327.06	–0.14	2.19
33X-5, 62–64	327.26	–0.23	2.06
33X-5, 82–84	327.46	–0.20	2.23
33X-5, 102–104	327.66	–0.21	2.19
33X-5, 122–124	327.86	–0.36	2.19
33X-5, 142–144	328.06	–0.36	2.29
33X-6, 2–4	328.17	–0.24	2.00
33X-6, 22–24	328.37	–0.37	1.99
33X-6, 42–44	328.57	–0.28	2.25
33X-6, 62–64	328.77	–0.42	2.19
33X-6, 82–84	328.97	–0.43	2.37
33X-6, 102–104	329.17	–0.34	2.00
33X-6, 122–124	329.37	–0.41	2.12
33X-6, 142–144	329.57	–0.47	2.06
33X-7, 2–4	329.68	–0.34	1.92
33X-7, 20–22	329.86	–0.43	2.11
33X-7, 42–44	330.08	–0.22	2.06
34X-1, 2–4	331.12		
34X-1, 22–24	331.32	–0.36	1.92
34X-1, 42–44	331.52		
34X-1, 62–64	331.72	–0.36	2.08
34X-1, 82–84	331.92	–0.44	2.16
34X-1, 102–104	332.12	–0.41	2.22
34X-1, 122–124	332.32	–0.36	2.29
34X-1, 142–144	332.52	–0.27	2.26
34X-2, 2–4	332.62	–0.21	2.18
34X-2, 22–24	332.82	–0.08	1.95
34X-2, 42–44	333.02	–0.20	2.14
34X-2, 62–64	333.22	–0.15	2.10
34X-2, 82–84	333.42	–0.22	2.13
34X-2, 102–104	333.62	–0.27	2.13
34X-2, 122–124	333.82	–0.01	2.30
34X-2, 142–144	334.02	–0.13	2.27
34X-3, 2–4	334.13	–0.25	2.06
34X-3, 22–24	334.33	–0.23	2.18
34X-3, 42–44	334.53	–0.29	2.11
34X-3, 62–64	334.73	–0.22	2.25
34X-3, 82–84	334.93	–0.46	2.03
34X-3, 102–104	335.13	–0.17	2.12
34X-3, 122–124	335.33	–0.20	2.07
34X-3, 142–144	335.53	–0.33	2.10
34X-4, 2–4	335.63		
34X-4, 22–24	335.83		
34X-4, 42–44	336.03	–0.27	2.10
34X-4, 62–64	336.23	–0.21	2.19
34X-4, 82–84	336.43	–0.24	2.02
34X-4, 102–104	336.63	–0.26	2.12
34X-4, 122–124	336.83	–0.27	2.05
34X-4, 142–144	337.03	–0.13	2.21
34X-5, 2–4	337.14	–0.24	1.96
34X-5, 22–24	337.34	–0.06	2.30
34X-5, 42–44	337.54	0.03	2.16
34X-5, 62–64	337.74	0.01	2.32
34X-5, 82–84	337.94	–0.07	2.10
34X-5, 102–104	338.14	–0.22	2.15
34X-5, 122–124	338.34		
34X-5, 142–144	338.54	–0.03	2.08
34X-6, 2–4	338.64	–0.27	2.19
34X-6, 22–24	338.84	–0.21	2.34
34X-6, 42–44	339.04	–0.12	2.04
34X-6, 62–64	339.24	0.04	2.16
34X-6, 82–84	339.44	0.07	2.08
34X-6, 102–104	339.64		
34X-6, 122–124	339.84	0.02	2.14
34X-6, 142–144	340.04	0.01	2.22
34X-7, 2–4	340.15	0.01	2.19
34X-7, 22–24	340.35	–0.10	2.16
34X-7, 42–44	340.55	–0.18	2.16
35X-1, 2–4	341.58		
35X-1, 22–24	341.78	0.01	2.23
35X-1, 42–44	341.98	–0.18	1.98
35X-1, 62–64	342.18		
35X-1, 82–84	342.38	–0.08	2.15
35X-1, 102–104	342.58	–0.23	2.19
35X-1, 122–124	342.78	–0.23	2.31
35X-1, 142–144	342.98	–0.25	2.21
35X-2, 2–4	343.09	–0.33	2.17
35X-2, 22–24	343.29	–0.31	2.31
35X-2, 42–44	343.49	–0.18	2.49
35X-2, 62–64	343.69	–0.25	2.26
35X-2, 82–84	343.89	–0.17	2.38
35X-2, 102–104	344.09	–0.27	2.13
35X-2, 122–124	344.29	–0.18	2.33
35X-2, 142–144	344.49		
35X-3, 2–4	344.60	–0.10	2.26
35X-3, 22–24	344.80	–0.19	2.38
35X-3, 42–44	345.00	0.01	2.24
35X-3, 62–64	345.20		
35X-3, 82–84	345.40	–0.16	2.15
35X-3, 102–104	345.60	–0.13	2.13
35X-3, 122–124	345.80	–0.17	2.15
35X-3, 142–144	346.00	–0.05	1.99
35X-4, 2–4	346.11	–0.20	2.08
35X-4, 22–24	346.31	–0.11	2.14
35X-4, 42–44	346.51	–0.18	1.95
35X-4, 62–64	346.71	–0.14	2.13
35X-4, 82–84	346.91	–0.16	2.15
35X-4, 102–104	347.11	–0.17	2.25
36X-1, 2–3	352.14	–0.21	2.20
36X-1, 22–23	352.34	–0.20	2.26
36X-1, 42–43	352.54	–0.21	2.26
36X-1, 62–63	352.74	–0.11	2.21
36X-1, 82–83	352.94	–0.30	2.07
36X-1, 102–103	353.14	–0.29	2.19
36X-1, 122–123	353.34	–0.32	2.36
36X-1, 142–143	353.54	–0.27	2.27
36X-2, 2–3	353.65	–0.36	2.29
36X-2, 22–23	353.85	–0.18	2.36
36X-2, 42–43	354.05	–0.24	2.12
36X-2, 62–63	354.25	–0.15	2.23
36X-2, 82–83	354.45	–0.09	2.18
36X-2, 102–103	354.65		
36X-2, 122–123	354.85	–0.23	2.24
36X-2, 142–143	355.05	–0.21	1.98
36X-3, 2–4	355.16	–0.43	1.41
36X-3, 22–24	355.36		
36X-3, 42–44	355.56	–0.30	2.17
36X-3, 62–64	355.76	–0.51	1.98

Appendix Table AT3 (continued).

Core, section, interval (cm)	Depth (mcd)	*Cibicidoides wuellerstorfi* $\delta^{13}C$ (‰)	*Cibicidoides wuellerstorfi* $\delta^{18}O$ (‰)
36X-3, 82–84	355.96	–0.49	2.12
36X-3, 102–104	356.16	–0.42	2.15
36X-3, 122–124	356.36	–0.45	2.25
36X-3, 142–144	356.56	–0.55	2.57
36X-4, 2–4	356.66	–0.42	2.53
36X-4, 22–24	356.86		
36X-4, 42–44	357.06	–0.29	2.45
36X-4, 62–64	357.26	–0.28	2.46
36X-4, 82–84	357.46	–0.26	2.21
36X-4, 102–104	357.66	–0.19	2.08
36X-4, 122–124	357.86	–0.41	2.36
36X-4, 142–144	358.06	–0.29	2.23
36X-6, 2–4	359.69	–0.24	2.11
36X-6, 22–24	359.89		
36X-6, 42–44	360.09	–0.28	2.09
36X-6, 62–64	360.29	–0.43	2.20
36X-6, 82–84	360.49		
36X-6, 102–104	360.69		
36X-6, 122–124	360.89	–0.43	2.17
36X-6, 142–144	361.09	–0.38	2.15
36X-7, 2–4	361.21	–0.38	2.39
36X-7, 22–24	361.41	–0.36	2.33
36X-7, 42–44	361.61	–0.33	2.29
37X-1, 2–4	362.60	–0.44	2.16
37X-1, 22–24	362.80	–0.30	2.32
37X-1, 42–44	363.00	–0.33	2.24
37X-1, 62–64	363.20	–0.28	2.29
37X-1, 82–84	363.40	–0.21	2.39
37X-1, 102–104	363.60		
37X-1, 122–124	363.80	–0.21	2.35
37X-1, 142–144	364.00	–0.25	2.39
37X-2, 2–4	364.12	–0.14	2.26
37X-2, 22–24	364.32	–0.22	2.20
37X-2, 42–44	364.52	–0.09	1.97
37X-2, 62–64	364.72	–0.21	2.09
37X-2, 82–84	364.92	–0.17	2.20
37X-2, 102–104	365.12	–0.36	2.18
37X-2, 122–124	365.32	–0.29	2.07
37X-2, 142–144	365.52	–0.29	2.26
37X-3, 2–4	365.62	–0.35	2.32
37X-3, 22–24	365.82	–0.28	2.49
37X-3, 42–44	366.02	–0.26	2.48
37X-3, 62–64	366.22	–0.20	2.41
37X-3, 82–84	366.42	–0.10	2.36
37X-3, 102–104	366.62	–0.10	2.36
37X-3, 122–124	366.82	–0.20	1.93
37X-3, 142–144	367.02	0.04	2.21
37X-4, 2–4	367.13	–0.07	2.18
37X-4, 22–24	367.33		
37X-4, 42–44	367.53		
37X-4, 62–64	367.73	–0.02	2.23
37X-4, 82–84	367.93	–0.15	2.11
37X-4, 102–104	368.13	–0.22	2.18
37X-4, 122–124	368.33	–0.21	2.26
37X-4, 142–144	368.53	–0.17	2.09
37X-5, 2–4	368.63	–0.21	2.19
37X-5, 22–24	368.83	–0.31	2.18
37X-5, 42–44	369.03		
37X-5, 62–64	369.23	–0.44	2.35
37X-5, 82–84	369.43		
37X-5, 102–104	369.63	–0.41	2.62
37X-5, 122–124	369.83		
37X-5, 142–144	370.03	–0.07	2.43
37X-6, 2–4	370.13	–0.02	2.34
37X-6, 22–24	370.33	0.09	2.35
37X-6, 42–44	370.53		
37X-6, 62–64	370.73	–0.12	2.29
37X-6, 82–84	370.93	–0.03	2.60
37X-6, 102–104	371.13	–0.07	2.44
37X-6, 122–124	371.33	–0.08	2.38
37X-6, 142–144	371.53	–0.19	2.46
37X-7, 2–4	371.64	–0.08	2.67
37X-7, 22–24	371.84	0.07	2.17
37X-7, 42–44	372.04		
38X-1, 2–4	373.06	–0.20	2.07
38X-1, 22–24	373.26	–0.42	2.26
38X-1, 42–44	373.46	–0.15	2.54
38X-1, 62–64	373.66	–0.10	2.15
38X-1, 82–84	373.86	–0.10	2.21
38X-1, 102–104	374.06	–0.29	2.37
38X-1, 122–124	374.26	–0.23	2.48
38X-1, 142–144	374.46	–0.41	2.56
38X-2, 2–4	374.57		
38X-2, 22–24	374.77		
38X-2, 42–44	374.97	–0.30	2.85
38X-2, 62–64	375.17		
38X-2, 82–84	375.37	–0.03	2.28
38X-2, 102–104	375.57	0.00	2.22
38X-2, 122–124	375.77	0.02	2.43
38X-2, 142–144	375.97	0.04	2.23
38X-3, 2–4	376.08	–0.17	2.32
38X-3, 22–24	376.28	–0.23	2.36
38X-3, 42–44	376.48	–0.19	2.30
38X-3, 62–64	376.68	–0.23	2.39
38X-3, 82–84	376.88		
38X-3, 102–104	377.08	–0.35	2.29
38X-3, 122–124	377.28	–0.33	2.25
38X-3, 142–144	377.48	–0.37	2.40
38X-4, 2–4	377.57	–0.38	2.33
38X-4, 22–24	377.77	–0.46	2.55
38X-4, 42–44	377.97	–0.53	2.57
38X-4, 62–64	378.17		
38X-4, 82–84	378.37	–0.60	2.68
38X-4, 102–104	378.57	–0.51	2.22
38X-4, 122–124	378.77	–0.57	2.50
38X-4, 142–144	378.97	–0.57	2.33
38X-5, 2–4	379.07	–0.56	2.39
38X-5, 22–24	379.27		
38X-5, 42–44	379.47		
38X-5, 62–64	379.67	–0.25	2.50
38X-5, 82–84	379.87	–0.17	2.06
38X-5, 102–104	380.07	–0.21	2.54
38X-5, 122–124	380.27	–0.20	2.31
38X-5, 142–144	380.47	–0.13	2.17
38X-6, 2–4	380.58	–0.10	2.26
38X-6, 22–24	380.78	–0.21	2.17
38X-6, 42–44	380.98	–0.20	2.46
38X-6, 62–64	381.18	–0.12	2.20
38X-6, 82–84	381.38	–0.16	2.23
38X-6, 102–104	381.58	–0.24	2.21
38X-6, 122–124	381.78	–0.23	2.08
38X-6, 142–144	381.98	–0.34	2.35
38X-7, 2–4	382.09	–0.18	2.35
38X-7, 22–24	382.29	–0.40	2.27
38X-7, 42–44	382.49	–0.48	2.24
39X-1, 2–4	383.52	–0.32	2.14
39X-1, 22–24	383.72	–0.69	2.00
39X-1, 42–44	383.92	–0.33	2.20
39X-1, 62–64	384.12	–0.36	2.17
39X-1, 82–84	384.32	–0.35	2.29
39X-1, 102–104	384.52	–0.33	2.25
39X-1, 122–124	384.72	–0.37	2.40
39X-1, 142–144	384.92	–0.38	2.33
39X-2, 2–4	385.03	–0.46	2.55
39X-2, 22–24	385.23	–0.53	2.57
39X-2, 42–44	385.43	–0.60	2.68
39X-2, 62–64	385.63	–0.51	2.22
39X-2, 82–84	385.83	–0.57	2.50
39X-2, 102–104	386.03	–0.57	2.33
39X-2, 122–124	386.23	–0.56	2.39

Appendix Table AT4. Benthic oxygen and carbon isotope data of Site 1241. (Continued on next eight pages.)

Core, section, interval (cm)	Depth (mcd)	*Cibicidoides wuellerstorfi* $\delta^{13}C$ (‰)	*Cibicidoides wuellerstorfi* $\delta^{18}O$ (‰)
202-1241A-			
7H-3, 10–12	61.55	–0.01	3.08
7H-3, 20–22	61.65	–0.16	3.03
7H-3, 30–32	61.75	–0.04	3.08
7H-3, 40–42	61.85	–0.06	3.04
7H-3, 50–52	61.95	–0.09	2.79
7H-3, 60–62	62.05	–0.02	2.80
7H-3, 70–72	62.15	–0.22	2.82
7H-3, 80–82	62.25	–0.11	2.84
7H-3, 90–92	62.35	–0.20	2.60
7H-3, 100–102	62.45	–0.39	2.86
7H-3, 110–112	62.55	–0.41	3.23
7H-3, 120–122	62.65	–0.50	3.05
7H-3, 130–132	62.75	–0.40	3.15
7H-3, 140–142	62.85	–0.19	3.22
7H-4, 0–2	62.94	0.01	2.87
7H-4, 10–12	63.04	–0.01	2.95
7H-4, 20–22	63.14	–0.06	3.05
7H-4, 30–32	63.24	–0.04	2.80
7H-4, 40–42	63.34	–0.10	2.92
7H-4, 50–52	63.44	–0.19	3.17
7H-4, 60–62	63.54	–0.15	2.98
7H-4, 70–72	63.64	–0.19	2.86
7H-4, 80–82	63.74	–0.21	3.30
7H-4, 90–92	63.84	–0.20	3.07
7H-4, 100–102	63.94	–0.29	3.52
7H-4, 110–112	64.04	–0.42	3.52
7H-4, 120–122	64.14	0.13	2.57
7H-4, 130–132	64.24	0.11	2.61
7H-4, 140–142	64.34	0.02	2.85
7H-5, 0–2	64.45	–0.14	2.93
7H-5, 10–12	64.55	0.02	2.98
7H-5, 20–22	64.65	–0.26	
7H-5, 30–32	64.75	–0.24	3.23
7H-5, 40–42	64.85	–0.48	3.40
7H-5, 50–52	64.95	–0.31	3.33
7H-5, 60–62	65.05	–0.26	3.39
7H-5, 70–72	65.15	–0.24	3.16
7H-5, 80–82	65.25	–0.06	3.40
7H-5, 90–92	65.35	–0.24	3.19
7H-5, 100–102	65.45	–0.38	3.03
7H-5, 110–112	65.55	–0.51	3.13
7H-5, 120–122	65.65	–0.51	3.35
7H-5, 130–132	65.75	–0.44	
7H-5, 140–142	65.85	–0.40	3.37
7H-6, 0–2	65.96	–0.34	3.24
7H-6, 10–12	66.06	–0.12	3.20
7H-6, 20–22	66.16	–0.11	3.18
7H-6, 30–32	66.26	0.02	3.20
7H-6, 40–42	66.36	–0.09	2.97
9H-3, 50–52	83.55	–0.62	2.81
9H-3, 60–62	83.65	–0.48	2.89
9H-3, 70–72	83.75	–0.64	2.93
9H-3, 80–82	83.85	–0.44	2.93
9H-3, 90–92	83.95	–0.32	2.48
9H-3, 100–102	84.05	–0.47	2.77
9H-3, 110–112	84.15	–0.17	2.86
9H-3, 120–122	84.25	–0.14	2.42
9H-3, 130–132	84.35	–0.26	2.57
9H-3, 140–142	84.45	–0.25	2.53
9H-4, 0–2	84.55	–0.19	
9H-4, 10–12	84.65	–0.27	2.53
9H-4, 20–22	84.75	–0.36	2.56
9H-4, 30–32	84.85	–0.22	2.76
9H-4, 40–42	84.95	–0.29	2.68
9H-4, 50–52	85.05	–0.32	2.57
9H-4, 60–62	85.15	–0.30	2.83
9H-4, 70–72	85.25	–0.40	2.89
9H-4, 80–82	85.35	–0.37	2.70
9H-4, 90–92	85.45	–0.18	2.75
9H-4, 100–102	85.55	–0.35	2.54
9H-4, 110–112	85.65	–0.20	2.66
9H-4, 120–122	85.75	–0.28	2.77
9H-4, 130–132	85.85	–0.14	2.64
9H-4, 140–142	85.95	–0.35	2.95
9H-5, 0–2	86.05	–0.41	2.74
9H-5, 10–12	86.15	–0.35	2.77
9H-5, 20–22	86.25	–0.31	2.74
9H-5, 30–32	86.35	–0.30	2.86
9H-5, 40–42	86.45	–0.16	2.82
9H-5, 50–52	86.55	–0.41	2.47
9H-5, 60–62	86.65	–0.17	2.60
9H-5, 70–72	86.75	–0.23	2.52
9H-5, 80–82	86.85	–0.14	2.40
9H-5, 90–92	86.95	–0.17	2.52
9H-5, 100–102	87.05	–0.33	2.53
9H-5, 110–112	87.15	–0.33	2.51
9H-5, 120–122	87.25	–0.30	2.43
9H-5, 130–132	87.35	–0.34	2.76
9H-5, 140–142	87.45	–0.18	2.48
9H-6, 0–2	87.56	–0.15	2.38
9H-6, 10–12	87.66	–0.37	2.34
9H-6, 20–22	87.76	–0.37	2.35
9H-6, 30–32	87.86	–0.31	2.33
9H-6, 40–42	87.96	–0.56	2.49
9H-6, 50–52	88.06	–0.38	2.65
9H-6, 60–62	88.16	–0.19	2.27
9H-6, 70–72	88.26	–0.58	2.15
9H-6, 80–82	88.36	–0.15	2.28
9H-6, 90–92	88.46	–0.18	2.38
9H-6, 100–102	88.56	–0.32	2.29
9H-6, 110–112	88.66	–0.20	2.30
9H-6, 120–122	88.76	–0.10	2.36
9H-6, 130–132	88.86	–0.13	2.59
9H-6, 140–142	88.96	–0.28	2.42
9H-7, 0–2	89.07	0.03	2.68
9H-7, 10–12	89.17	–0.20	2.24
10H-2, 10–12	92.22	–0.07	2.50
10H-2, 20–22	92.32	–0.09	2.37
10H-2, 30–32	92.42	–0.12	2.37
10H-2, 40–42	92.52	–0.04	2.34
10H-2, 50–52	92.62	0.04	2.65
10H-2, 60–62	92.72	–0.01	2.39
10H-2, 70–72	92.82	0.05	2.29
10H-2, 80–82	92.92	–0.02	2.27
10H-2, 90–92	93.02	0.05	2.37
10H-2, 100–102	93.12	0.08	2.45
10H-2, 110–112	93.22	–0.02	2.62
10H-2, 120–122	93.32	–0.16	2.41
10H-2, 130–132	93.42	–0.37	2.49
10H-2, 140–142	93.52	–0.20	2.42
10H-3, 0–2	93.62		2.28
10H-3, 10–12	93.72	–0.08	2.24
10H-3, 20–22	93.82	0.11	2.10
10H-3, 30–32	93.92	0.08	2.39
10H-3, 40–42	94.02	0.05	2.38
10H-3, 50–52	94.12	0.08	2.14
10H-3, 60–62	94.22	–0.05	2.27
10H-3, 70–72	94.32	–0.19	2.23
10H-3, 80–82	94.42	–0.13	2.46
10H-3, 90–92	94.52	–0.16	2.44
10H-3, 100–102	94.62	–0.20	2.66
10H-3, 110–112	94.72	–0.28	2.72
10H-3, 120–122	94.82	–0.33	2.81
10H-3, 130–132	94.92	–0.36	2.70
10H-3, 140–142	95.02	–0.14	2.72
10H-4, 0–2	95.12	–0.10	2.46
10H-4, 10–12	95.22	–0.03	2.34

Appendix Table AT4 (continued).

Core, section, interval (cm)	Depth (mcd)	*Cibicidoides wuellerstorfi* $\delta^{13}C$ (‰)	*Cibicidoides wuellerstorfi* $\delta^{18}O$ (‰)
10H-4, 20–22	95.32	0.15	2.25
10H-4, 30–32	95.42	–0.11	2.10
10H-4, 40–42	95.52	–0.11	2.39
10H-4, 50–52	95.62	–0.07	2.28
10H-4, 60–62	95.72	–0.18	2.31
10H-4, 70–72	95.82	–0.33	2.51
10H-4, 80–82	95.92	–0.35	2.55
10H-4, 90–92	96.02	–0.44	2.38
10H-4, 100–102	96.12	–0.27	2.62
10H-4, 110–112	96.22	–0.41	2.19
10H-4, 120–122	96.32	–0.16	2.57
10H-4, 130–132	96.42	–0.25	2.57
10H-4, 140–142	96.52	0.04	2.34
10H-5, 0–2	96.62	0.11	2.31
10H-5, 10–12	96.72	–0.02	2.18
10H-5, 20–22	96.82	0.11	2.14
10H-5, 30–32	96.92	0.18	2.30
10H-5, 40–42	97.02	0.14	2.31
10H-5, 50–52	97.12	–0.17	2.24
10H-5, 60–62	97.22	–0.11	2.39
10H-5, 70–72	97.32	–0.27	2.48
10H-5, 80–82	97.42	–0.48	2.32
10H-5, 90–92	97.52	–0.14	2.51
10H-5, 100–102	97.62	–0.31	2.76
10H-5, 110–112	97.72	–0.26	2.66
10H-5, 120–122	97.82	–0.18	2.28
10H-5, 130–132	97.92	–0.31	2.33
10H-5, 140–142	98.02	–0.16	2.15
10H-6, 0–2	98.12	–0.19	2.33
10H-6, 10–12	98.22	–0.14	2.26
10H-6, 20–22	98.32	0.07	2.35
10H-6, 30–32	98.42	0.04	2.40
10H-6, 40–42	98.52	0.10	2.23
10H-6, 50–52	98.62	0.08	2.42
10H-6, 60–62	98.72	–0.01	2.26
11H-4, 20–22	105.93	–0.04	2.45
11H-4, 30–32	106.03	–0.03	2.37
11H-4, 40–42	106.13	0.04	2.05
11H-4, 50–52	106.23	0.03	2.19
11H-4, 60–62	106.33	0.08	2.47
11H-4, 70–72	106.43	–0.15	2.49
11H-4, 80–82	106.53	–0.02	2.48
11H-4, 90–92	106.63	0.04	2.46
11H-4, 100–102	106.73	–0.13	2.42
11H-4, 110–112	106.83	–0.09	2.49
11H-4, 120–122	106.93	–0.14	2.53
11H-4, 130–132	107.03	–0.31	2.50
11H-4, 140–142	107.13	–0.17	2.69
11H-5, 0–2	107.24	–0.23	2.68
11H-5, 10–12	107.34	–0.16	2.85
11H-5, 20–22	107.44	–0.14	2.58
11H-5, 30–32	107.54	–0.02	2.35
11H-5, 40–42	107.64	–0.22	2.27
11H-5, 50–52	107.74	0.00	2.43
11H-5, 60–62	107.84	–0.04	2.35
11H-5, 70–72	107.94	0.00	2.42
11H-5, 80–82	108.04	–0.07	2.35
11H-5, 90–92	108.14	–0.21	2.29
11H-5, 100–102	108.24	–0.19	2.42
11H-5, 110–112	108.34	–0.22	2.46
12H-2, 140–142	115.01	–0.18	2.25
12H-3, 0–2	115.12	–0.35	2.17
12H-3, 10–12	115.22	–0.22	2.33
12H-3, 20–22	115.32	–0.32	2.15
12H-3, 30–32	115.42	–0.12	2.33
12H-3, 40–42	115.52	–0.12	2.46
12H-3, 50–52	115.62	–0.12	2.57
12H-3, 60–62	115.72	–0.10	2.48
12H-3, 70–72	115.82	–0.14	2.40
12H-3, 80–82	115.92	–0.24	2.36
12H-3, 90–92	116.02	–0.25	2.36
12H-3, 100–102	116.12	–0.46	2.44
12H-3, 110–112	116.22	–0.42	2.56
12H-3, 120–122	116.32	–0.30	2.53
12H-3, 130–132	116.42	–0.31	2.54
12H-3, 140–142	116.52	–0.17	2.37
12H-4, 0–2	116.63	–0.04	2.51
12H-4, 10–12	116.73	–0.02	2.27
12H-4, 20–22	116.83	–0.12	2.35
12H-4, 30–32	116.93	–0.11	2.39
12H-4, 40–42	117.03	–0.05	2.30
12H-4, 50–52	117.13	–0.08	2.34
12H-4, 60–62	117.23	–0.14	2.38
12H-4, 70–72	117.33	–0.09	2.50
12H-4, 80–82	117.43	–0.06	2.40
12H-4, 90–92	117.53	–0.17	2.22
12H-4, 100–102	117.63	–0.24	2.33
12H-4, 110–112	117.73		
12H-4, 120–122	117.83	–0.15	2.43
12H-4, 130–132	117.93	–0.21	2.45
12H-4, 140–142	118.03	–0.11	2.36
12H-5, 0–2	118.14	–0.18	2.55
12H-5, 10–12	118.24	–0.18	2.49
12H-5, 20–22	118.34	–0.03	2.53
12H-5, 30–32	118.44	–0.14	2.50
12H-5, 40–42	118.54	–0.23	2.36
12H-5, 50–52	118.64	–0.13	2.30
12H-5, 60–62	118.74	–0.21	2.15
12H-5, 70–72	118.84	–0.23	2.26
12H-5, 80–82	118.94	–0.30	2.33
12H-5, 90–92	119.04	–0.20	2.38
12H-5, 100–102	119.14	–0.39	2.34
12H-5, 110–112	119.24	–0.07	2.48
13H-3, 40–42	125.41	0.25	2.47
13H-3, 50–52	125.51	0.21	2.54
13H-3, 60–62	125.61	0.21	2.17
13H-3, 70–72	125.71	0.09	2.09
13H-3, 80–82	125.81		
13H-3, 90–92	125.91	0.21	2.29
13H-3, 100–102	126.01	0.08	2.28
13H-3, 110–112	126.11	0.08	2.06
13H-3, 120–122	126.21	–0.11	2.37
13H-3, 130–132	126.31	0.06	2.46
13H-3, 140–142	126.41	0.05	2.48
13H-4, 0–2	126.52	0.00	2.50
13H-4, 10–12	126.62	–0.02	2.56
13H-4, 20–22	126.72		
13H-4, 30–32	126.82	0.11	2.61
13H-4, 40–42	126.92	–0.02	2.41
13H-4, 50–52	127.02	–0.19	2.26
13H-4, 60–62	127.12	–0.12	2.43
13H-4, 70–72	127.22	–0.18	2.44
13H-4, 80–82	127.32	–0.05	2.24
13H-4, 90–92	127.42	–0.14	2.17
13H-4, 100–102	127.52	–0.33	2.46
13H-4, 110–112	127.62	–0.33	
13H-4, 120–122	127.72	–0.55	2.56
13H-4, 130–132	127.82	–0.20	2.63
13H-4, 140–142	127.92	–0.08	2.34
13H-5, 0–2	128.02	0.02	2.53
13H-5, 10–12	128.12	–0.05	2.58
13H-5, 20–22	128.22	0.00	2.48
13H-5, 30–32	128.32	–0.03	2.44
13H-5, 40–42	128.42	–0.16	2.44
13H-5, 50–52	128.52	–0.13	2.39
13H-5, 60–62	128.62	–0.13	2.43
13H-5, 70–72	128.72	–0.13	2.46
13H-5, 80–82	128.82	–0.20	2.44

Appendix Table AT4 (continued).

Core, section, interval (cm)	Depth (mcd)	*Cibicidoides wuellerstorfi* $\delta^{13}C$ (‰)	*Cibicidoides wuellerstorfi* $\delta^{18}O$ (‰)
13H-5, 90–92	128.92	–0.18	2.41
13H-5, 100–102	129.02	–0.32	2.56
13H-5, 110–112	129.12	–0.24	2.48
14H-1, 50–52	132.57	–0.02	2.29
14H-1, 60–62	132.67	–0.13	2.36
14H-1, 70–72	132.77	–0.11	2.23
14H-1, 80–82	132.87	–0.01	2.37
14H-1, 90–92	132.97	0.01	2.28
14H-1, 100–102	133.07	–0.06	2.22
14H-1, 110–112	133.17	0.00	2.31
14H-1, 120–122	133.27	–0.05	2.47
14H-1, 130–132	133.37	–0.08	2.36
14H-1, 140–142	133.47	–0.22	2.44
14H-2, 0–2	133.58	–0.31	2.47
14H-2, 10–12	133.68	–0.03	2.31
14H-2, 20–22	133.78	–0.04	2.49
14H-2, 30–32	133.88	–0.04	2.37
14H-2, 40–42	133.98	0.09	2.28
14H-2, 50–52	134.08	0.15	2.36
14H-2, 60–62	134.18	0.05	2.28
14H-2, 70–72	134.28	0.12	2.32
14H-2, 80–82	134.38	0.11	2.42
14H-2, 90–92	134.48	0.11	2.19
14H-2, 100–102	134.58	0.22	2.33
14H-2, 110–112	134.68	0.12	2.17
14H-2, 120–122	134.78	–0.15	2.27
14H-2, 130–132	134.88	0.09	2.37
14H-2, 140–142	134.98	–0.18	2.40
14H-3, 0–2	135.09	–0.01	2.56
14H-3, 10–12	135.19	–0.28	2.45
14H-3, 20–22	135.29	–0.22	2.48
14H-3, 30–32	135.39	–0.20	2.46
14H-3, 40–42	135.49	–0.29	2.56
14H-3, 50–52	135.59	–0.27	2.66
14H-3, 60–62	135.69	–0.04	2.77
14H-3, 70–72	135.79	0.08	2.30
14H-3, 80–82	135.89	0.11	2.72
14H-3, 90–92	135.99	0.07	2.50
14H-3, 100–102	136.09	0.01	2.29
14H-3, 110–112	136.19	0.11	2.33
14H-3, 120–122	136.29	0.20	2.44
14H-3, 130–132	136.39	0.06	2.29
14H-3, 140–142	136.49	–0.05	2.40
14H-4, 0–2	136.60	–0.03	2.55
14H-4, 10–12	136.70	0.01	2.54
14H-4, 20–22	136.80	0.00	2.71
14H-4, 30–32	136.90	–0.10	2.60
14H-4, 40–42	137.00	–0.01	2.66
14H-4, 50–52	137.10	0.03	2.65
14H-4, 60–62	137.20	0.14	2.48
14H-4, 70–72	137.30	–0.18	2.37
14H-4, 80–82	137.40	0.07	2.31
14H-4, 90–92	137.50	0.05	2.36
14H-4, 100–102	137.60	–0.12	2.41
14H-4, 110–112	137.70	–0.17	2.43
14H-4, 120–122	137.80	–0.30	2.47
14H-4, 130–132	137.90	–0.15	2.58
14H-4, 140–142	138.00	–0.45	2.50
14H-5, 0–2	138.11	–0.27	2.62
14H-5, 10–12	138.21	–0.32	2.62
14H-5, 20–22	138.31	–0.22	2.56
14H-5, 30–32	138.41	–0.30	2.49
14H-5, 40–42	138.51	–0.14	2.44
14H-5, 50–52	138.61	–0.06	2.62
14H-5, 60–62	138.71	–0.08	2.52
14H-5, 70–72	138.81	–0.01	2.47
14H-5, 80–82	138.91	0.05	2.32
14H-5, 90–92	139.01	–0.02	2.39
14H-5, 100–102	139.11	0.00	2.40
14H-5, 110–112	139.21	0.00	2.48
14H-5, 120–122	139.31	–0.12	2.38
14H-5, 130–132	139.41	–0.11	2.38
14H-5, 140–142	139.51	–0.22	2.39
14H-6, 0–2	139.62	–0.41	2.60
14H-6, 10–12	139.72	–0.38	2.70
14H-6, 20–22	139.82	–0.48	2.75
14H-6, 30–32	139.92	–0.54	2.85
14H-6, 40–42	140.02	–0.65	2.79
14H-6, 50–52	140.12	–0.33	2.48
14H-6, 60–62	140.22	–0.49	2.70
14H-6, 70–72	140.32	–0.36	2.57
15H-3, 0–2	145.14	–0.29	2.47
15H-3, 10–12	145.24	–0.07	2.24
15H-3, 20–22	145.34	–0.14	2.28
15H-3, 30–32	145.44	–0.28	2.31
15H-3, 40–42	145.54	–0.08	2.48
15H-3, 50–52	145.64	–0.04	2.29
15H-3, 60–62	145.74	0.16	2.47
15H-3, 70–72	145.84	–0.02	2.39
15H-3, 80–82	145.94	0.05	2.22
15H-3, 90–92	146.04	–0.15	2.27
15H-3, 100–102	146.14	–0.15	2.23
15H-3, 110–112	146.24	–0.08	2.25
15H-3, 120–122	146.34	–0.34	2.16
15H-3, 130–132	146.44	–0.26	2.16
15H-3, 140–142	146.54	–0.40	2.01
15H-4, 0–2	146.65	–0.44	2.24
15H-4, 10–12	146.75	–0.15	2.31
15H-4, 20–22	146.85	–0.41	2.42
15H-4, 30–32	146.95	–0.56	2.46
15H-4, 40–42	147.05	–0.38	2.55
15H-4, 50–52	147.15	–0.23	2.28
15H-4, 60–62	147.25	–0.16	2.41
15H-4, 70–72	147.35	–0.18	2.35
15H-4, 80–82	147.45	–0.29	2.00
15H-4, 90–92	147.55	–0.16	2.31
15H-4, 100–102	147.65	0.00	2.16
15H-4, 110–112	147.75	–0.25	2.04
15H-4, 120–122	147.85	0.04	2.20
15H-4, 130–132	147.95	0.22	2.35
15H-4, 140–142	148.05	0.06	2.49
15H-5, 0–2	148.16	–0.32	2.33
15H-5, 10–12	148.26	–0.04	2.23
15H-5, 20–22	148.36		2.35
15H-5, 30–32	148.46	–0.08	2.20
15H-5, 40–42	148.56	–0.29	2.35
15H-5, 50–52	148.66	–0.34	2.24
15H-5, 60–62	148.76	–0.25	2.46
15H-5, 70–72	148.86	–0.30	2.45
15H-5, 80–82	148.96	–0.24	2.62
15H-5, 93–95	149.09	–0.24	2.41
15H-5, 100–102	149.16	–0.35	2.51
15H-5, 110–112	149.26	–0.17	2.50
15H-5, 120–122	149.36	–0.20	2.42
15H-5, 130–132	149.46	–0.14	2.31
15H-5, 140–142	149.56	0.01	2.55
15H-6, 0–2	149.67		2.47
15H-6, 10–12	149.77	0.04	2.63
15H-6, 20–22	149.87	–0.11	2.48
15H-6, 30–32	149.97	0.01	2.44
15H-6, 40–42	150.07	–0.05	2.44
15H-6, 50–52	150.17	–0.04	2.36
15H-6, 60–62	150.27	–0.04	2.38
15H-6, 70–72	150.37	–0.16	2.52
15H-6, 80–82	150.47	–0.08	2.36
15H-6, 90–92	150.57	–0.07	2.51
15H-6, 100–102	150.67	–0.10	2.37
15H-6, 110–112	150.77	–0.03	2.55

Appendix Table AT4 (continued).

Core, section, interval (cm)	Depth (mcd)	*Cibicidoides wuellerstorfi* $\delta^{13}C$ (‰)	*Cibicidoides wuellerstorfi* $\delta^{18}O$ (‰)
15H-6, 120–122	150.87	–0.27	2.44
16H-4, 70–72	158.39	–0.19	2.04
16H-4, 80–82	158.49	0.03	1.97
16H-4, 90–92	158.59		
16H-4, 100–102	158.69	0.18	2.34
16H-4, 110–112	158.79	0.24	2.27
16H-4, 120–122	158.89		2.47
16H-4, 130–132	158.99	0.21	2.51
16H-4, 140–142	159.09	0.09	2.29
16H-5, 0–2	159.20	0.12	2.44
16H-5, 10–12	159.30	0.01	2.57
16H-5, 20–22	159.40		
16H-5, 30–32	159.50		
16H-5, 40–42	159.60		
16H-5, 50–52	159.70	0.07	2.53
16H-5, 60–62	159.80		
16H-5, 70–72	159.90	0.21	2.19
16H-5, 80–82	160.00		
16H-5, 90–92	160.10		
16H-5, 100–102	160.20	0.32	2.29
16H-5, 110–112	160.30	0.35	2.14
16H-5, 120–122	160.40	0.39	2.28
16H-5, 130–132	160.50	0.41	2.35
16H-5, 140–142	160.60	0.19	2.57
16H-6, 0–2	160.71	0.14	2.36
16H-6, 10–12	160.81		
16H-6, 20–22	160.91		
16H-6, 30–32	161.01	0.26	2.50
16H-6, 40–42	161.11	0.24	2.41
16H-6, 50–52	161.21	0.25	2.36
16H-6, 60–62	161.31	0.14	2.58
16H-6, 70–72	161.41		2.19
16H-6, 80–82	161.51	0.22	2.43
16H-6, 90–92	161.61	0.08	2.23
17H-4, 30–32	168.06	–0.20	2.87
17H-4, 45–47	168.21	–0.15	2.37
17H-4, 60–62	168.36		
17H-4, 75–77	168.51	–0.03	2.38
17H-4, 90–92	168.66	–0.02	2.61
17H-4, 105–107	168.81	0.00	2.38
17H-4, 120–122	168.96	0.04	2.32
17H-4, 135–137	169.11	0.00	2.64
17H-5, 0–2	169.26	–0.03	2.43
17H-5, 15–17	169.41		
17H-5, 30–32	169.56	–0.19	2.55
17H-5, 45–47	169.71	–0.22	2.55
17H-5, 60–62	169.86	–0.21	2.55
17H-5, 75–77	170.01	–0.22	2.73
17H-5, 90–92	170.16		
17H-5, 105–107	170.31	0.12	2.37
17H-5, 120–122	170.46	0.01	2.51
17H-5, 135–137	170.61	0.08	2.34
17H-6, 0–2	170.77	0.07	2.48
17H-6, 15–17	170.92	0.05	2.20
17H-6, 30–32	171.07	0.12	2.15
17H-6, 45–47	171.22	–0.13	2.44
17H-6, 60–62	171.37	0.02	2.16
17H-6, 75–77	171.52	–0.03	2.12
17H-6, 90–92	171.67		
17H-6, 105–107	171.82	–0.03	2.24
17H-6, 120–122	171.97	0.14	2.62
17H-6, 135–137	172.12		
202-1241B-			
8H-2, 100–102	73.16	–0.15	3.03
8H-2, 110–112	73.26	0.03	2.75
8H-2, 120–122	73.36	–0.01	2.57
8H-2, 130–132	73.46	–0.15	2.44
8H-2, 140–142	73.56	0.00	2.86
8H-3, 0–2	73.67	–0.22	3.09
8H-3, 10–12	73.77	–0.38	3.08
8H-3, 20–22	73.87	–0.25	3.01
8H-3, 30–32	73.97	–0.39	2.97
8H-3, 40–42	74.07	–0.30	2.97
8H-3, 50–52	74.17	–0.36	2.94
8H-3, 60–62	74.27	–0.37	2.93
8H-3, 70–72	74.37	–0.35	2.91
8H-3, 80–82	74.47		
8H-3, 90–92	74.57	–0.21	3.02
8H-3, 100–102	74.67	–0.28	2.74
8H-3, 110–112	74.77	–0.30	2.69
8H-3, 120–122	74.87	–0.29	2.56
8H-3, 130–132	74.97		
8H-3, 140–142	75.07	–0.30	2.60
8H-4, 0–2	75.17	–0.21	3.02
8H-4, 10–12	75.27	–0.41	2.81
8H-4, 20–22	75.37	–0.19	3.07
8H-4, 30–32	75.47	–0.27	2.84
8H-4, 40–42	75.57	–0.18	2.62
8H-4, 50–52	75.67		
8H-4, 60–62	75.77		
8H-4, 70–72	75.87		
8H-4, 80–82	75.97		
8H-4, 90–92	76.07		
8H-4, 100–102	76.17		
8H-4, 110–112	76.27	–0.03	2.91
8H-4, 120–122	76.37	–0.05	2.43
8H-4, 130–132	76.47	0.01	2.57
8H-4, 140–142	76.57	0.05	2.62
8H-5, 0–2	76.67	0.14	2.67
8H-5, 10–12	76.77	0.06	2.57
8H-5, 20–22	76.87	–0.07	2.81
8H-5, 30–32	76.97	–0.04	2.75
8H-5, 40–42	77.07	–0.01	2.95
8H-5, 43–45	77.10	–0.05	2.70
8H-5, 50–52	77.17	0.15	2.48
8H-5, 60–62	77.27	–0.07	2.57
8H-5, 70–72	77.37	–0.32	2.66
8H-5, 80–82	77.47	–0.24	2.79
8H-5, 90–92	77.57	–0.48	2.57
8H-5, 100–102	77.67	–0.49	2.72
8H-5, 110–112	77.77	–0.31	2.61
8H-5, 120–122	77.87	–0.65	2.58
12H-2, 130–132	119.31	–0.11	2.36
12H-2, 140–142	119.41	–0.16	2.31
12H-3, 0–2	119.51	0.01	2.36
12H-3, 10–12	119.61	–0.01	2.44
12H-3, 20–22	119.71	0.10	2.46
12H-3, 30–32	119.81	0.14	2.39
12H-3, 40–42	119.91	0.11	2.39
12H-3, 50–52	120.01	–0.03	2.32
12H-3, 60–62	120.11	–0.06	2.40
12H-3, 70–72	120.21	–0.17	2.43
12H-3, 80–82	120.31	–0.08	2.53
12H-3, 90–92	120.41	–0.13	2.57
12H-3, 100–102	120.51	–0.35	2.42
12H-3, 110–112	120.61	–0.15	2.56
12H-3, 120–122	120.71	0.01	2.52
12H-3, 130–132	120.81	–0.03	2.39
12H-3, 140–142	120.91	0.06	2.36
12H-4, 0–2	121.02	0.01	2.37
12H-4, 10–12	121.12	0.03	2.17
12H-4, 20–22	121.22	0.08	2.20
12H-4, 30–32	121.32	0.11	2.36
12H-4, 40–42	121.42	0.28	2.49
12H-4, 50–52	121.52	0.09	2.35
12H-4, 60–62	121.62	0.15	2.35
12H-4, 70–72	121.72	0.10	2.33
12H-4, 80–82	121.82	0.06	2.21

Appendix Table AT4 (continued).

Core, section, interval (cm)	Depth (mcd)	*Cibicidoides wuellerstorfi* $\delta^{13}C$ (‰)	*Cibicidoides wuellerstorfi* $\delta^{18}O$ (‰)
12H-4, 90–92	121.92	–0.04	2.37
12H-4, 100–102	122.02	–0.12	2.51
12H-4, 110–112	122.12	–0.06	2.45
12H-4, 120–122	122.22	0.04	2.64
12H-4, 130–132	122.32	0.06	2.59
12H-4, 140–142	122.42	0.23	2.51
12H-5, 0–2	122.53	0.14	2.34
12H-5, 10–12	122.63	0.21	2.51
12H-5, 20–22	122.73	0.24	2.46
12H-5, 30–32	122.83	–0.01	2.43
12H-5, 40–42	122.93	0.17	2.42
12H-5, 50–52	123.03	0.27	2.42
12H-5, 60–62	123.13	–0.05	2.58
12H-5, 70–72	123.23	0.03	2.42
12H-5, 80–82	123.33	–0.08	2.52
12H-5, 90–92	123.43	–0.09	2.43
12H-5, 100–102	123.53	–0.10	2.50
12H-5, 110–112	123.63	0.01	2.56
12H-5, 120–122	123.73	0.13	2.54
12H-5, 130–132	123.83	0.09	2.53
12H-5, 140–142	123.93	0.14	2.64
12H-6, 0–2	124.03	0.12	2.51
12H-6, 10–12	124.13	0.14	2.33
12H-6, 20–22	124.23	0.11	2.47
12H-6, 30–32	124.33	0.18	2.61
12H-6, 40–42	124.43	0.09	2.50
12H-6, 50–52	124.53	–0.09	2.52
12H-6, 60–62	124.63	–0.07	2.51
12H-6, 70–72	124.73	0.04	2.52
12H-6, 80–82	124.83	0.00	2.35
12H-6, 90–92	124.93	0.03	2.62
12H-6, 100–102	125.03	–0.01	2.56
12H-6, 110–112	125.13	–0.02	2.55
12H-6, 120–122	125.23	0.01	2.48
12H-6, 130–132	125.33	0.16	2.37
14H-2, 110–112	140.38	–0.18	2.32
14H-2, 120–122	140.48	–0.16	2.38
14H-2, 130–132	140.58	–0.12	
14H-2, 140–142	140.68	–0.21	2.46
14H-3, 0–2	140.79	0.06	2.60
14H-3, 10–12	140.89		2.45
14H-3, 20–22	140.99	0.17	2.34
14H-3, 30–32	141.09	0.11	2.69
14H-3, 40–42	141.19		2.25
14H-3, 50–52	141.29	–0.15	2.40
14H-3, 60–62	141.39	–0.23	2.40
14H-3, 70–72	141.49	–0.24	2.45
14H-3, 80–82	141.59	–0.30	2.35
14H-3, 90–92	141.69	–0.28	2.29
14H-3, 100–102	141.79	–0.20	2.49
14H-3, 110–112	141.89	–0.27	2.56
14H-3, 120–122	141.99	–0.15	2.29
14H-3, 130–132	142.09		2.56
14H-3, 140–142	142.19	–0.19	2.38
14H-4, 0–2	142.30	–0.16	2.47
14H-4, 10–12	142.40	–0.16	2.29
14H-4, 20–22	142.50	–0.18	2.20
14H-4, 30–32	142.60	–0.36	2.16
14H-4, 40–42	142.70	–0.21	2.28
14H-4, 50–52	142.80	–0.32	2.36
14H-4, 60–62	142.90	–0.30	2.42
14H-4, 70–72	143.00	–0.19	2.33
14H-4, 80–82	143.10	–0.12	2.56
14H-4, 90–92	143.20	–0.23	2.46
14H-4, 100–102	143.30	–0.19	2.49
14H-4, 110–112	143.40	–0.06	2.38
14H-4, 120–122	143.50	–0.18	2.26
14H-4, 130–132	143.60	–0.09	2.08
14H-4, 140–142	143.70	–0.01	2.40
14H-5, 0–2	143.81	0.02	2.55
14H-5, 10–12	143.91	0.06	2.61
14H-5, 20–22	144.01	0.07	2.45
14H-5, 30–32	144.11	–0.02	2.41
14H-5, 40–42	144.21	0.01	2.34
14H-5, 50–52	144.31	–0.05	2.12
14H-5, 60–62	144.41	–0.20	2.30
14H-5, 70–72	144.51	–0.12	2.33
14H-5, 80–82	144.61	–0.05	2.40
14H-5, 90–92	144.71		
14H-5, 100–102	144.81	–0.35	2.57
14H-5, 110–112	144.91	–0.25	2.46
14H-5, 120–122	145.01	–0.59	2.41
14H-5, 130–132	145.11	–0.54	2.45
16H-2, 30–32	161.66	0.02	2.25
16H-2, 45–47	161.81	0.01	2.48
16H-2, 60–62	161.96	–0.01	2.16
16H-2, 75–77	162.11	0.02	2.19
16H-2, 90–92	162.26	0.00	2.27
16H-2, 105–107	162.41	–0.13	2.41
16H-2, 120–122	162.56	0.13	2.32
16H-2, 135–137	162.71	0.06	2.31
16H-3, 0–2	162.87	0.07	2.46
16H-3, 15–17	163.02	0.04	2.39
16H-3, 30–32	163.17	–0.05	2.52
16H-3, 45–47	163.32	0.05	2.37
16H-3, 60–62	163.47	0.05	2.40
16H-3, 75–77	163.62		2.53
16H-3, 90–92	163.77	0.07	2.09
16H-3, 105–107	163.92		
16H-3, 120–122	164.07	–0.09	2.30
16H-3, 135–137	164.22	0.18	2.43
16H-4, 0–2	164.38	0.01	2.39
16H-4, 15–17	164.53	0.15	2.53
16H-4, 30–32	164.68	0.37	2.32
16H-4, 45–47	164.83	0.32	2.50
16H-4, 60–62	164.98		
16H-4, 75–77	165.13	0.21	2.21
16H-4, 90–92	165.28	0.23	2.46
16H-4, 105–107	165.43	0.26	2.61
16H-4, 120–122	165.58	0.13	2.39
16H-4, 135–137	165.73		
16H-5, 0–2	165.88	0.14	2.43
16H-5, 15–17	166.03	–0.10	2.49
16H-5, 30–32	166.18	0.12	2.13
16H-5, 45–47	166.33		
16H-5, 60–62	166.48	0.03	2.41
16H-5, 75–77	166.63	0.09	2.11
16H-5, 90–92	166.78	–0.01	2.29
16H-5, 105–107	166.93	–0.06	2.24
16H-5, 120–122	167.08		
16H-5, 135–137	167.23		
16H-6, 0–2	167.37	–0.16	2.45
16H-6, 15–17	167.52	–0.26	2.63
16H-6, 30–32	167.67	–0.33	2.58
16H-6, 45–47	167.82	–0.15	3.00
16H-6, 60–62	167.97	–0.35	2.70
17H-2, 0–2	172.30	–0.05	2.35
17H-2, 15–17	172.45	0.15	2.43
17H-2, 30–32	172.60	0.10	2.33
17H-2, 45–47	172.75	0.01	2.55
17H-2, 60–62	172.90	0.07	2.27
17H-2, 75–77	173.05	0.21	2.29
17H-2, 90–92	173.20	0.01	2.35
17H-2, 105–107	173.35	–0.10	2.60
17H-2, 120–122	173.50	0.06	2.39
17H-2, 135–137	173.65	0.16	2.22
17H-3, 0–2	173.81	–0.01	2.57
17H-3, 15–17	173.96	–0.06	2.41

Appendix Table AT4 (continued).

Core, section, interval (cm)	Depth (mcd)	*Cibicidoides wuellerstorfi* $\delta^{13}C$ (‰)	*Cibicidoides wuellerstorfi* $\delta^{18}O$ (‰)
17H-3, 30–32	174.11	–0.20	2.55
17H-3, 45–47	174.26	–0.11	2.58
17H-3, 60–62	174.41		
17H-3, 75–77	174.56	0.17	2.25
17H-3, 90–92	174.71		
17H-3, 105–107	174.86	0.21	2.65
17H-3, 120–122	175.01	0.21	2.70
17H-3, 135–137	175.16	0.21	2.43
17H-4, 0–2	175.31	0.17	2.04
17H-4, 15–17	175.46	0.24	2.91
17H-4, 30–32	175.61	0.07	2.01
17H-4, 45–47	175.76	–0.21	2.56
17H-4, 60–62	175.91	–0.25	2.67
17H-4, 75–77	176.06	–0.27	2.76
17H-4, 90–92	176.21	–0.31	2.58
17H-4, 105–107	176.36	–0.06	2.67
17H-4, 120–122	176.51	–0.07	2.39
17H-4, 135–137	176.66	–0.05	2.36
202-1241C-			
3H-4, 0–2	58.21	–0.46	3.41
3H-4, 10–12	58.31	–0.41	3.81
3H-4, 20–22	58.41	–0.44	3.60
3H-4, 30–32	58.51	–0.57	3.75
3H-4, 40–42	58.61	–0.33	3.67
3H-4, 50–52	58.71	–0.30	3.24
3H-4, 60–62	58.81	–0.17	3.10
3H-4, 70–72	58.91	0.03	3.06
3H-4, 80–82	59.01	–0.01	2.88
3H-4, 90–92	59.11	–0.01	2.58
3H-4, 100–102	59.21	–0.42	2.74
3H-4, 110–112	59.31	–0.03	2.95
3H-4, 120–122	59.41	–0.20	3.05
3H-4, 130–132	59.51	0.04	
3H-4, 140–142	59.61	–0.36	3.31
3H-5, 0–2	59.72	–0.91	3.47
3H-5, 10–12	59.82	–0.46	3.45
3H-5, 20–22	59.92	–0.36	3.56
3H-5, 30–32	60.02	–0.30	3.65
3H-5, 40–42	60.12	–0.10	3.08
3H-5, 50–52	60.22	–0.09	2.67
3H-5, 60–62	60.32	–0.15	3.04
3H-5, 70–72	60.42	–0.36	2.89
3H-5, 80–82	60.52	–0.55	3.25
3H-5, 90–92	60.62	–0.60	3.40
3H-5, 100–102	60.72	–0.65	3.62
3H-5, 110–112	60.82	–0.66	3.69
3H-5, 120–122	60.92	–0.68	3.46
3H-5, 130–132	61.02	–0.62	3.51
3H-5, 140–142	61.12	–0.48	3.28
3H-6, 0–2	61.23	–0.04	2.65
3H-6, 10–12	61.33	0.02	2.71
3H-6, 20–22	61.43	–0.10	2.88
4H-2, 30–32	66.46	0.05	2.49
4H-2, 40–42	66.56	0.15	2.62
4H-2, 50–52	66.66	0.04	2.81
4H-2, 60–62	66.76	0.05	2.89
4H-2, 70–72	66.86	0.04	2.94
4H-2, 80–82	66.96	–0.23	2.89
4H-2, 90–92	67.06	–0.29	2.86
4H-2, 100–102	67.16	–0.25	3.00
4H-2, 110–112	67.26	–0.04	2.96
4H-2, 120–122	67.36	0.12	2.96
4H-2, 130–132	67.46	0.10	2.72
4H-2, 140–142	67.56		
4H-3, 0–2	67.67	0.08	2.59
4H-3, 10–12	67.77	0.01	2.77
4H-3, 20–22	67.87	–0.22	
4H-3, 30–32	67.97	–0.35	3.18
4H-3, 40–42	68.07	–0.14	3.05
4H-3, 50–52	68.17	–0.20	3.25
4H-3, 60–62	68.27	–0.21	3.53
4H-3, 70–72	68.37	–0.16	3.05
4H-3, 80–82	68.47	–0.01	3.16
4H-3, 90–92	68.57	0.17	3.40
4H-3, 100–102	68.67	–0.04	2.82
4H-3, 110–112	68.77	–0.01	2.91
4H-3, 120–122	68.87	0.24	2.78
4H-3, 130–132	68.97	0.10	2.71
4H-3, 140–142	69.07		
4H-4, 0–2	69.19		2.95
4H-4, 10–12	69.29	0.00	3.21
4H-4, 20–22	69.39	0.04	3.03
4H-4, 30–32	69.49	0.03	3.26
4H-4, 40–42	69.59	–0.02	2.99
4H-4, 50–52	69.69	0.03	2.88
4H-4, 60–62	69.79	–0.05	2.90
4H-4, 70–72	69.89	0.04	2.84
4H-4, 80–82	69.99	–0.02	2.95
4H-4, 90–92	70.09	–0.08	2.88
4H-4, 100–102	70.19	–0.09	3.14
4H-4, 110–112	70.29	–0.10	3.07
4H-4, 120–122	70.39	0.16	
4H-4, 130–132	70.49	0.04	2.79
4H-4, 140–142	70.59	0.09	2.84
4H-5, 0–2	70.70	0.01	2.65
4H-5, 10–12	70.80	–0.03	3.06
4H-5, 20–22	70.90	0.00	2.97
4H-5, 30–32	71.00	0.02	3.13
4H-5, 40–42	71.10	–0.27	2.93
4H-5, 50–52	71.20	–0.26	2.84
4H-5, 60–62	71.30	–0.34	2.94
4H-5, 70–72	71.40	–0.32	3.16
4H-5, 80–82	71.50	–0.31	2.86
4H-5, 90–92	71.60	–0.32	2.95
4H-5, 100–102	71.70	–0.15	2.63
4H-5, 110–112	71.80	0.00	3.11
4H-5, 120–122	71.90	0.08	2.66
4H-5, 130–132	72.00		
4H-5, 140–142	72.10		
4H-6, 0–2	72.21		
4H-6, 10–12	72.31	–0.07	2.86
4H-6, 20–22	72.41	–0.06	2.75
4H-6, 30–32	72.51	–0.04	2.54
4H-6, 40–42	72.61	–0.16	2.72
4H-6, 50–52	72.71	–0.15	2.78
4H-6, 60–62	72.81	–0.47	2.78
4H-6, 70–72	72.91	0.01	3.05
4H-6, 80–82	73.01	–0.17	3.34
4H-6, 90–92	73.11	–0.22	3.22
5H-2, 140–142	77.95	–0.43	2.64
5H-3, 0–2	78.06	–0.51	2.90
5H-3, 10–12	78.16	–0.50	2.68
5H-3, 20–22	78.26	–0.46	2.70
5H-3, 30–32	78.36	–0.57	2.55
5H-3, 40–42	78.46	–0.40	2.55
5H-3, 50–52	78.56	–0.24	2.38
5H-3, 60–62	78.66	–0.28	2.28
5H-3, 70–72	78.76	–0.17	2.23
5H-3, 80–82	78.86	–0.19	2.49
5H-3, 90–92	78.96	–0.18	2.34
5H-3, 100–102	79.06	–0.31	2.31
5H-3, 110–112	79.16	–0.38	2.57
5H-3, 120–122	79.26	–0.16	2.40
5H-3, 130–132	79.36	–0.18	2.41
5H-3, 140–142	79.46	–0.30	2.37
5H-4, 0–2	79.56	–0.23	2.52
5H-4, 10–12	79.66	–0.20	2.53
5H-4, 20–22	79.76	–0.02	2.60

Appendix Table AT4 (continued).

Core, section, interval (cm)	Depth (mcd)	*Cibicidoides wuellerstorfi* $\delta^{13}C$ (‰)	*Cibicidoides wuellerstorfi* $\delta^{18}O$ (‰)
5H-4, 30–32	79.86	–0.12	2.60
5H-4, 40–42	79.96	–0.23	2.60
5H-4, 50–52	80.06	–0.09	2.56
5H-4, 60–62	80.16	0.06	2.55
5H-4, 70–72	80.26	0.06	2.67
5H-4, 80–82	80.36	0.03	
5H-4, 90–92	80.46	0.06	2.58
5H-4, 100–102	80.56	0.06	2.48
5H-4, 110–112	80.66	–0.04	2.39
5H-4, 120–122	80.76	0.02	2.53
5H-4, 130–132	80.86	–0.04	2.59
5H-4, 140–142	80.96	–0.12	2.49
5H-5, 0–2	81.06	–0.10	2.60
5H-5, 10–12	81.16	–0.06	2.49
5H-5, 20–22	81.26	0.09	2.56
5H-5, 30–32	81.36	–0.08	2.42
5H-5, 40–42	81.46	0.08	2.45
5H-5, 50–52	81.56	0.08	2.56
5H-5, 60–62	81.66	–0.05	2.64
5H-5, 70–72	81.76	0.09	2.51
5H-5, 80–82	81.86	–0.13	2.43
5H-5, 90–92	81.96	–0.03	2.72
5H-5, 100–102	82.06	–0.05	2.64
5H-5, 110–112	82.16	0.06	2.71
5H-5, 120–122	82.26	–0.05	2.55
5H-5, 130–132	82.36	–0.11	2.48
5H-5, 140–142	82.46	–0.06	2.52
5H-6, 0–2	82.57	–0.18	2.63
5H-6, 10–12	82.67	–0.11	2.59
5H-6, 20–22	82.77	–0.39	2.76
5H-6, 30–32	82.87	–0.39	2.98
5H-6, 40–42	82.97	–0.40	2.80
5H-6, 50–52	83.07	–0.60	3.07
5H-6, 60–62	83.17	–0.61	3.17
5H-6, 70–72	83.27	–0.66	2.90
5H-6, 80–82	83.37	–0.45	2.99
5H-6, 90–92	83.47	–0.45	2.87
6H-3, 20–22	89.23	–0.19	2.26
6H-3, 30–32	89.33	–0.18	2.40
6H-3, 40–42	89.43	–0.34	2.44
6H-3, 50–52	89.53	–0.34	2.49
6H-3, 60–62	89.63	–0.34	2.40
6H-3, 70–72	89.73	–0.27	2.62
6H-3, 80–82	89.83	–0.26	2.44
6H-3, 90–92	89.93	–0.22	2.67
6H-3, 100–102	90.03	–0.13	2.29
6H-3, 110–112	90.13	0.06	2.35
6H-3, 120–122	90.23	0.08	2.24
6H-3, 130–132	90.33	–0.12	2.10
6H-3, 140–142	90.43	–0.10	2.21
6H-4, 0–2	90.53	–0.28	2.55
6H-4, 10–12	90.63	–0.15	2.20
6H-4, 20–22	90.73	0.06	2.45
6H-4, 30–32	90.83	–0.17	2.66
6H-4, 40–42	90.93	–0.13	2.61
6H-4, 50–52	91.03	0.04	2.37
6H-4, 60–62	91.13	–0.10	2.47
6H-4, 70–72	91.23	–0.27	2.43
6H-4, 80–82	91.33	–0.12	2.47
6H-4, 90–92	91.43	–0.08	2.38
6H-4, 100–102	91.53	0.09	2.09
6H-4, 110–112	91.63	–0.13	2.31
6H-4, 120–122	91.73	0.01	2.23
6H-4, 130–132	91.83	–0.28	2.25
6H-4, 140–142	91.93	–0.24	2.33
6H-5, 0–2	92.03	–0.15	2.35
6H-5, 10–12	92.13	–0.26	2.38
7H-2, 100–102	98.82	–0.11	2.36
7H-2, 110–112	98.92	–0.18	2.57
7H-2, 120–122	99.02	–0.16	2.65
7H-2, 130–132	99.12	–0.08	2.59
7H-2, 140–142	99.22	–0.10	2.42
7H-3, 0–2	99.32	0.04	2.55
7H-3, 10–12	99.42	0.04	2.22
7H-3, 20–22	99.52	–0.05	2.52
7H-3, 30–32	99.62	0.03	2.38
7H-3, 40–42	99.72	0.07	2.09
7H-3, 50–52	99.82	–0.05	2.44
7H-3, 60–62	99.92	–0.21	2.55
7H-3, 70–72	100.02	–0.36	
7H-3, 80–82	100.12	–0.11	2.56
7H-3, 90–92	100.22	–0.22	2.43
7H-3, 100–102	100.32	–0.23	2.17
7H-3, 110–112	100.42	–0.09	2.30
7H-3, 120–122	100.52	–0.08	2.08
7H-3, 130–132	100.62	–0.17	2.48
7H-3, 140–142	100.72	–0.25	2.52
7H-4, 0–2	100.82	–0.22	2.53
7H-4, 10–12	100.92	–0.39	2.10
7H-4, 20–22	101.02	–0.14	2.61
7H-4, 30–32	101.12	–0.12	2.26
7H-4, 40–42	101.22	–0.14	2.62
7H-4, 50–52	101.32		
7H-4, 60–62	101.42	–0.27	2.14
7H-4, 70–72	101.52	–0.40	2.22
7H-4, 80–82	101.62	–0.26	2.42
7H-4, 90–92	101.72	–0.62	2.43
7H-4, 100–102	101.82	–0.46	2.51
7H-4, 110–112	101.92	–0.13	2.38
7H-4, 120–122	102.02	–0.19	2.30
7H-4, 130–132	102.12	–0.14	2.31
7H-4, 140–142	102.22	–0.19	
7H-5, 0–2	102.32		
7H-5, 10–12	102.42	–0.14	2.25
7H-5, 20–22	102.52	–0.10	2.27
7H-5, 30–32	102.62	–0.13	2.61
7H-5, 40–42	102.72	–0.17	2.43
7H-5, 50–52	102.82	–0.13	2.28
7H-5, 60–62	102.92	–0.30	2.19
7H-5, 70–72	103.02	–0.44	2.11
7H-5, 80–82	103.12		2.20
7H-5, 90–92	103.22	–0.35	2.70
7H-5, 100–102	103.32	–0.19	2.46
7H-5, 110–112	103.42	–0.21	2.71
7H-5, 120–122	103.52	–0.34	2.56
7H-5, 130–132	103.62	–0.15	2.49
7H-5, 140–142	103.72	–0.07	2.53
7H-6, 0–2	103.82	–0.02	2.45
7H-6, 10–12	103.92	–0.17	2.24
7H-6, 20–22	104.02	–0.13	2.20
7H-6, 30–32	104.12	–0.03	2.31
7H-6, 40–42	104.22	–0.19	2.35
7H-6, 50–52	104.32	–0.25	2.60
7H-6, 60–62	104.42	–0.20	2.29
7H-6, 70–72	104.52	–0.28	2.16
7H-6, 80–82	104.62	–0.32	2.40
7H-6, 90–92	104.72	–0.39	2.50
7H-6, 100–102	104.82	–0.32	2.39
7H-6, 110–112	104.92	–0.30	2.58
7H-6, 120–122	105.02	–0.19	2.42
7H-6, 130–132	105.12	–0.15	2.39
7H-6, 140–142	105.22	–0.17	2.30
7H-7, 0–2	105.32	–0.19	2.29
7H-7, 10–12	105.42	–0.24	2.16
7H-7, 20–22	105.52	–0.18	2.30
7H-7, 30–32	105.62	–0.26	2.34
7H-7, 40–42	105.72	–0.30	2.55
7H-7, 50–52	105.82	–0.47	2.52

Appendix Table AT4 (continued).

Core, section, interval (cm)	Depth (mcd)	*Cibicidoides wuellerstorfi* $\delta^{13}C$ (‰)	*Cibicidoides wuellerstorfi* $\delta^{18}O$ (‰)
7H-7, 60–62	105.92	–0.01	2.41
8H-2, 0–2	108.36	–0.23	2.56
8H-2, 10–12	108.46	–0.18	2.55
8H-2, 20–22	108.56	–0.24	2.64
8H-2, 30–32	108.66	–0.17	2.63
8H-2, 40–42	108.76	0.06	2.26
8H-2, 50–52	108.86	–0.02	2.43
8H-2, 60–62	108.96	0.04	2.26
8H-2, 70–72	109.06	0.06	2.36
8H-2, 80–82	109.16	0.07	2.40
8H-2, 90–92	109.26	0.02	2.37
8H-2, 100–102	109.36	0.02	2.37
8H-2, 110–112	109.46	–0.09	2.33
8H-2, 120–122	109.56	0.04	2.69
8H-2, 130–132	109.66	–0.08	2.50
8H-2, 140–142	109.76	0.02	2.64
8H-3, 0–2	109.86	–0.06	2.52
8H-3, 10–12	109.96	–0.04	2.40
8H-3, 20–22	110.06	–0.26	2.42
8H-3, 30–32	110.16	–0.06	2.42
8H-3, 40–42	110.26	–0.15	2.44
8H-3, 50–52	110.36	–0.23	2.05
8H-3, 60–62	110.46	–0.17	2.15
8H-3, 70–72	110.56		2.31
8H-3, 80–82	110.66	–0.11	2.54
8H-3, 90–92	110.76	–0.06	2.48
8H-3, 100–102	110.86	–0.05	2.46
8H-3, 110–112	110.96	–0.06	2.41
8H-3, 120–122	111.06	–0.01	2.52
8H-3, 130–132	111.16	–0.05	2.52
8H-3, 140–142	111.26	–0.03	2.50
8H-4, 0–2	111.36	0.06	2.44
8H-4, 10–12	111.46	–0.02	2.31
8H-4, 20–22	111.56		2.37
8H-4, 30–32	111.66	–0.01	2.37
8H-4, 40–42	111.76	0.05	2.59
8H-4, 50–52	111.86	–0.07	2.35
8H-4, 60–62	111.96	–0.02	2.61
8H-4, 70–72	112.06	0.01	2.52
8H-4, 80–82	112.16	–0.02	2.44
8H-4, 90–92	112.26	–0.01	2.43
8H-4, 100–102	112.36	–0.09	2.56
8H-4, 110–112	112.46	–0.05	2.48
8H-4, 120–122	112.56	–0.18	2.42
8H-4, 130–132	112.66	–0.05	2.56
8H-4, 140–142	112.76	0.01	2.45
8H-5, 0–2	112.86	–0.04	2.64
8H-5, 10–12	112.96	0.08	2.22
8H-5, 20–22	113.06	0.01	2.51
8H-5, 30–32	113.16	–0.19	2.33
8H-5, 40–42	113.26	0.01	2.50
8H-5, 50–52	113.36	–0.08	2.28
8H-5, 60–62	113.46	0.05	2.45
8H-5, 70–72	113.56	0.00	2.41
8H-5, 80–82	113.66	0.12	2.40
8H-5, 90–92	113.76	0.08	2.43
8H-5, 100–102	113.86	–0.06	2.26
8H-5, 110–112	113.96	–0.09	2.43
8H-5, 120–122	114.06	–0.16	2.42
8H-5, 130–132	114.16	–0.22	2.41
8H-5, 140–142	114.26	–0.17	2.33
8H-6, 0–2	114.36	–0.26	2.25
8H-6, 10–12	114.46	–0.24	2.27
8H-6, 20–22	114.56	–0.35	2.36
8H-6, 30–32	114.66	–0.41	2.58
8H-6, 40–42	114.76	–0.07	2.64
8H-6, 50–52	114.86	–0.08	2.38
8H-6, 60–62	114.96	–0.33	2.17
13H-5, 110–112	129.12	–0.24	2.48
9H-3, 90–92	129.14	–0.26	2.76
9H-3, 100–102	129.24	–0.14	2.64
9H-3, 110–112	129.34	–0.20	2.26
9H-3, 120–122	129.44	–0.10	2.37
9H-3, 130–132	129.54	–0.01	2.41
9H-3, 140–142	129.64	0.11	2.61
9H-4, 0–2	129.74	–0.11	2.45
9H-4, 10–12	129.84	0.00	2.43
9H-4, 20–22	129.94	0.01	2.49
9H-4, 30–32	130.04	–0.06	2.26
9H-4, 40–42	130.14	–0.15	2.34
9H-4, 50–52	130.24	–0.11	2.43
9H-4, 60–62	130.34	–0.07	2.33
9H-4, 70–72	130.44		2.37
9H-4, 80–82	130.54	–0.11	2.30
9H-4, 90–92	130.64	–0.21	2.31
9H-4, 100–102	130.74	–0.20	2.35
9H-4, 110–112	130.84	–0.23	2.53
9H-4, 120–122	130.94	–0.15	2.67
9H-4, 130–132	131.04	–0.20	2.22
9H-4, 140–142	131.14	–0.05	2.61
9H-5, 0–2	131.25	–0.27	2.12
9H-5, 10–12	131.35	–0.11	2.21
9H-5, 20–22	131.45	–0.12	2.29
9H-5, 30–32	131.55	0.10	2.25
9H-5, 40–42	131.65	–0.09	2.50
9H-5, 50–52	131.75	–0.10	2.29
9H-5, 60–62	131.85	–0.14	2.47
9H-5, 70–72	131.95	–0.17	2.39
9H-5, 80–82	132.05	–0.16	2.50
9H-5, 90–92	132.15	–0.13	2.55
9H-5, 100–102	132.25	–0.16	2.53
9H-5, 110–112	132.35	–0.20	2.37
9H-5, 120–122	132.45	–0.15	2.25
9H-5, 130–132	132.55	–0.18	2.41
11H-2, 90–92	150.97	–0.02	2.42
11H-2, 100–102	151.07	–0.25	2.29
11H-2, 110–112	151.17	–0.36	2.25
11H-2, 120–122	151.27	–0.15	2.23
11H-2, 130–132	151.37	0.07	2.52
11H-2, 140–142	151.47	0.00	2.41
11H-3, 0–2	151.57	0.05	2.41
11H-3, 10–12	151.67	–0.04	2.33
11H-3, 20–22	151.77	–0.17	2.43
11H-3, 30–32	151.87	–0.29	2.43
11H-3, 40–42	151.97	–0.07	2.36
11H-3, 50–52	152.07	–0.17	2.62
11H-3, 60–62	152.17	–0.21	2.35
11H-3, 70–72	152.27	–0.09	2.65
11H-3, 80–82	152.37	–0.18	2.43
11H-3, 90–92	152.47	–0.60	2.48
11H-3, 100–102	152.57	–0.25	2.55
11H-3, 110–112	152.67	–0.22	2.47
11H-3, 120–122	152.77	–0.23	2.50
11H-3, 130–132	152.87	0.04	2.46
11H-3, 140–142	152.97	0.07	2.29
11H-4, 0–2	153.07	0.17	2.54
11H-4, 10–12	153.17	–0.03	2.50
11H-4, 20–22	153.27	0.20	2.50
11H-4, 30–32	153.37	0.13	2.32
11H-4, 40–42	153.47	0.12	2.35
11H-4, 50–52	153.57	0.03	2.42
11H-4, 60–62	153.67		
11H-4, 70–72	153.77	0.09	2.43
11H-4, 80–82	153.87	0.09	2.44
11H-4, 90–92	153.97	0.05	2.50
11H-4, 100–102	154.07	–0.08	2.47
11H-4, 110–112	154.17	–0.04	2.52
11H-4, 120–122	154.27	–0.03	2.51

Appendix Table AT4 (continued).

		Cibicidoides wuellerstorfi	
Core, section, interval (cm)	Depth (mcd)	$\delta^{13}C$ (‰)	$\delta^{18}O$ (‰)
11H-4, 130–132	154.37	0.02	2.76
11H-4, 140–142	154.47	0.01	2.31
11H-5, 0–2	154.57	0.02	2.52
11H-5, 10–12	154.67	0.16	2.29
11H-5, 20–22	154.77	0.03	2.44
11H-5, 30–32	154.87	0.21	2.49
11H-5, 40–42	154.97	0.10	2.51
11H-5, 50–52	155.07	0.27	2.44
11H-5, 60–62	155.17	0.15	2.62
11H-5, 70–72	155.27	0.31	2.34
11H-5, 80–82	155.37	0.23	2.36
11H-5, 90–92	155.47	0.27	2.33
11H-5, 100–102	155.57		
11H-5, 110–112	155.67	–0.09	2.24
11H-5, 120–122	155.77	–0.31	2.38
11H-5, 130–132	155.87	–0.27	2.35
11H-5, 140–142	155.97	0.14	2.39
11H-6, 0–2	156.08	0.18	2.30
11H-6, 10–12	156.18	0.26	2.60
11H-6, 20–22	156.28	0.16	2.45
11H-6, 30–32	156.38	0.11	2.39
11H-6, 40–42	156.48	0.29	2.47
11H-6, 50–52	156.58	0.29	2.23
11H-6, 60–62	156.68	0.05	2.39
11H-6, 70–72	156.78	0.10	2.50
11H-6, 80–82	156.88	0.19	2.22
11H-6, 90–92	156.98	0.28	2.39
11H-6, 100–102	157.08	0.13	2.20
11H-6, 110–112	157.18	0.17	2.31
11H-6, 120–122	157.28	0.13	2.28
11H-6, 130–132	157.38	0.11	2.38
11H-6, 140–142	157.48	0.07	2.52
11H-7, 0–2	157.58	0.10	2.11
11H-7, 10–12	157.68	0.13	2.23
11H-7, 20–22	157.78	0.06	2.16